The Effect of Morphological Variations at the Human Ankle and Hip Joints on their Biomechanical Function

A Thesis

Submitted to the Faculty

of

Drexel University

by

Ramya Namani

in partial fulfillment of the

requirements for the degree

of

Doctor of Philosophy

September 2015

Acknowledgments

I would like to express my gratitude to my advisor Dr. Sorin Siegler for his tremendous support throughout my PhD program. His knowledge and passion for Biomechanics motivated me every day to develop my career in Biomechanics. He is one of the kindest and humble persons I have known.

I would like to thank other committee members Dr. Jack Zhou, Dr. Sriram Balasubramanian, Dr. Fred Allen and Dr. John Lacontora for their time and their valuable feedback in writing my thesis.

I would like to thank Dr. Javad Parvizi from Rothman institute for his guidance and collaboration with the hip project.

My sincere gratitude to my academic advisor, Dr. Alan Lau for his tremendous support and pushing me to finish my PhD on time. He is one of the most knowledgeable as well as kind persons I have met at Drexel.

I would like to thank International Society of Biomechanics for their support in awarding me a dissertation grant and a travel grant. The dissertation grant supported me to pursue the project and the travel grant gave me an opportunity to attend ISB conference and present my work and get feedback from some experts in Biomechanics field.

Lastly, I would thank all the staff of Drexel University for helping me in completing this program smoothly.

TABLE OF CONTENTS

LIST OF TABLES

LIST OF FIGURES

ABSTRACT

The Effect of Morphological Variations at the Human Ankle and Hip Joints on their Biomechanical Function
Ramya Namani
Sorin Siegler, Ph.D.

The morphology of the articular surfaces of bones and the insertion sites of ligaments crossing anatomical human joints were reported to vary greatly amongst individuals. These morphological variations could be the main cause for the observed large variations in the joint mechanical function. The goal of this study is to explore the causal relationship between the joint morphology and mechanics in two specific joints- ankle and hip joint. To achieve this goal, six experimentally validated numerical models of the ankle joint complex, were developed from morphological data, obtained from magnetic resonance images of six cadaveric lower limbs and six numerical models of hip joints were developed from morphological data obtained from computer tomographic scans of six healthy hip joints. The morphology of the bone is systematically varied and the resulting mechanical function such as range of motion of the joint, flexibility of the joint and forces in the ligaments are compared with the change in morphology. Since all models used identical material properties and were subjected to identical loads and boundary conditions, it was concluded that the observed variations in mechanical behavior of the joint were due to variations in morphology. The results suggested that the morphological variations could be the main cause for the large variations observed in joint mechanics and could influence the mechanical consequences of ligament injuries and surgical procedures such as joint fusion and joint replacement.

CHAPTER 1: INTRODUCTION

The morphology of the articular surfaces of bones and the insertion sites of ligaments crossing anatomical human joints were reported to vary greatly amongst individuals. Similar high inter-subject variability has been reported for the passive mechanical characteristics of human joints. However, very few studies explored the causal relations between joint morphology and joint mechanical behavior. Preliminary studies from our laboratory provided early evidence for an existence of such causal relationship. In those studies image-based, subject specific, three dimensional models of the ankle were used to explore the causal relationship between various morphological parameters and mechanical behavior of the ankle joint. Identifying these causal relationships may have significant impact on clinical management of various musculoskeletal disorders and may guide the development of individualized, subject specific treatment procedures.

Main Goal

To explore the causal relationship between the variations in joint morphology and the variations in joint mechanics in two specific joints.

1. Ankle Joint Complex– irregular joint
2. Hip Joint- close to spherical joint

These two joints represent two extremes of joint complexity with the hip being adequately represented by a simple ball-and-socket, three degrees of freedom joint and the ankle as a complex and irregular six-degrees-of-freedom joint.

Specific Aims

1. To study the effect of change in orientation of Calcaneofibular ligament (CFL) on Range of Motion(ROM), flexibility and force in CFL

   Hypothesis: The Orientation of the CFL effects ankle kinematics and flexibility and force in CFL.

2. To study the effect of change in morphology of sustentaculum tali on ROM, flexibility and force in CFL.

   Hypothesis: Shape of sustentaculum tali effects ankle kinematics and flexibility and force in CFL.

3. The effect of variations in the geometry of the femur on interference pattern.

   Hypothesis:

   1. Change in femoral neck orientation effects patterns of interference
   2. The shape of proximal femur effects patterns of interference

CHAPTER 2: BACKGROUND

Variations in Morphology

Anatomical studies [1-3] on the human joints reported large inter-subject variations in morphology of bones and soft tissue attachment sites. Examples of the former include variations in the shape and inclination of the sustentaculum tali of the calcaneus [1, 3, 4], abnormal shape of femur and acetabulum leading to femoroacetabular impingement [2] while examples of the later include variations in size of the Anterior Tibiotalar Ligament and variations in orientation of the Calcaneo-Fibular Ligament (CFL) [3, 5].

Variations in Mechanics

Experimental in vitro and in vivo biomechanical studies [6-9] on the human ankle, hip and knee joints reported large variations in the mechanical behavior. Such variations were reported in range of motion [8-10], kinematic coupling [8], orientation of an assumed fixed axis of rotation [6, 7] and variations in stiffness and flexibility characteristics [11]. Some studies [12, 13] reported that there is a restricted ROM in hips with femoroacetabular impingement compared to normal subjects. These variations were primarily attributed to variations in experimental techniques but no systematic studies into the nature and source of these inter-subject variations were reported.

Morphology-Mechanics Relationship

There were few studies in which the researchers have studied the relation between morphology and mechanical behavior in various human joints. Anderson et al [14]

studied that the effect of articular surface geometry of hip joint on cartilage stress. Eckhoff et.al, [15] studied the effect of variations in the knee joint axis of rotation on knee joint kinematics. Researchers have studied the relationship between the articular facets and range of motion of hand joints in the evolution of hand joint [16, 17] and found that the larger the difference in the curvature of the mutual facets, the greater the degree of movement. A previously developed image-based, subject-specific, numerical model of the ankle joint [18, 19], demonstrated that the large inter-subject variability in the stiffness characteristics of the ankle joint can be explained by the morphological variations in the shape of the sustentaculum tali. This provided an early indication suggesting the validity of the assumption that the inter-subject variability in the mechanical function of the ankle is causally related to inter-subject variability in the underlying bone and soft-tissue morphology.

In the following section the variations in morphology, variations in mechanics and morphology-mechanics relationship in Ankle and hip joints will be discussed in detail specific to the specific aims of the study.

Ankle Joint

The ankle joint complex is a complex joint composed of four bones-tibia, talus, fibula and calcaneus, stabilized by several ligaments and traversed by a number of tendons. The unique design of the ankle makes it a very stable joint. This joint has to be stable in order to withstand 1.5 times your body weight when you walk and up to eight times your body

weight when you run. The muscles, tendons, and ligaments that support the ankle joint work together to propel the body. The articular surfaces of each bone are covered by cartilage which acts as cushion between the bones. Ankle joint complex is divided into two joints- ankle joint (talocrural joint) and subtalar joint (talocalcaneal joint) (
Figure 1).

The ankle joint is a hinge joint. This joint plays a major role in dorsiflexion and plantar flexion. The ankle joint is composed of the three bones: fibula (calf bone), tibia (shin bone), and talus (ankle bone). The tibia and fibula form the ankle mortise which consists of the medial and lateral malleoli [20] . In the distal end of the ankle mortise sits the trochlea tali, the upper surface of the talus. This allows the articular surfaces to glide upon each other and assures the cartilage surfaces to move freely. The ankle joint is bound by the strong deltoid ligament and three lateral ligaments: the anterior talofibular ligament, the posterior talofibular ligament, and the calcaneofibular ligament.

The bony anatomy of the subtalar joint (SJ) is less complex as it basically consists of two bones-talus and calcaneus. This joint plays major role in the inversion and eversion motion. The main ligament of the joint is interosseous ligament between talus and calcaneus. It runs through the sinus tarsi, a canal between the articulations of the two bones. The other ligaments that form weaker connections between talus and calcaneus are anterior talocalcaneal, posterior talocalcaneal, medial and lateral talocalcaneal ligaments.

a) Ankle and Subtalar joints (Ankle Anatomy [21])

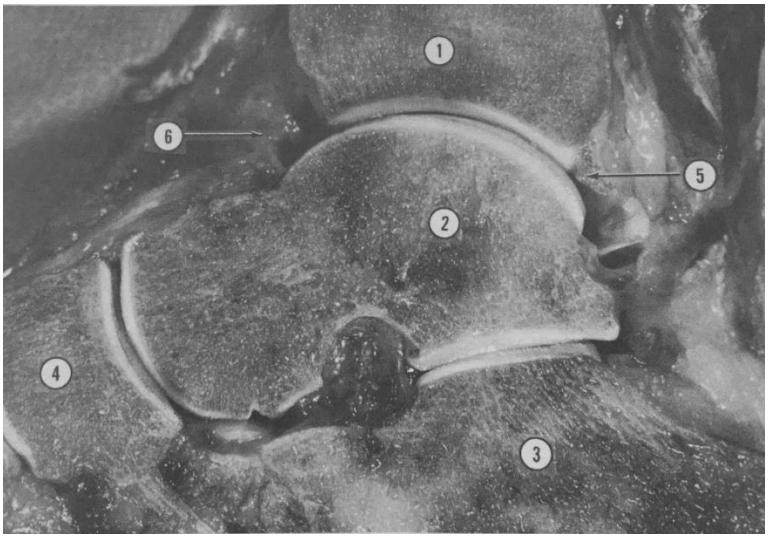

b) Sagittal cross-section of Ankle (1, tibia; 2, talus; 3, calcaneus; 4, navicular; 5, deep component of tibiofibular ligament forming a labrum; 6, anterior adipose body with large anterior joint cavity) (Sarrafian, 1993 [3])

Figure 1. Ankle joint anatomy

Variations in Morphology of Bones in Ankle Joint

Distal Tibia

The lower end of the tibia is formed by five surfaces: inferior, anterior, posterior, lateral and medial surface (Figure 2). The inferior surface articulates with the trochlear surface of the talus. The lateral border of the tibia is larger than the medial and the anterior border is longer that the posterior. Geometrically, this surface is a section of a frustum of a cone with an average medial conical angle of $22^{o}\pm4^{o}$ ranging from 0^{o} to 35^{o} [3].

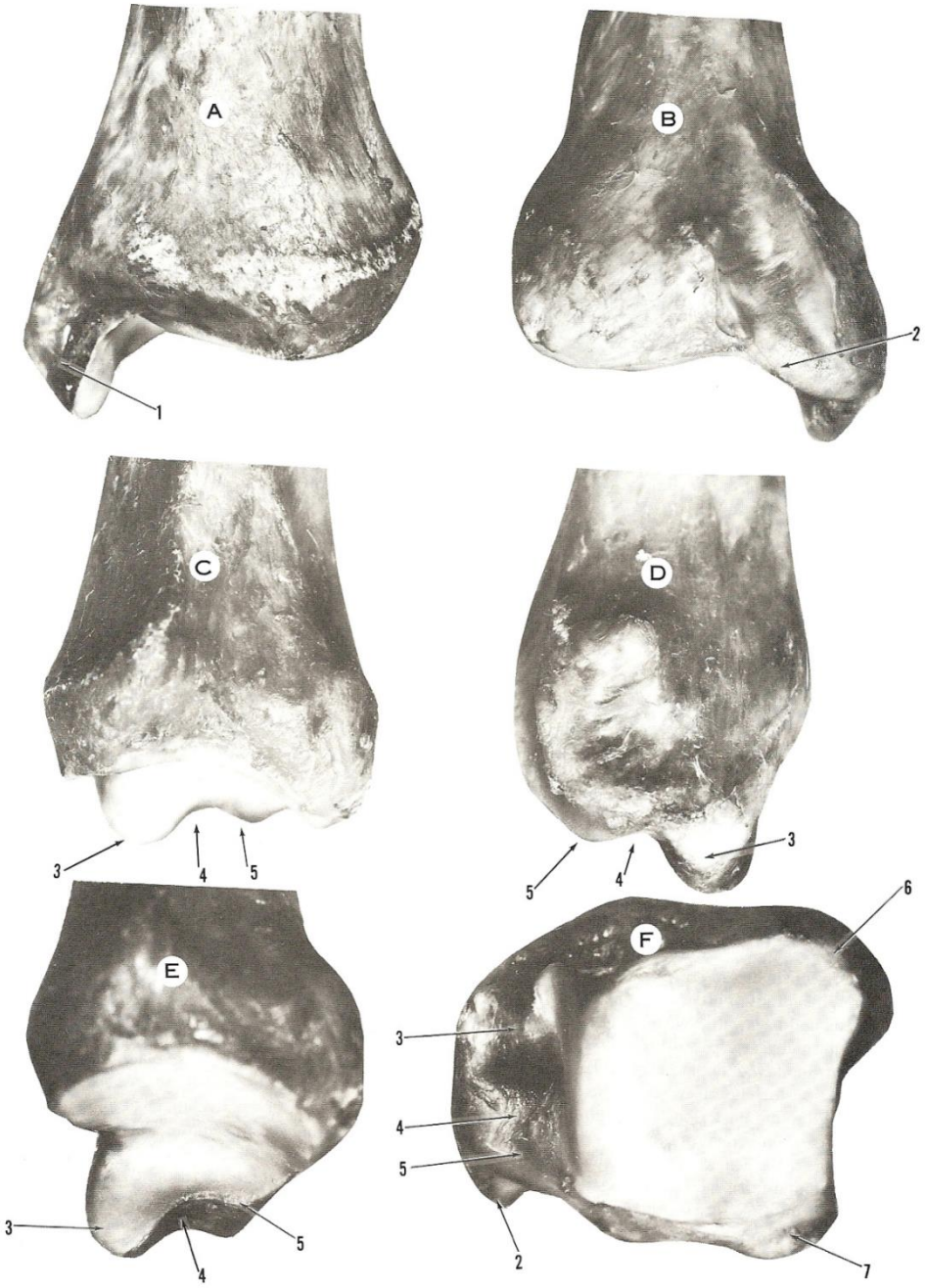

Figure 2. Tibia-General features

A) Anterior aspect of left distal tibia. (B) Posterior aspect of distal tibia. (C) Lateral aspect of distal tibia. (D) Medial aspect of distal tibia. (E) Lateral aspect of medial malleolus. (F) Inferior view of distal tibia. 1, medial malleolus; 2, sulcus for tibialis posterior tendon; 3, anterior colliculus; 4, intercolliculus groove; 5, posterior colliculus; 6, anterior tibial tubercle; 7, posterior tibial tubercle (Sarrafian, 1993 [3]).

In any position of talus, the tibial plafound covers only two-thirds of the talar surface. With the long axis of tibia, the tibial plafound makes an angle of 93.3 degrees ±3.2 degrees.

Talus

Talus is the intercalated bone located between the ankle bimalleolar fork and the tarsus. The superior face forms the ankle joint, or tibiotalar joint, with the tibia plafond and lateral mallelous of the fibula. The inferior face forms the subtalar joint with the calcaneus. The talus is divided into three distinct regions: the body, the neck, and the head [3] (Figure 3).

The body of the talus has five surfaces: superior, lateral, medial, posterior, and inferior. The superior or trochlear surface of the talus is pulley shaped and articulates with distal surface of tibia. The lateral segment of the surface is wider than the medial. The medial border is straight and the lateral border is oblique, so the trochlear surface is wedge shaped and narrower posteriorly.

The length and width of the talus was measured for 100 dry tali. The average length (L) was 48mm, with a maximum of 60mm and a minimum of 40mm. The average width (W) was 37mm with a maximum of 45mm and a minimum of 30 mm [3] (Figure 4).

The body and the neck of the talus are not coaxial. In the horizontal plane, the neck shifts medially and makes an angle of declination with the long axis of the trochlea tali. In sagittal plane, the neck is deviated downward relative to the talar body and makes an angle of inclination (Figure 5).

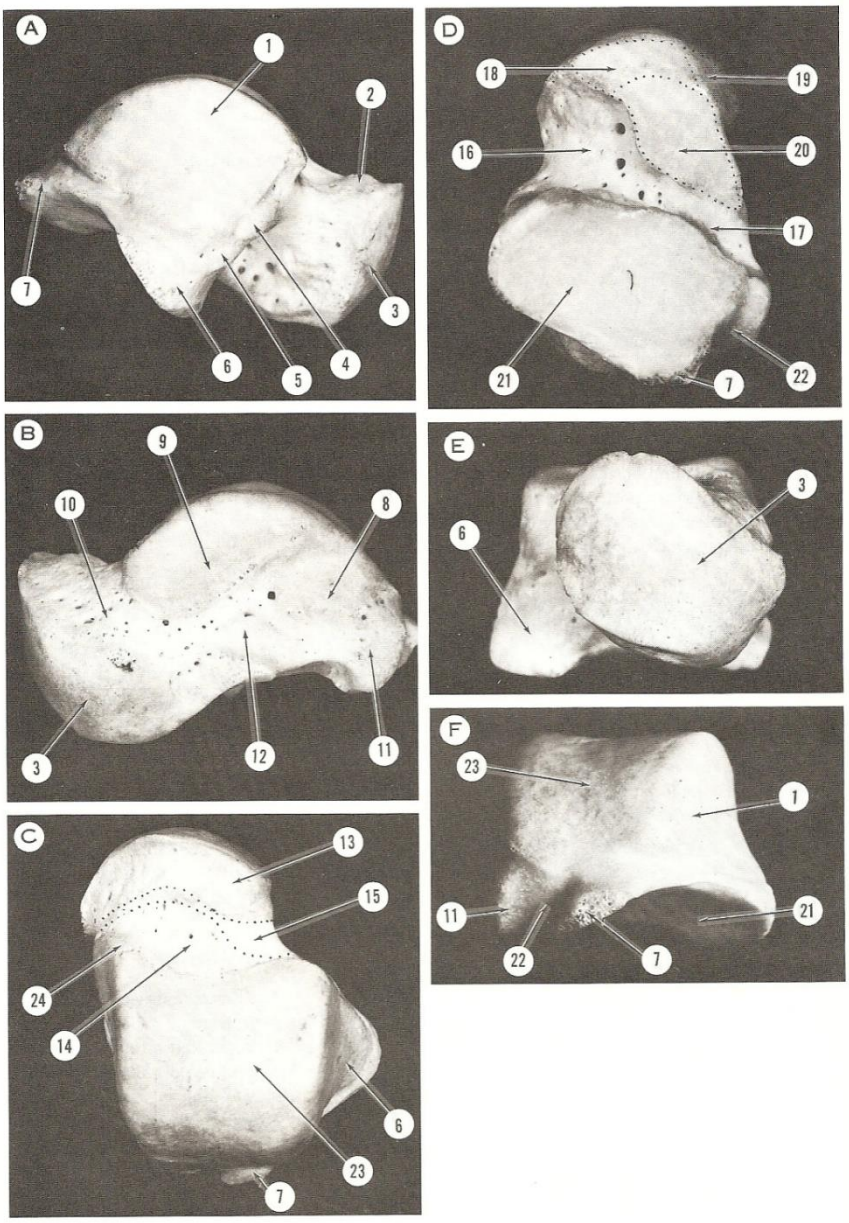

Figure 3. Talus- General features.

A) Lateral aspect. (B) Medial aspect. (C) Superior aspect. (D) Inferior aspect. (E) Anterior aspect. (F) Posterior aspect. (1, articular surface - facies malleolus lateralis; 2, cervical collar; 3, articular surface - facies articularis navicularis; 4, 5, tubercles for insertions of anterior talofibular ligaments; 6, lateral process; 7, posterolateral tubercle; 8, oval surface for insertion of talotibial component of deltoid ligament; 9, articular surface - facies malleolaris medialis; 10, talar neck; 11, posteromedial tubercle; 12, tubercle of insertion of deltoid ligament; 13, segment of talar neck located within talonavicular joint; 14, segment of talar neck located within talotibial joint; 15, extra-articular segment of talar neck where a bursa may be found against which glides medial root of inferior extensor retinaculum; 16, sinus tarsi; 17, canalis tarsi; 18, anterior calcaneal articular surface of the talar head; 19, articular segment of talar head corresponding to superomedial and inferior calcaneonavicular ligaments; 20, middle calcaneal articular surface of talar neck; 21, posterior calcaneal articular surface of the talar body; 22, canal of the flexor hallucis longus tendon; 23, trochlear surface; 24, anteromedial extension of trochlear)(Sarrafian, 1993[3]).

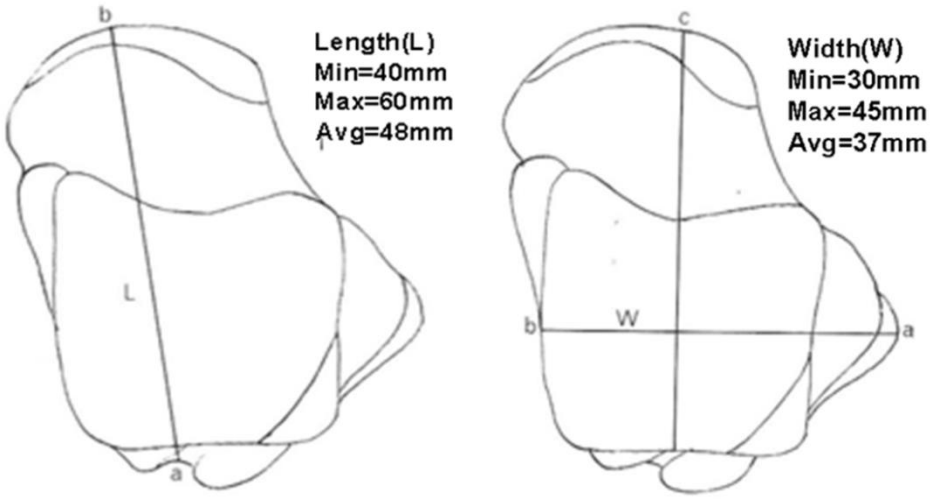

Figure 4. Length and Width of talus (Sarrafian, 1993 [3], modified).

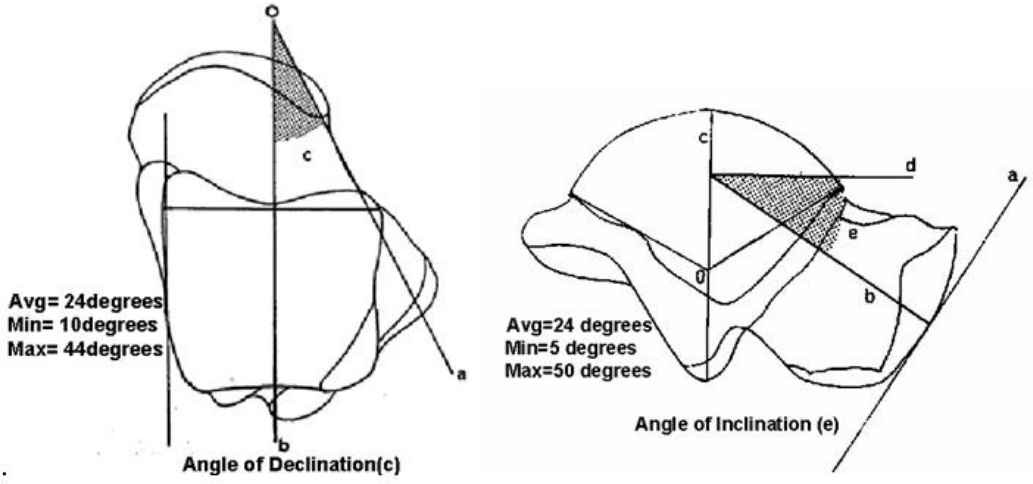

Figure 5. Angle of Declination (c) and Angle of Inclination (e) Angle of Talar neck relative to the body. (Sarrafian, 1993 [3], modified)

The morphology of the trochlear surface resembles to a frustum of a cone whose apex is directed medially and whose apical angle varies considerably from individual to

individual, 24 degrees ± 6 degrees with a range of 0 degrees to 38 degrees [22] (Figure 6). According to Inman's assumption the axis of rotation of talus within the mortise is a fixed axis, which is the intermalleolar axis. Later, It has been shown by many researchers [8, 10, 23-25] that the axis of rotation of the talus within the mortise is not about a fixed axis, rather it rotates about a variable axis in all three planes (dorsi-plantar flexion, inversion-eversion, and internal-external rotation) (Figure 7).

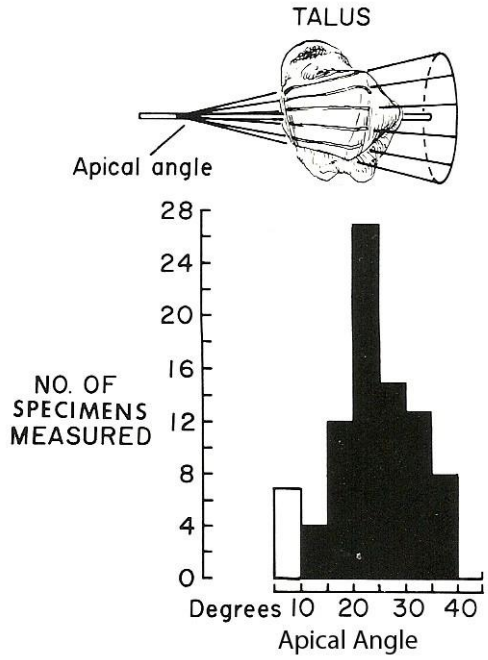

Figure 6. Trochlea of talus-variations in apical angles of conical surfaces (Inman, 1991[22])

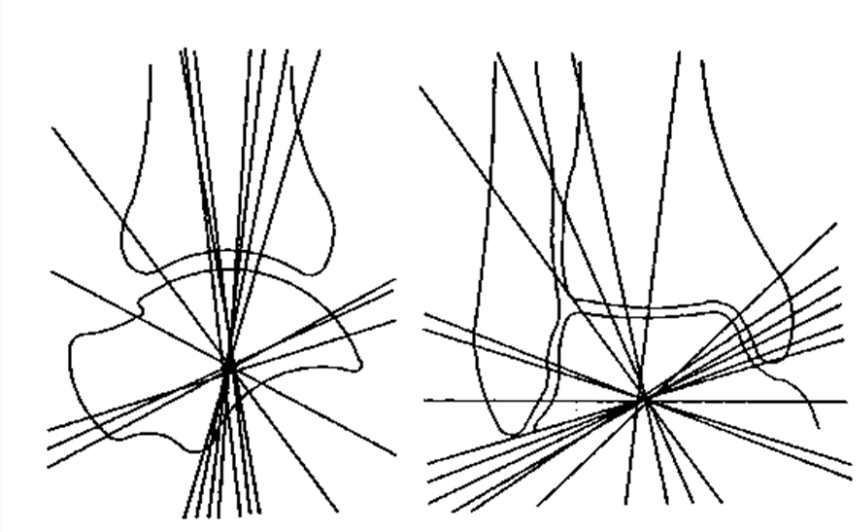

Figure 7. Variable axis of rotation of Ankle joint.
Coronal and Sagittal projections of Plantar-Dorsiflexion, Pronation-Supination, and Medial-Lateral rotation axes (Lundberg, 1989[10])

The inferior surface of the talus generally has three articular facets: anterior, medial, and posterior. However, many variations of the articular facets have been observed Figure 8). The common configuration of articular surface is having four distinct surfaces as shown in Figure 8A. In other instances, two surfaces fuse through a direct anterior extension from the posterior calcaneal surface.

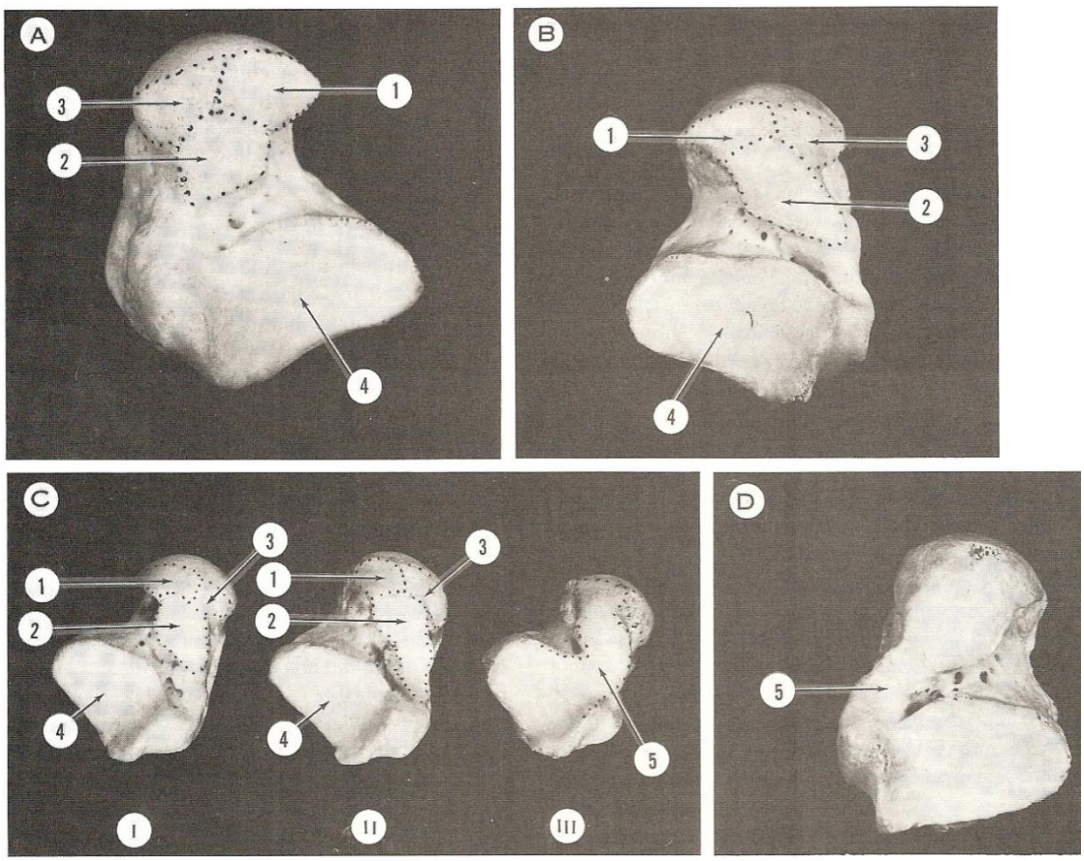

Figure 8. Talus- Variations of the inferior articular surfaces
(A) Common configuration of the articular surfaces. (B) Posterior extension of the middle calcaneal surface. (C) (I) moderate posterior extension of middle calcaneal surface. (II) Marked posterior extension of middle calcaneal surface. (III) Fusion (5) of all articular surfaces, obliterating the tarsal canal and a segment of the sinus tarsi. (D) Fusion (5) of the middle and posterior calcaneal surfaces on the medial aspect of the tarsal canal, which is still maintained. (1, anterior calcaneal articular surface of the talar head; 2, middle calcaneal articular surface of talar neck; 3, articular segment of talar head corresponding to superomedial and inferior calcaneonavicular ligament; 4, posterior calcaneal articular surface of talar body) (Sarrafian, 1993[3]).

Calcaneous

The calcaneus, also called the heel bone, is a large bone that forms the foundation of the rear part of the foot. The calcaneus connects with the talus and cuboid bones. The connection between the talus and calcaneus forms the subtalar joint. Figure 9 shows that the lateral, medial, superior, inferior and anterior surfaces of calcaneous.

The calcaneus has several functional morphological features that vary from subject to subject such as: configuration of the anterior, middle, and posterior articulating facets, inclination of the posterior articular surface, and inclination and size of the sustentaculum tali.

The length, width, height and inclination angle of the calcaneus vary between subjects (Figure 10 and Figure 11). In a study with 50 calcanei, the average length (L) is 75 mm with a minimum of 48 mm and a maximum of 98 mm. The average width (W) is 40 mm with a minimum of 26 mm and a maximum of 53 mm. The average height (H), approximately 50% of the length, is 40 mm with a minimum of 33 mm and a maximum of 47 mm [3]. The average value of inclination angle of the posterior calcaneal surface is 65 degrees (min=55 degrees, max=75 degrees).

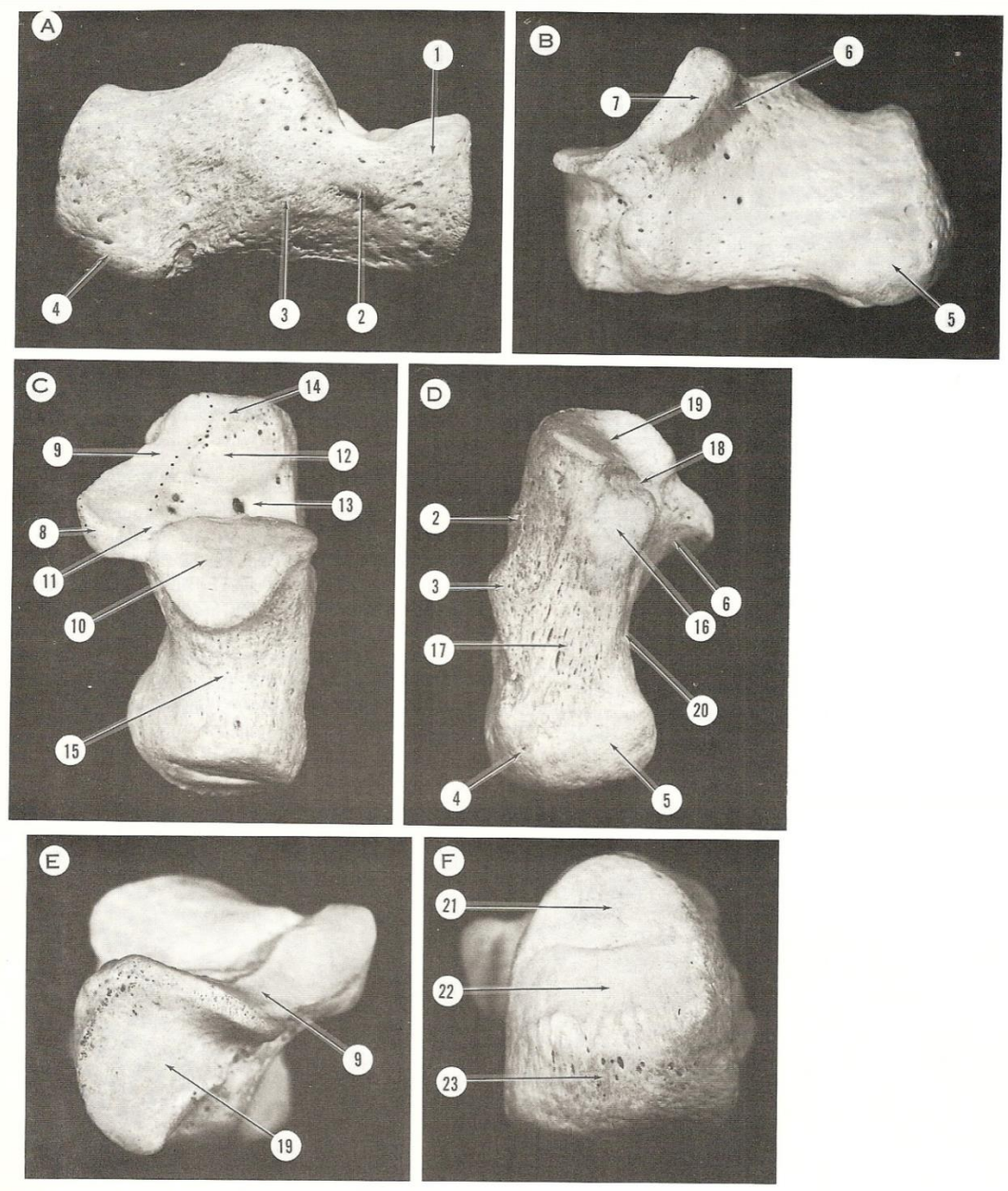

Figure 9. Calcaneus-General features
(A) Lateral surface. (B) Medial Surface. (C) Superior surface. (D) Inferior surface. (E) Anterior surface. (F) Posterior surface. (1, great apophysis; 2, trochlear process; 3, eminentia retrotrochlearis; 4, lateral tuberosity; 5, medial tuberosity; 6, canal for flexor hallucis longus tendon; 7, medial surface of sustentaculum tali; 8, posterior border of sustentaculum tali; 9, fused anterior and middle talar articular surfaces; 10, posterior talar articular surface; 11, canalis tarsi; 12, sinus tarsi - bony eminence; 13, sinus tarsi - fossa calcanei; 14, sinus tarsi - insertion surface of bifurcate ligament; 15, posterior third of superior surface; 16, anterior tuberosity of inferior surface; 17, longitudinally striated inferior surface; 18, coronoid fossa; 19, cuboidal articular surface; 20, medial calcaneal canal; 21, upper third of posterior surface, corresponding to pre-Achilles bursa; 22, 23, middle and lower thirds of posterior surface, corresponding to insertion of Achilles tendon) (Sarrafian, 1993[3]).

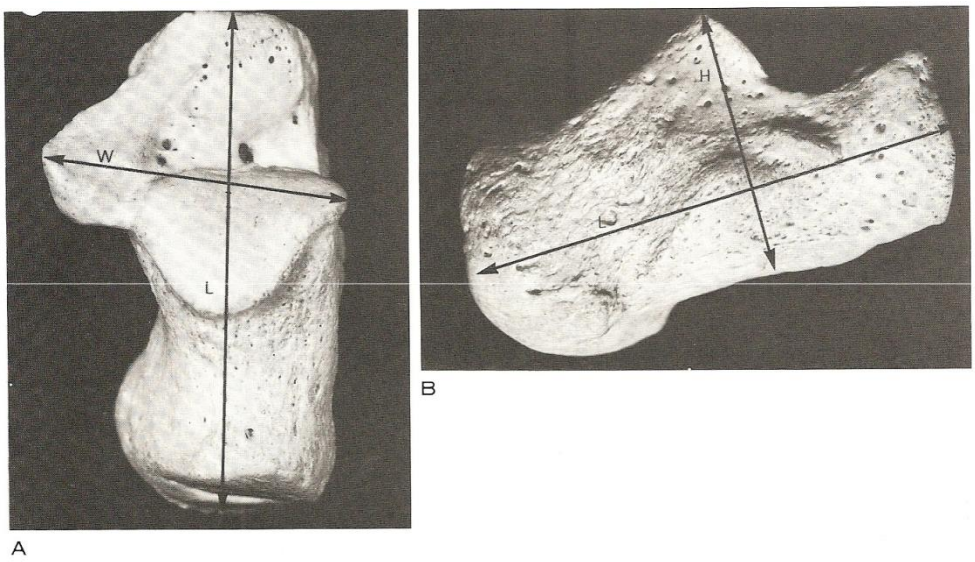

Figure 10. Length and Width of calcaneus
(A) Superior View. (B) Lateral View. (L, length; W, width; H, height) (Sarrafian, 1993[3])

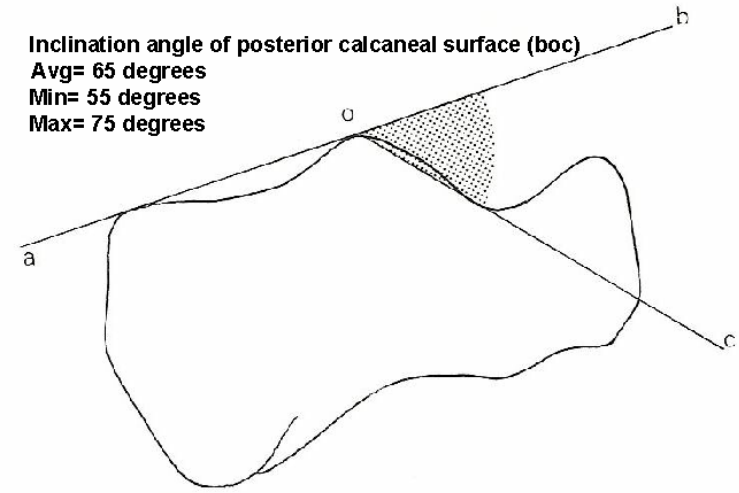

Figure 11. Inclination angle of the posterior calcaneal surface (Sarrafian, 1993[3]).

Variations in the articular facets of the calcaneus have been described by many authors [1, 26-28]. Bunning and Barnett [26] concluded that the Calcanei are classifiable into three types according to the number of superior articular facets present. In type A, the anterior and middle surfaces are separate, in type B the anterior and middle facets are

confluent and in type C calcanei the anterior, middle and posterior facets are united into a single facet (Figure 12).

This morphological variability of the calcaneal facets could result from differences in gait or other habit influencing these articular areas post-natally or it could be indicative of genetically determined variations. Sarrafian divided these into few more categories Figure 13).

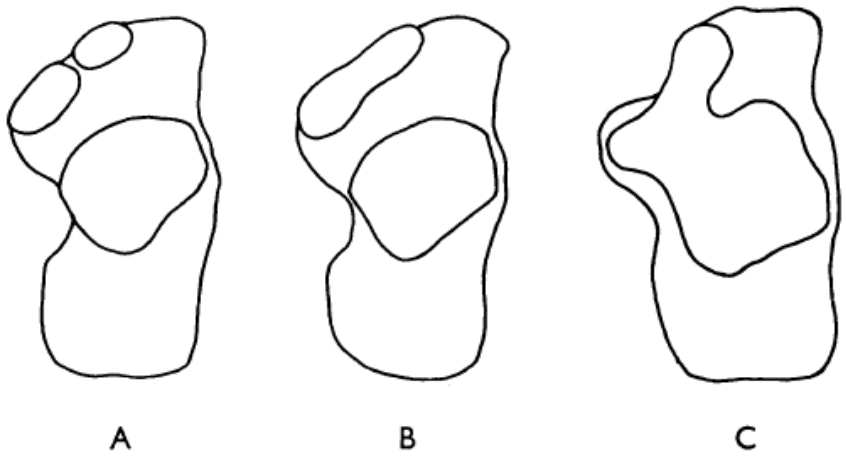

Figure 12. The three types of calcaneus (Bunning, 1965[26]).

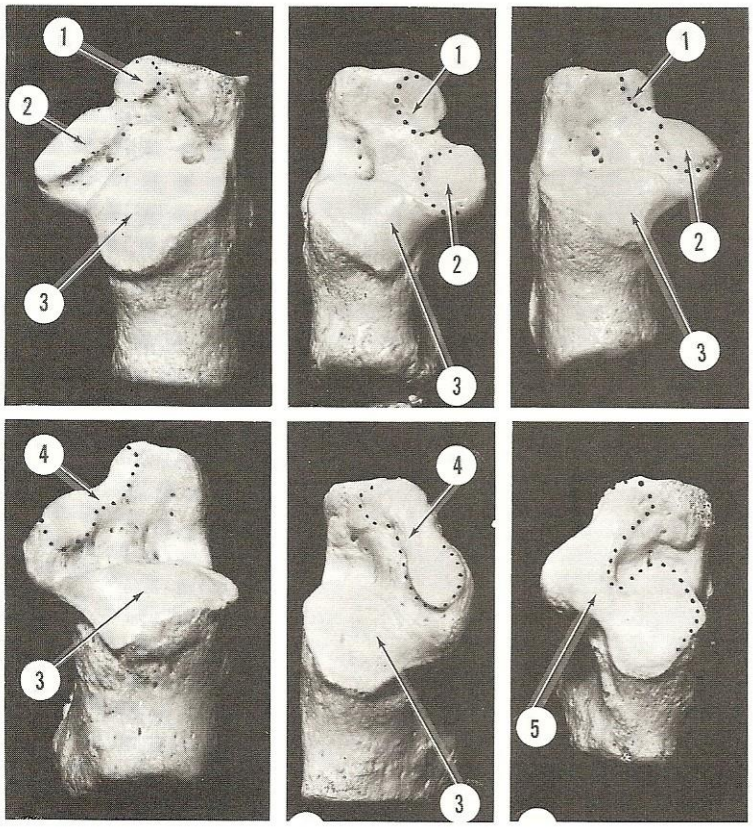

Figure 13. Variations of the articular surface of calcaneus
1, anterior talar articular surface; 2, middle talar articular surface; 3, posterior talar articular surface; 4, fused anterior and middle talar articular surfaces; 5, fused anterior, middle, and posterior talar articular surfaces (Sarrafian, 1993[3]).

The frequencies of occurrence of variations in Calcanei by various authors into these three classes are shown in the Figure 14.

Author	Number of Calcanei	Occurrence (%)		
		Type A	Type B	Type C
Laidlaw*†	750	32	69	
Bunning and Barnet‡	Veddah 10	0	60	40
	African 492	36	63	1
	British 194	67	33	0
	Indian 78	22	78	0
Present series	50	34	64	2
Padmanabhan	Indian 272	35	65	

* Laidlaw reports complete absence of the anterior facet in 0.9%.
† Laidlaw PP: The os calcis, part II. J Anat Physiol 33:168, 1905
‡ Bunning PSC, Barnett CH: A comparison of adult and foetal talocalcaneal

Figure 14. Frequency of occurrence of variations in calcanei (Sarrafian, 1993[3]).

Sustentaculum Tali

The Sustentaculum tali is a bracket like projection, triangular with a posterior base and an anterior apex. This surface projects anteromedially and is inclined downward and anteriorly at an average angle of 46^{o} (maximum 60^{o}, minimum 30^{o}) (Figure 15) [3].

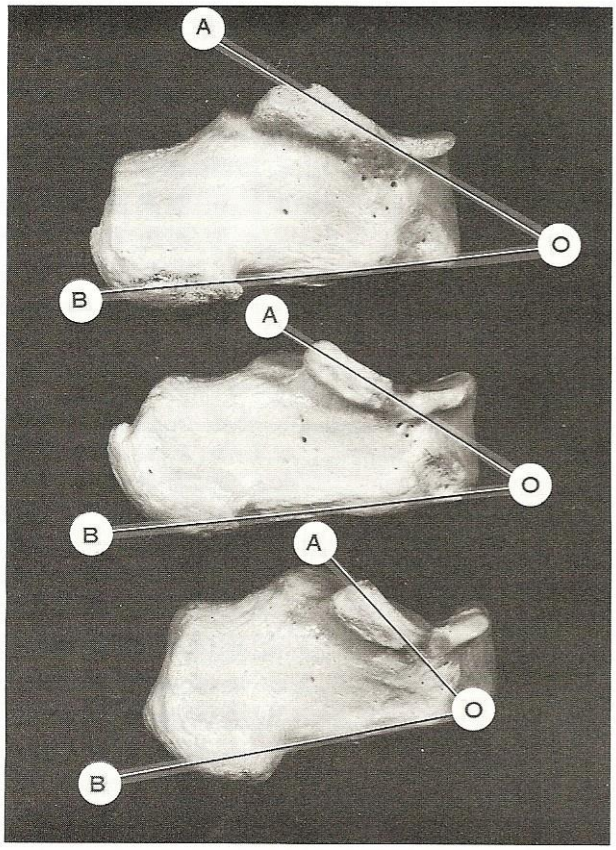

Figure 15. Variable inclination of sustentaculum tali (AOB) (Sarrafian, 1993**[3]).**

The width and length of sustentaculum tali are variable. The width of the sustentaculum tali was on an average of 13mm (maximum 18mm, minimum 8mm). The ratio of the sustentacular width to total width of os calcis at the same level is on average 0.33 (maximum 0.47, minimum 0.23) [3]. These values may be correlated with the supportive function of the sustentaculum tali relative to the talar head. Incompetent sustentaculum tali may fall into a group with minimum value or lower. The sustentaculum tali can also be classified as long or short. A long sustentaculum is continuous through its border with the processus anterior, which is then in association with a fusion of the facies articularis media and anterior. A short sustentaculum ends suddenly anteriorly and a notch separates the two articular surfaces (Figure 13).

Variations in Orientation of Ligaments

The ankle joint complex is stabilized by various ligaments. The ankle joint, is composed of the tibio-talar articulation. It is stabilized laterally by the anterior talo-fibular ligament (ATFL) and the calcaneofibular ligament (CFL) medially by the deltoid ligament, and posteriorly by the robust posterior talofibular ligament (PTFL). The ATFL lies within the capsular layers but is a distinct structure. The CFL crosses both ankle and subtalar joints. All of the ligaments of the ankle joint complex vary in structure, insertion, orientation, and size from subject to subject. Of particular interest to this study is the calcaneofibular ligament of the lateral collateral ligament and their susceptibility to inversion injuries. Inversion injuries to the ankle are among the most common problems in musculoskeletal care, representing 10% of all visits to the emergency room [29, 30]. The incidence of inversion ankle injuries is reported as one in 10,000 people per day. Up to 20% of patients sustaining an inversion injury to the ankle will experience persistent symptoms such as functional instability, recurrent sprains or chronic pain [31].

Calcaneofibular Ligament

The calcaneofibular ligament (CFL) is a cordlike oval ligament 20 mm to 30 mm in length and 3 mm to 8 mm in diameter [3, 32] (Figure 16).

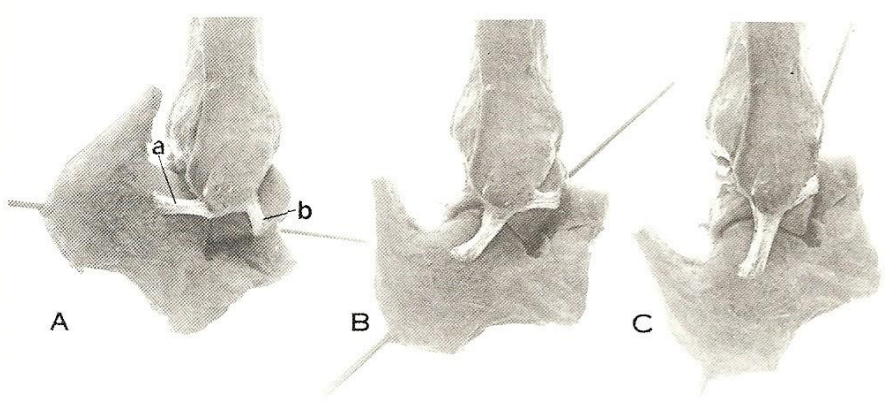

Figure 16. Calcaneofibular ligament
(A) Plantarflexion; (B) Neutral; (C) Dorsiflexion. (a, calcaneofibular ligament; b, anterior talofibular ligament.) (Inman, 1991[22]).

CFL runs from the tip of the lateral malleolus of the fibula downward and slightly backward to a tubercle on the lateral surface of the calcaneus. The location of the calcaneal insertion is variable. In a study of 750 calcanei, the typical location in neutral position (Figure 16) occurs in 64.5%; anterior location, 25.5%; posterior location, 5.5%; downward location, 4.5% [33]. The variable insertions result in variable obliquity of the ligament orientation relative to the long axis of the fibula [3]. In a study based on 30 dissected specimens and observing 55 ankles during surgery, the angle between the CFL and the long axis of fibula varied in different subjects-74.66% has orientation of 10^{o} to 45^{o}; 18.66% has orientation of 0^{o}; 45 subjects has 80^{o} to 90^{o} orientation; 2.66% are fanshaped [5] (Figure 17).

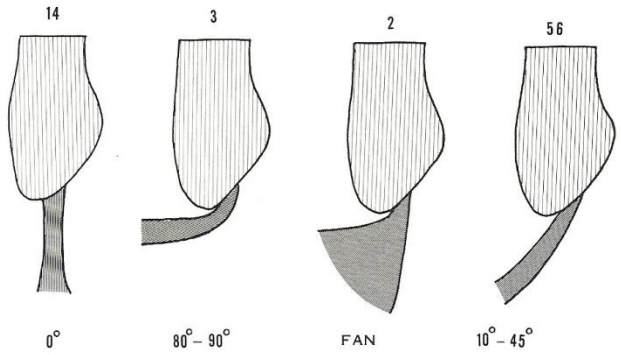

Figure 17. Calcaneofibular ligament - variable orientation (Sarrafian, 1993[3]).

Variations in Mechanics

The passive kinematic properties of the ankle are the result of a complex interaction between bony articular morphology and ligament constraints. These properties are reported to be variable among individuals. The basic patterns of motion however, are primarily determined by the geometric features of the articulating surfaces of the talus, and of the tibia and fibula, i.e. the trochlear surface and the tibial/fibular mortise.

Terminology of the Motion

The main motions at ankle joint complex are Dorsiflexion-Plantarflexion, Inversion-Eversion, Internal-External rotations. The motion about intermalleolar axis (Z axis)is the Dorsi-Plantar flexion, the motion about long axis of tibia (Y axis) is the Internal-External Rotations, the motion perpendicular to the Z and Y axis is Inversion-Eversion motion about X axis (Figure 18).

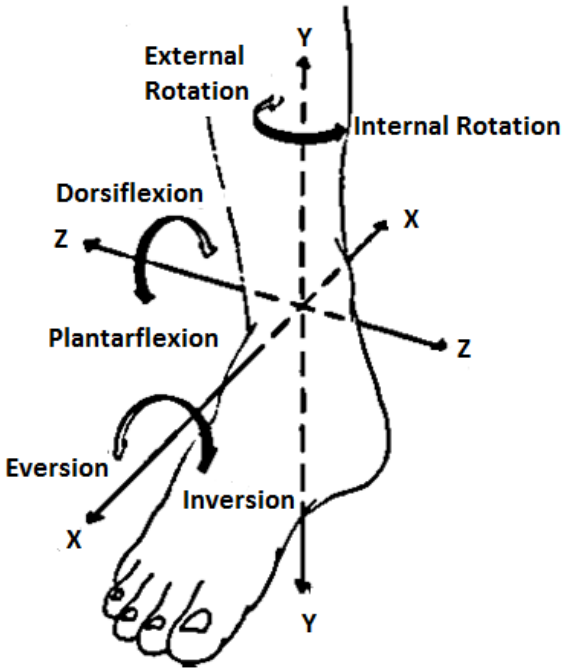

Figure 18. Axes of motion of the Ankle joint (Sarrafian, 1993[3],modified)

Table 1 Range of Motion – Dorsi / Plantarflexion

Dorsiflexion (deg)	Plantarflexion (deg)	References
20-25	35-40	[34]
21.9-27.9	21-36	[7]
20.75-27.25	36.6-45.24	[8]

Table 2. Range of Motion – Internal / External

Internal(deg)	External(deg)	References
22-36	16-28	[8]

Table 3. Range of Motion - Inversion / Eversion

Inversion (deg)	Eversion (deg)	References
12.5-19.5	11.42-20.32	[8]
18-20	10-14	[34]
30	20	[3]

Ankle joint Motion

Dorsiflexion and plantar flexion are the major components of the motion at the talocrural joint. The ROM of normal ankle joint is 10.2 degrees dorsiflexion (min=6 degrees to max=16 degrees) and 14.2 degrees plantarflexion (min=13 degrees, max=17 degrees) [35], 5-6 degrees external rotation [36, 37], 8.2 degrees (standard deviation =0.5 degree), 13.8 degrees inversion (standard deviation=1 degree), 5 degrees inversion (standard deviation = 0.6 degrees) [37].

The ankle joint is considered initially as a one-degrees of freedom joint with a fixed axis of rotation [38]. Later several studies [8, 39] concluded that the axis of rotation of the talus within the mortise is not about a fixed axis, rather, it rotates about a variable axis in all three planes (dorsi-plantar flexion, inversion-eversion and internal–external rotation) (Figure 19).

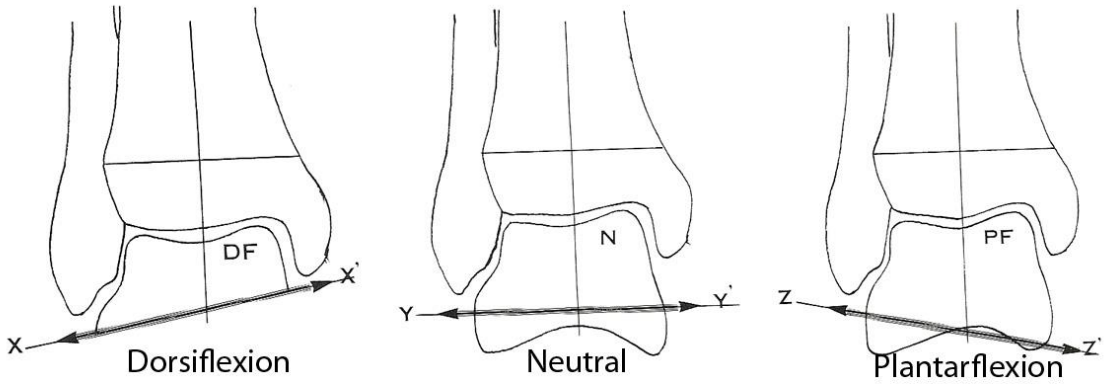

Figure 19. Ankle joint- multiple axis of rotation (Sarrafian, 1993[3]).

Subtalar joint Motion

The axis of subtalar joint is oblique, oriented upward, anteriorly and medially [40, 41]. The motion of subtalar joint can be studied by vectorising the motion into three components: longitudinal, vertical and transverse. Later the motion at subtalar joint is studied by describing the motion as that of a screw [41]. The subtalar motion is variable. In inversion motion the ROM is 25 degrees to 30 degrees and in eversion the ROM in 5 to 10 degrees [3].

Ankle Joint Coordinate System

Ankle joint complex is composed of talocrural and the subtalar joints. The coordinate system for these joined is defined considering the motions of the respective bones.

Ankle Joint (Talocrural Joint): The articulation formed between the talus and the tibia/fibula.

Subtalar Joint (Talocalcaneal Joint): The articulation between the talus and the calcaneus.

Ankle Joint Complex: The combination of ankle joint and subtalar joint.

The major motions about an anatomical joint coordinate system are rotations; plantarflexion / dorsiflexion, inversion / eversion, and internal / external rotation. Plantar/Dorsiflexion is about the Intermalleolar axis (Z), internal/external motion is about the line coincident with the long axis of tibia-fibula (Y) and the inversion/eversion is about the common perpendicular to Z and Y axis [42].

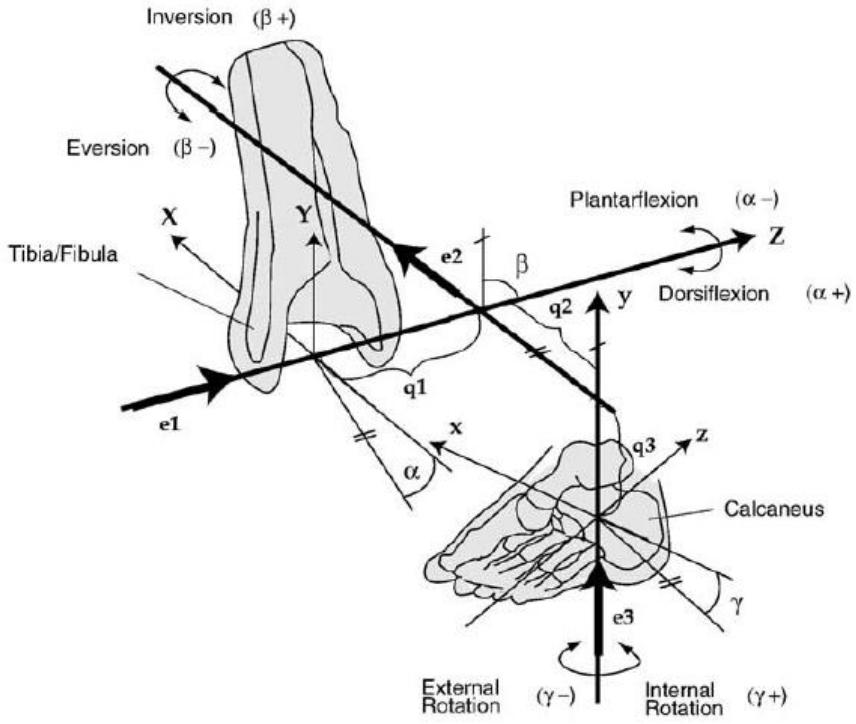

Figure 20. Joint Coordinate System of Ankle Joint Complex
α–dorsiflexion/plantarflexion, β-inversion/eversion, γ-internal/external, q1-medial/lateralshift, q2-anterior/posterior drawer, q3-compression/distraction (Wu, 2002[42]).

Effect of morphology on Ankle Joint motion

Initially the motion of the ankle joint is studied by approximating the surface of talus to cylinder. Later Inman [22] proposed that the trochlea of the talus is rarely a section of cylinder but is a section of a frustum of a cone whose apex is directed medially whose

apical angle varies from individual to individual. This concept is relied on assumption that the talocrural joint as a one-degree freedom joint with a fixed axis of rotation. Later several studies concluded that the axis of rotation of the talus within the mortise is not about a fixed axis, rather, it rotates about a variable axis in all three planes (dorsi-plantar flexion, inversion-eversion and internal–external rotation).

The motion of ankle joint depends mainly on the surface of talus. From dorsiflexion to plantarflexion at the ankle joint, the articulating surfaces of the talus and malleoli remain in contact. Due to the conical contour of trochlea as defined by Inman[22], Plantar flexion of the talus induces a functional varus or supination [43]. Barnett and Napier [23] correlated the wedge contour of the talus to internal rotation. During plantar flexion the medial surface of talus has tendency to separate from medial malleolar surface which is neutralized by the internal rotation produced due to the wedge surface of talus trochlea.

Effect of Morphology on Subtalar Joint motion

The axis of subtalar joint is oblique, oriented upward, anteriorly and medially.[22, 41]. The motion components at the subtalar joint can be determined from a simple vectorial analysis of the subtalar joint axis components, which are longitudinal, vertical and transverse. The greater longitudinal component generates supination-pronation motion, the vertical component generates abduction-adduction, and the lesser transverse component generates flexion-extension. Later, Manter [41] described the motion a the subtalar joint as screw motion. The motion at the subtalar joint is guided by the contour of the articular surfaces, their orientation, and the intrinsic and extrinsic ligaments. The

posterior calcaneal surface may be considered as a male ovoid surface and the posterior talar articular surface as female ovoid. A male ovoid surface moving on a female ovoid surface slides, rolls and spins (Figure 21). The rolling is in a direction opposite to sliding. A female ovoid surface moving on a male ovoid surface slide rolls and spins (Figure 22). The rolling is in the motion of sliding. A convex male surface oriented transversely will generate only the motion of flexion-extension, where as a surface oriented longitudinally will generate only the motion of supination-pronation. The degree of orientation of the articular surfaces affects the amplitude of the motion components. The posterior calcaneal surface has an inclination angle with an average of 65 degrees (min=55 degrees, max=75 degrees). A larger inclination angle provides more flexion component to the motion. The posterior talar articulating surface has declination angle with average 37 degrees (min=26 degrees, max=50 degrees). A greater declination angle orients the surface in a longitudinal direction that will increase the flexion-extension component, whereas a smaller declination angle orients the surface more transversely and increases the supination-pronation component.

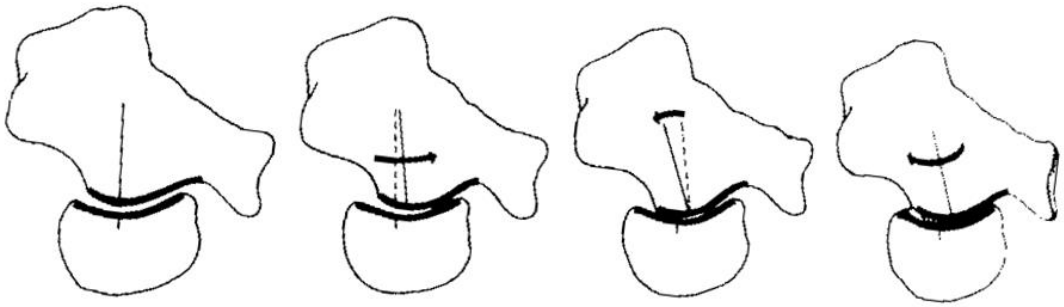

Figure 21. Subtalar joint motion- A male ovoid surface moving on a female ovoid surface (Sarrafian, 1993[3]).

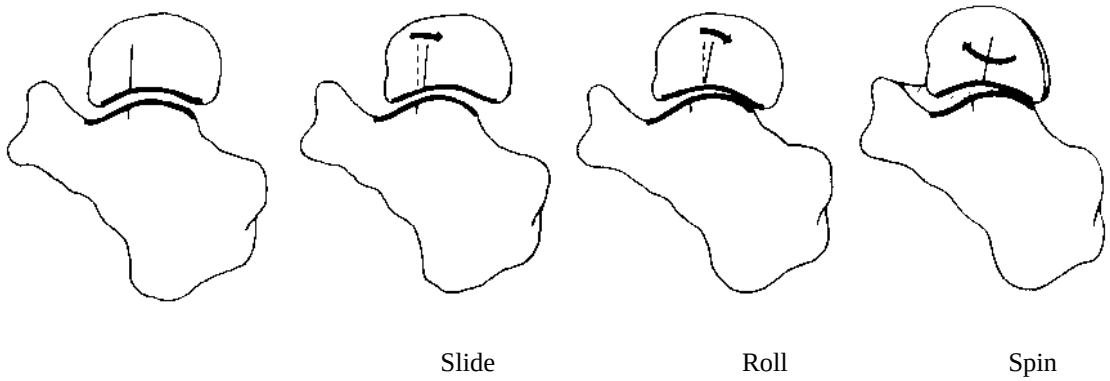

Figure 22. Subtalar joint motion - A female ovoid surface moving on a male ovoid surface (Sarrafian, 1993[3]).

Effect of Ligament Orientation on Mechanics:

The tension in CFL ligament is reported to be variable. In some subjects this ligament is tensed in dorsiflexion and relaxed in plantarflexion. However, in other subjects the effect is reversed or no change in tension [3]. This variability in tension in CFL may be explained due to the variability in the insertion sites of the ligament [3, 5].

Hip Joint Morphology

Hip joint is a ball and socket joint at the junction of pelvis and leg. The rounded head of femur forms the ball which fits in the cup shaped socket called acetabulum (Figure 23).

The joint is stabilized due to the ball and socket joint fit, strong ligaments gives additional stability for the joint. The femoral head comprises nearly two-thirds of a sphere, whereas the mating acetabulum forms a hemisphere of the same diameter. The cartilaginous surfaces of the femur and the acetabulum are not perfectly conforming, in that the femoral head corresponds more to a conchoids than a sphere. This permits the hip

joint to undergo movement in an assortment of motion axes that allow flexion-extension, abduction-adduction, and internal-external rotation [44]. The femoral head and acetabulum are covered by a cartilage. The thickness of cartilage varies between 1.15 mm and 1.46 mm [45]. The acetabular rim is covered by labrum with variable thickness from 2-3 mm [46]. The labrum is wider and thinner in the anterior region and thicker in the posterior region. The hip labrum has many functions, including shock absorption, joint lubrication, pressure distribution, and aiding in stability, with damage to the labrum associated with osteoarthritis.

Figure 23. Hip joint anatomy (Hip Anatomy[47]).

Variations in Morphology of Hip Joint- Effect on Joint function

Ideal hip joint is a ball and socket joint. Any changes in the morphology affecting the sphericity of joint may limit the range of motion causing cartilage wear and tear and leading to osteoarthritis of the joint. Dysplasia and Femoroacetabular impingement are two pathological conditions that are caused due to abnormal morphology of hip joint. In this study the effect of variations in the morphology of the hip joint on Femoroacetabular interference pattern is being studied.

Femoroacetabular Impingement (FAI)

Femoro-Acetabular Impingement (FAI) is defined as the interference between the femoral head-neck junction and the acetabular rim often leading to osteoarthritis [48-50]. Previous studies [48, 49, 51] have suggested that the early interference at the hip joint and FAI are due to abnormal morphology of hip joint having non-spherical femur and or excessive acetabular coverage can restrict range of motion and leading to pathological conditions such as Femoroacetabular Impingement (FAI), dysplasia etc. In a study with more than 600 surgical dislocations and after damage pattern inspection, Ganz et al [48] proposed that FAI as a mechanism for the development of early osteoarthritis for most non dysplastic hip joints. Surgical treatment of the femoroacetabular impingement focuses on improving the clearance for hip motion.

Physical Examination

Examination of the hip often reveals limitation of motion particularly the internal rotation and adduction in flexion. This test is done with the patient supine, the hip is rotated internally as it is flexed passively to approximately 90 degree and adducted (Figure 24) [48]. Forceful additional internal rotation induces shearing forces at the labrum and creating a sharp pain when there is a chondral lesion, a labral lesion, or both [48].

Figure 24. Femoro Acetabular Impingement-Clinical assessment.
90 degrees flexion with adduction and internal rotation (Tannast, 2007[2]).

Radiographic Assessment

The next step in FAI assessment is taking an orthograde AP radiographs with patient in standing position. Careful observation of these radiographs reveal bony prominence in the anterolateral head and neck junction, reduced offset of the femoral head-neck junction and changes on the acetabular rim such as double line that is seen with rim ossification. Magnetic Resonance Image data are very sensitive and specific for detecting non spherical femoral head, labral and chondral lesions.

Types of FAI

Depending on the pattern and various stages of chondral and labral injuries FAI is distinguished into three types (Figure 25).

1. CAM FAI: Cam FAI is caused by abnormal femoral head with increasing radius against the acetabular rim during hip flexion leading to chondral abrasion and labral detachment.
2. Pincer FAI: This type of impingement occurs because extra bone extends out over the normal rim of the acetabulum. The labrum can be crushed under the prominent rim of the acetabulum.
3. Mixed type: Most patients (86%) have a combination of both forms of impingement, which is called “mixed pincer and cam impingement,” with only a minority (14%) having the pure femoroacetabular impingement forms of either cam or pincer impingement [49].

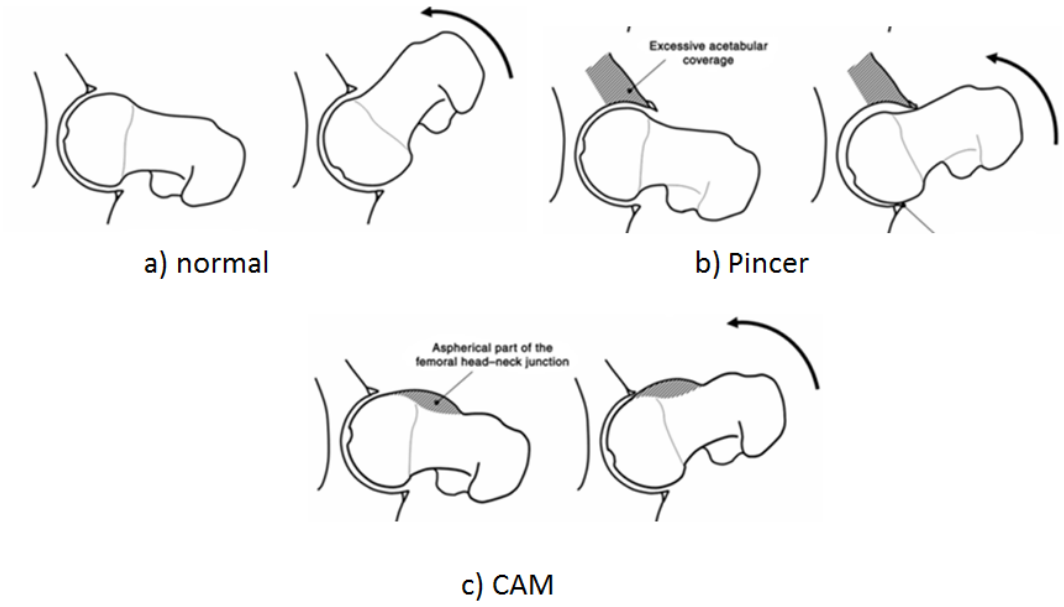

Figure 25. Types of Femoroacetabular Impingement.
a) Normal hip joint with sufficient joint clearance for unrestricted range of motion. b) Pincer impingement, with excessive acetabular over coverage. c) CAM impingement, with aspherical femoral head near femoral head-neck junction (Tannast, 2007[2]).

FAI Surgery

Surgical treatment for treating CAM impingement comprise of mainly removing any non-spherical portion of the head, thereby improving the neck offset and subsequent clearance. This process is called femoral neck osteoplasty. Pincer impingement is treated by reducing the anterior over coverage bony prominence at the acetabular rim [48].

Post-surgical results

In both open and arthroscopic surgical techniques FAI surgery success depends on complete restoration of head-neck offset and elimination of pain in the joint in extreme range of motion. Failure to completely address the bony impingement lesions of the hip is the most common reason for unsuccessful hip arthroscopy and subsequent revision surgery [52-54]. On the other hand, over resection may lead to hip instability, dysplasia, and dislocation [54, 55]. Phillip et al, [52] studied hip revisions on 37 hips. In this study, 36 of 37 patients had radiographic evidence of impingement that was either unaddressed or inadequately addressed at the time of index procedure and concluded that 13% of hip arthroscopies performed at this major referral center were revision arthroscopies for persistent impingement. In another study, Heyworth et al, [53] reviewed 24 revision hip arthroscopy cases performed in 23 patients. In 13 of 24 cases (54%), patients had no significant improvement at any point after the primary hip arthroscopy. Unaddressed or undertreated bony impingement lesions were found in 19 of 24 cases (79%) and concluded that Failure to address bony impingement lesions of the hip and a tight psoas tendon are key factors in unsuccessful hip arthroscopy and may require revision surgery and failure of labral repairs may be the result of unrecognized bony impingement at the time of initial surgery.

The post-surgical revisions suggests that there might be other parameters that other morphological abnormalities, in addition to the ones addressed by the surgery may be contributing to the early interference conditions.

Previous studies [12, 56] used computer 3D models of hip to study the kinematics of hip joint in presence of FAI. Similar approach is followed in this model based study to

evaluate the effect of variations in a number of morphological parameters of the proximal femur and the acetabulum on patterns of interference at the hip are investigated using a computerized 3D model of hip joint.

Hip Joint Mechanics

The major motions about hip joint anatomical joint coordinate system are rotations flexion/extension, abduction/adduction and internal/external rotations. Flexion/extension is about the line joining Anterior superior iliac spine (ASIS) points (Z), internal/external motion is about the line coincident with the long axis of tibia-fibula (Y) and the abduction/adduction is about the common perpendicular to Z and Y axis (Figure 26) [42].

Hip joint flexion varied from 90 to 150 degrees (mean 120 degrees), extension from 0 to 35 degrees (mean 9.5 degrees), abduction from 15 to 55 degrees (mean 38.5 degrees), adduction from 15 to 45 degrees (mean 30.5 degrees), internal rotation from 20 to 50 degrees (mean 32.5 degrees), and external rotation from 10 to 55 degrees (mean 33.6 degrees) [9, 57].

The hip joint plays a significant role in the human osteoarticular system, both in terms of locomotion and as a load-bearing joint for the torso by transmitting weight to different areas of the pelvis. During normal activities, the peak value of the joint force averages 2.1 to 5.5 body weight (BW), and they may reach values in excess of 8 BW during accidental stumbling [58].

There were studies in the past which describes the relation between the change in the morphology on interference pattern showing that the joints with FAI have restricted range

of motion [12, 49]. In a computer model based study Bedi et al[12], described that the surgical treatment improves hip joint kinematics. Similar technique is used in this model based study to find the relationship between the morphological parameters of the hip joint such as femoral neck-shaft angle, alpha angle, femoral anteversion and pistol grip deformity on the interference pattern of hip joint.

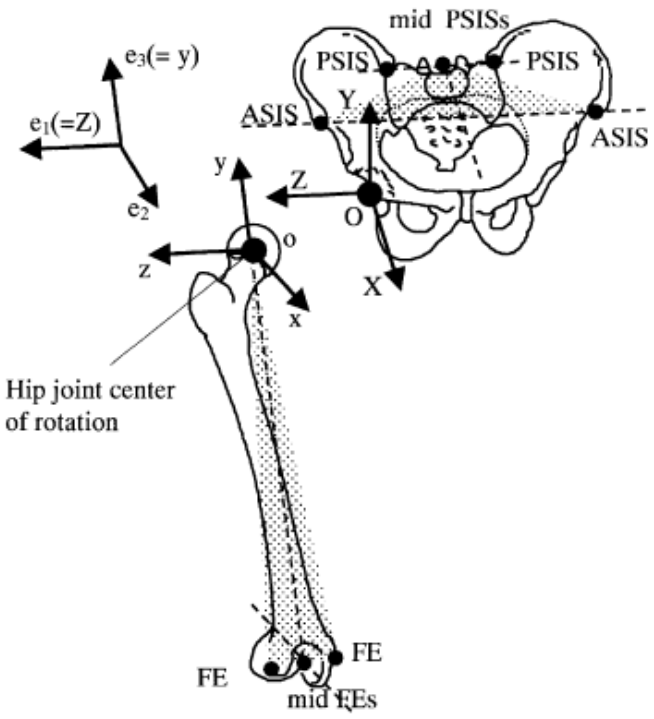

Figure 26. Joint Coordinate System of hip joint (Wu, 2002[42]).

Determining Center of hip Joint:

The normal human hip joint is treated as a ball and socket joint, with the center of rotation defined as the center of hip joint. The location of the hip center of rotation has been estimated using either a ‘‘functional’’ approach [59, 60] or a ‘‘prediction’’ approach

[61-63]. The prediction approach uses regression equations (REs) with the independent variables describing the geometry of the pelvis. This approach uses external bone reference according to which they determine the position of the center of rotation, using a series of empirical equations.

In the functional approach the hip joint center is calculated as the center of the best sphere described by the trajectory of markers placed on the thigh during several trials of hip rotations.[64].

In this study, the center of rotation hip joint is determined as the average of the centers of spheres fitting the femur and acetabulum.

Hip Morphological Parameters

The morphological parameters such as femoral neck-shaft angle, CEA angle, extrusion index, femoral anteversion/retroversion, alpha angle, neck offset angle, pistol grip deformity are considered as crucial parameters for femoroacetabular impingement [49, 51].

Femoral neck-shaft angle

The angle between femoral neck and femoral shaft in the sagittal plane is Femoral-neck-shaft angle. The normal range of femoral neck-shaft angle is 126^{o}-139^{o} [65, 66]. Femoral neck-shaft angle less than 125^{o} is defined as coxavara [51] and neck-shaft angle greater than 140^{o} is defined as coxavalga [66, 67] (Figure 27). It was found that coxavara has been recognized as a cause of cam impingement [51]. The normal neck-neck-shaft angle produces the lowest stress on the femoral neck and acetabulum because of the orientation

of an optimal lever arm that produces a mechanical advantage for biomechanical function [66].

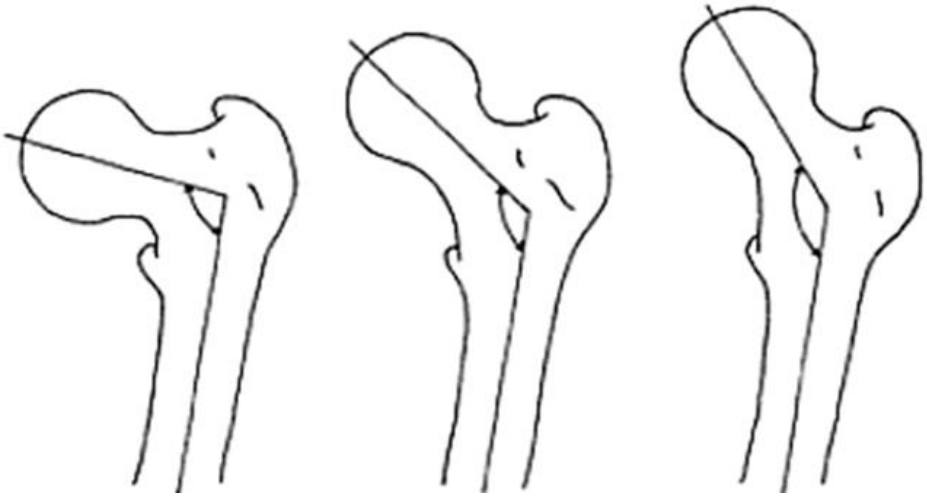

a) Coxavara (<125º) b) Normal (126º-139º) c) Coxavalga (>140º)

Figure 27. Variations in femoral Neck-Shaft angle (Hammer, 2007[68]).

Through years the conditions coxavara and coxavalga have been corrected surgically by following intertrochanteric osteotomy [69, 70]. In this procedure a wedge is cut near the femoral neck region and the femoral head is aligned on the cut plane of femoral shaft (Figure 28).

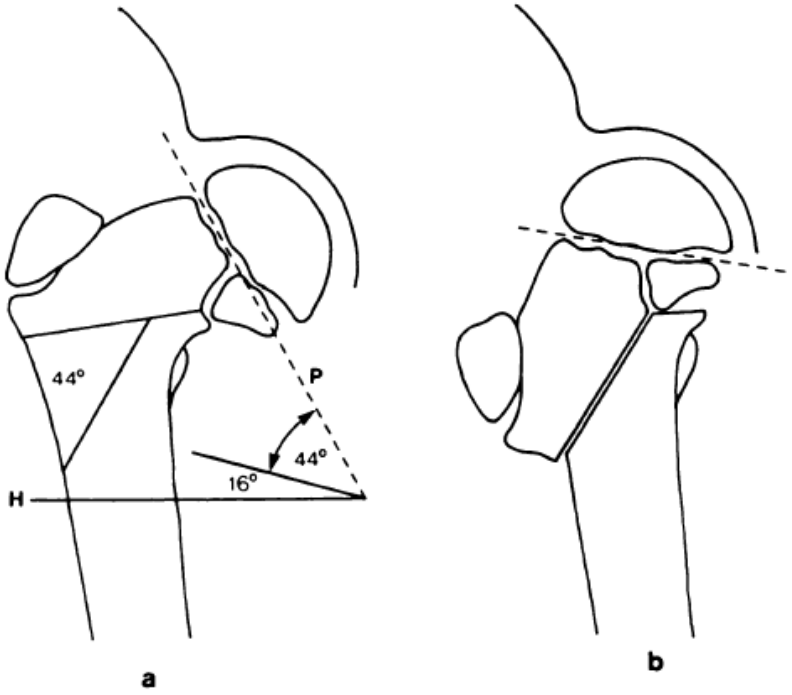

Figure 28 Intertrochanteric Osteotomy of femur (Cordes, 1991[70]).
Pre-operative planning to correct coxavara (a) tracing of the pre-operative radiograph, P represents the plane of the growth plate, H is a horizontal line drawn several centimeters below the lesser trochanter. A 44° closing wedge osteotomy is required to correct the inclination of the growth plate to 16° b) after the osteotomy the triangular metaphyseal fragment and the displaced femoral head are supported by the calcar femorale.

Femoral Anteversion or Angle of Torsion

Femoral neck anteversion is defined as the angle between an imaginary transverse line that runs medially to laterally through the knee joint and an imaginary transverse line passing through the center of the femoral head and neck. The normal value of femoral anteversion is 15 degrees-20 degrees (Cibulka, 2004).

Femur is said to have excessive or increased femoral anterversion if angle of anteversion is greater than 20 degrees and if the anteversion angle is less than 15 degrees the

condition is femoral retroversion (Figure 29). The condition femoral retroversion has been recognized as a cause for cam impingement.

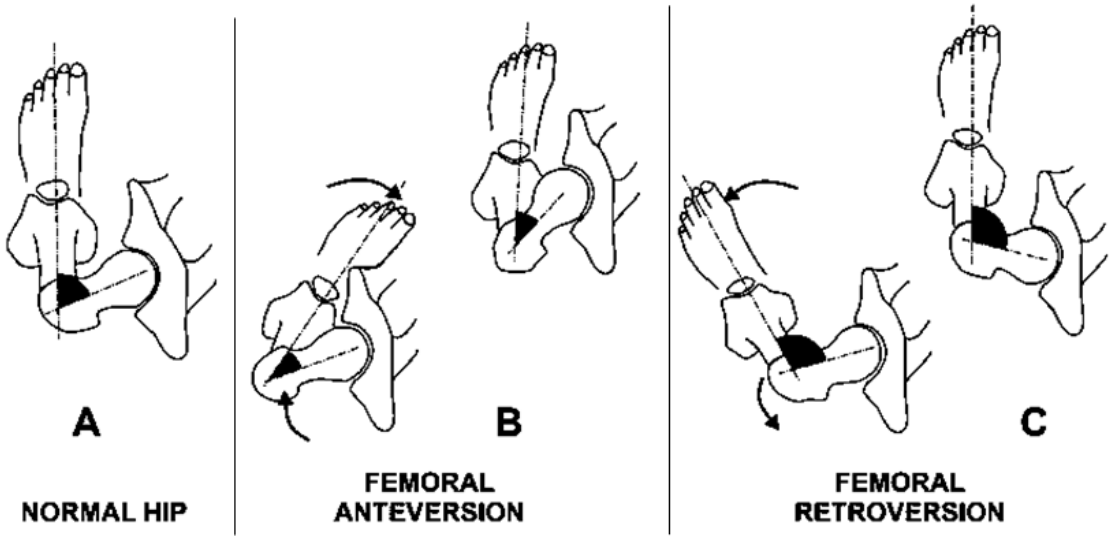

Figure 29. A) Normal hip B) Excessive Femoral Anteversion C) Femoral Retroversion (Clippinger, 2007[71]).

In order to correct femoral retroversion and excessive anteversion the surgical process derotational osteotomy is followed in which the femoral shaft is cut and rotated till the anteversion angle falls to normal range and fixed at that position with plates and screws (Figure 30)[72].

a) After performing the osteotomy, the femur is rotated to achieve the desired correction.
b) The osteotomy is then stabilized with an intramedullary nail to maintain the correction while the bone heals.

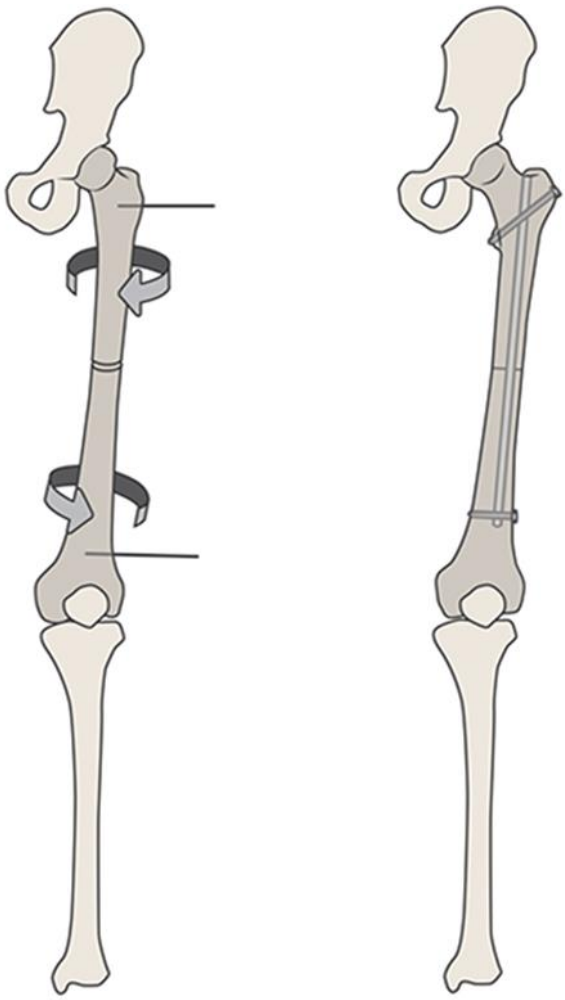

a) b)

Figure 30. Femoral Derotation Osteotomy-technique to correct femoral retroversion (Osteotomy [73]).

Pistol Grip deformity

The pistol grip deformity is considered as a radiographic sign of cam impingement [48, 51, 74]. In this deformity the shape of proximal femur resembles a flintlock pistol (Figure 31). The femoral head neck off set is decreased in the superior femoral neck at the head-neck junction.

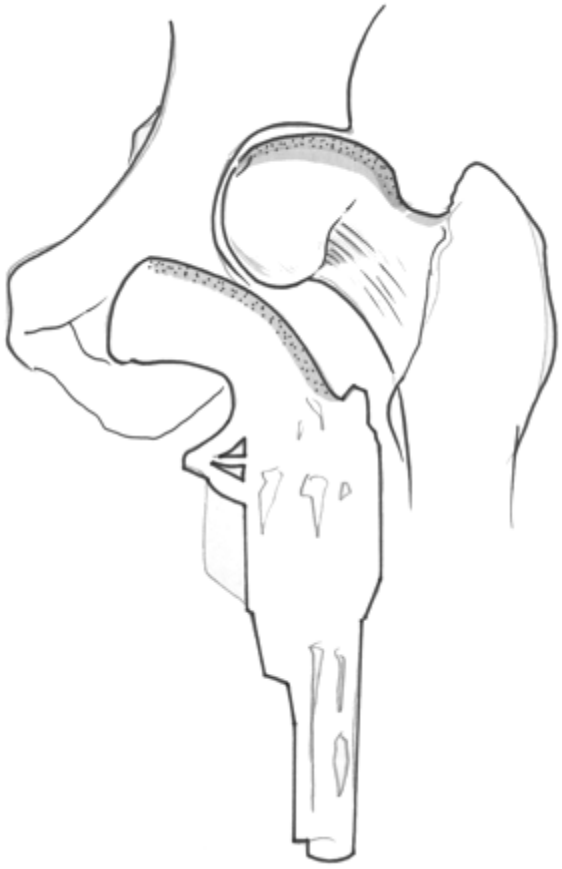

Figure 31. Pistol Grip Deformity of hip joint (Reid, 2010[75]).

CHAPTER 3: METHODOLOGY

The following two methods are followed to discuss the morphology–mechanics relationship in ankle and hip joints.

1. *Model Development:* Develop image-based, subject-specific, three-dimensional numerical models of the ankle and of the hip joints to provide the means of exploring the causal relationship between morphology and mechanical behavior.
2. *Effect of Morphology on Passive Mechanical Properties:* Using the numerical models, perform dynamic simulations following systematic variations in morphology

METHODOLOGY PART 1: MODEL DEVELOPMENT

Image-based, subject-specific, three-dimensional numerical models of the ankle and the hip joints are developed to explore the relationship between morphology and mechanical behavior. Specifically, such models will provide the means to explore the effect of bone morphology and location of insertion sites of ligaments on the kinematics and passive structural characteristics of the ankle and hip joints.

Ankle Joint

Step 1: Image Processing

Six models of the ankle joint complex are developed from magnetic resonance image data obtained with a 1.5 Tesla commercial General Electric Signa magnetic resonance

image scanner from six non-pathological un-embalmed cadaveric legs (average age 71.5 years, 2 males and 4 females) with a spatial resolution of the spatial resolution is 0.35mm x 0.7mm x 2.1mm. These MR images are then processed using ANALYZE^{TM} software to produce 3D numerical models of the articulating bones and the regions of insertion of surrounding ligaments. The process involves segmenting the bones of interest (tibia, fibula, talus, and calcaneus) in each MR slice (Figure 32a) followed by 3D spatial filtering, 3D interpolation and rendering to create .stl files representing the 3D geometry of each bone (Figure 32b). In addition, the regions of insertion of ligaments are identified, marked and exported from the image processing software.

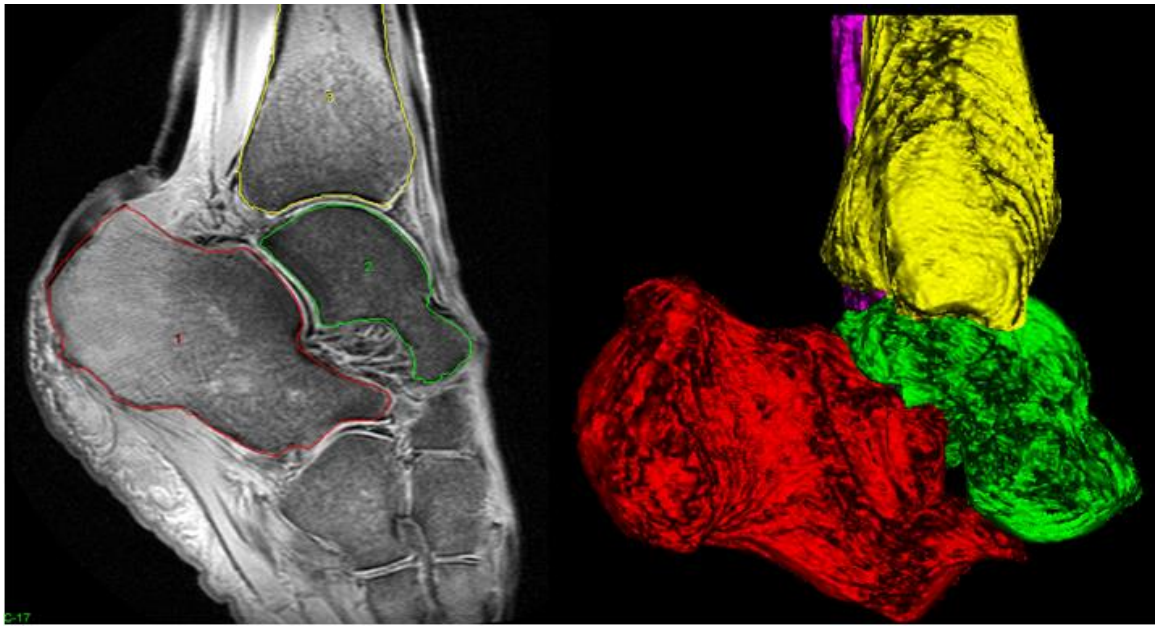

Figure 32. Image processing of ankle MRI
a) Example of the segmentation process used to obtain the contours of the bones in each 2-D slice(left), b) 3D model of bones after rending process(right)

Step 2: Post Processing

The rendered data obtained from Analyze™ is processed using Geomagic Studio 12™ to filter scanned artifacts, to fit the surface with polygons, to remove rough contours using a 3D smoothing algorithm (Figure 33). Decimate polygons option is used to reduce model size so that the resulting geometry can be efficiently handled by the dynamic simulation program (Figure 33). In addition, various morphological parameters of the bones and ligament insertion sites are measured at this stage and this information is later used in the development of the subject-specific dynamic simulation model.

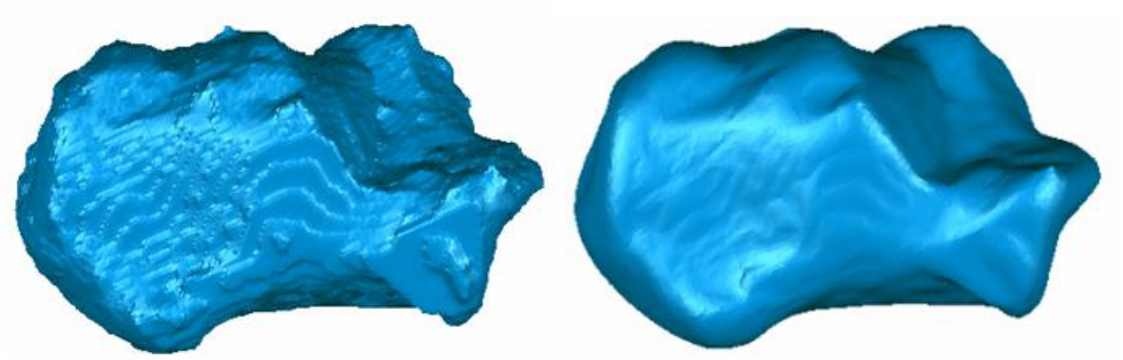

Before **After**

Figure 33. CAD surface before and after smoothing the surface

Step 3: Rigid Body Dynamic Model

Three dimensional bone morphology and ligament insertion sites are imported into a dynamic simulation software environment ADAMS™ (Figure 34). All the simulations were solved with ADAMS default integrator, GSTIFF [76] with step size of 0.01 and an integrator error 0.001. ADAMS uses a Newton-Raphson predictor-corrector numerical

algorithm to solve the dynamic equations based on the motion time history and current motion trajectory. The dynamic analysis involves developing and then integrating the non-linear ordinary differential equations [76, 77] (equation 1). Equation 2 describes the boindary conditions.

$$\boldsymbol{M\ddot{q} + \phi_q^T \lambda - A^T F(q, \dot{q}) = 0} \qquad \textbf{Equation 1}$$

$$\boldsymbol{\phi(q, t) = 0} \qquad \textbf{Equation 2}$$

M is the mass matrix of the system, q is the set of coordinates representing displacements, ϕ_q is the gradient of the constraints at any given state, F is the set of applied forces and gyroscopic terms of the inertia forces, and A^T is the matrix that projects the applied forces in the direction of q. ϕ is the set of configuration and applied motion constraints.

Equation 1 is a second order ordinary differential equation and equation 2 is an algebraic equation. The solution algorithm converts equation 1 and equation 2 to first order differential algebraic equations and then uses previously developed integrators, including the GSTIFF, I3, and S12 formulations, to solve the system of equations[76, 77].

Contact Properties

An Interference Detection Algorithm (RAPID^{TM}) [78] is used to establish contact between the bones where the properties of the contact are defined by the material properties of cartilage. The contact force between articular surfaces is defined as a non-linear function of penetration depth, x and penetration velocity, $\dot{x}$.

$$\boldsymbol{Force = kx^{e} + c_2\dot{x}} \qquad \textbf{Equation 3}$$

The values of *k*, *e* and c_2 in equation 3 are considered from the properties of articular cartilage [79-81]. These contact properties are explained in detail in Appendix A.

Ligament Properties

The material properties of each ligament element were described using a tension-only, non-linear load (*T*)–strain (ε) relationship:

$$\boldsymbol{T(\varepsilon) = A(e^{B\varepsilon} - 1) + c_1\dot{\varepsilon}} \qquad \textbf{Equation 4}$$

The constants *A*, *B* and damping coefficient c_1=1 N*s/mm, are obtained from literature [82] and detailed description is given in Appendix A. Table 4 shows the list of ligaments with nonlinear load-strain constants used in equation 4.

The ligaments of the AJC were represented with single or multiple line elements depending on their geometries (Figure 35). Cylindrical ligaments with relatively small diameter-to-length ratio such as the CFL were represented by a single element. Ligaments with relatively large diameter-to-length ratio, such as the PTTL were represented by multiple elements. This multi-element representation enabled the simulation of recruitment of different ligament fibers under different loading conditions.

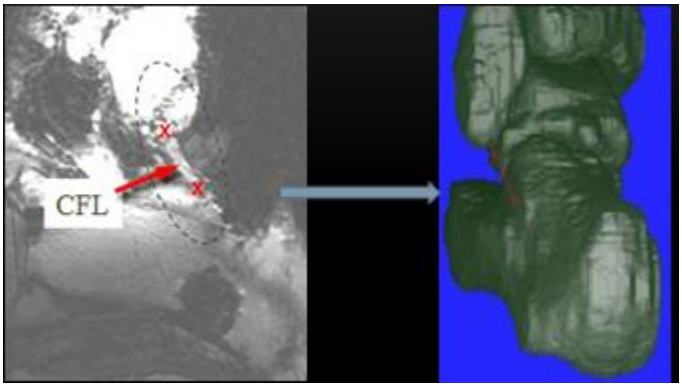

Figure 34. Procedure for identifying the ligaments from the MR images

Figure 35. 3D rendering in ADAMS showing the representation of the ligaments used in the model. The lateral collateral group consisting of three ligaments: the anterior talofibular ligament—ATFL, the calcaneofibular ligament—CFL, and the posterior talofibular ligament—PTFL (two elements). The medial collateral ligament group consists of three ligaments: the anterior tibio-talar ligament—ATTL, the tibio-calcaneal ligament—TCL (two elements), and the deep posterior tibio-talar ligament—PTTL (four elements). The subtalar group consists of two ligaments: the cervical ligament—CL (four elements), and the interosseos ligament—ITCL (10 elements).

Table 4. Ligament nonlinear load-strain properties

Group	Name of Ligament	Number of Elements	A	B
Lateral Collateral Ligament group	anterior talofibular ligament—ATFL	1	7.18	12.5
	calcaneofibular	1	0.20	49.63

	ligament—CFL			
	posterior talofibular ligament—PTFL	2	0.14	44.35
The medial collateral ligament group	the anterior tibio-talar ligament—ATTL	1	2.06	20.11
	the tibio-calcaneal ligament—TCL	2	0.51	45.99
	the deep posterior tibio-talar ligament—PTTL	4	1.34	28.65
Subtalar group	the cervical ligament—CL	4	0.0609	28.65
	the interosseos ligament—ITCL	10	0.261	28.65

Based on Grood and Suntay measures [83] calculated for the ankle joint coordinate system [8, 42]. Boundary conditions consisting of a fixed tibia-fibula and free calcaneus and talus are provided. The model is then loaded through cyclic moments corresponding to dorsiflexion/plantarflexion; inversion/eversion; internal rotation/external rotation. The output measures provide detailed description of the range of motion of ankle joint complex, kinematic coupling, and flexibility of the joint, the joint contact forces and their

locations on the bones and the forces and deformation of the surrounding ligaments. Figure 36 shows the dynamic model created in ADAMS-VIEW™ software. Figure 37 shows the flexibility characteristics of ankle joint complex.

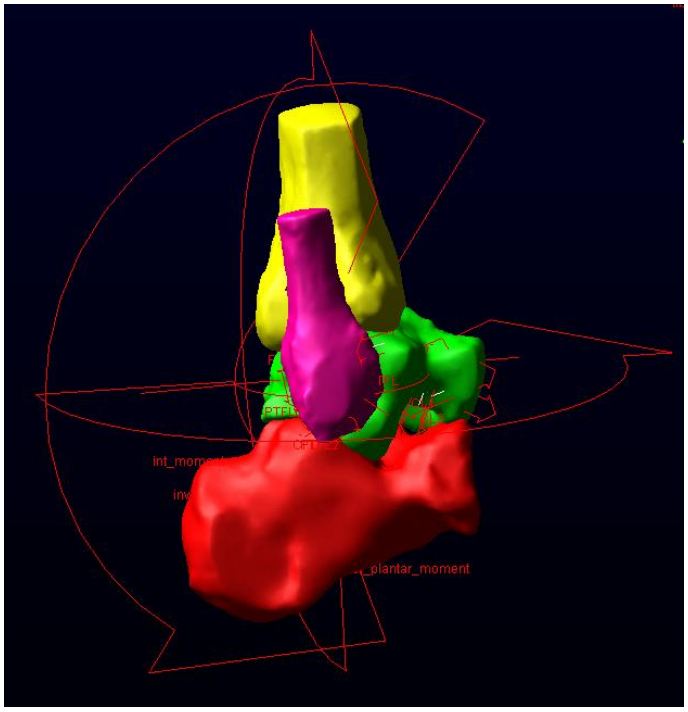

Figure 36. Dynamic model of ankle joint in ADAMS™ environment

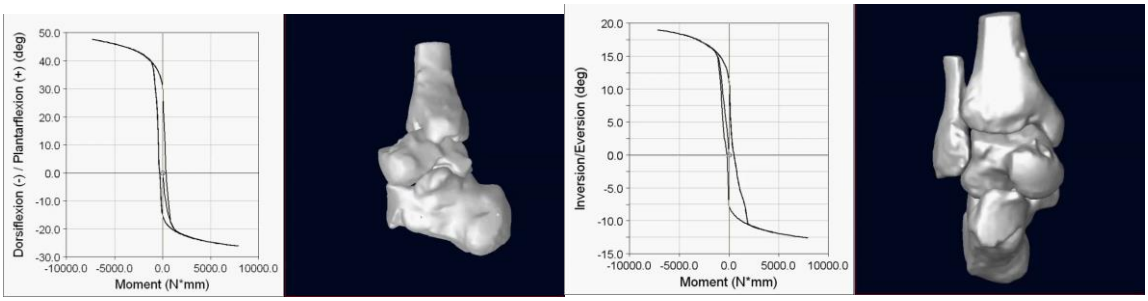

a) Dorsiflexion/Platarflexiononon b) Inversion/Eversion

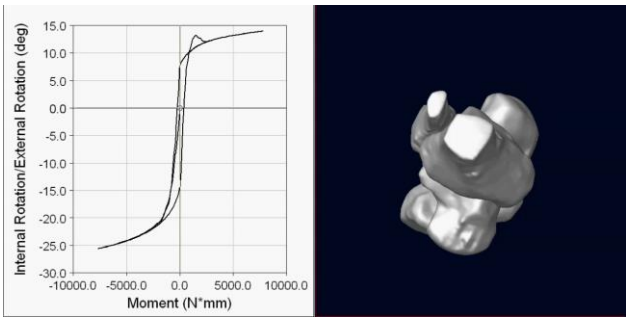

c) Internal/External rotation

Figure 37. Flexibility characteristics of Ankle Joint Complex in a) Dorsiflexion / Plantarflexion, b) Inversion / Eversion, c) Internal / External rotations

Hip Joint

Step 1: Image Processing

Computer Tomography (CT) images of hips with resolution of 0.8 mm*0.8 mm*2 mm are obtained from six non-pathalogical non-symptomatic subjects and ten of those diagnosed with a condition referred to as Femoro Acetabular Impingement (FAI) are acquired. These CT images are then processed using ANALYZE^{TM} software to produce 3D numerical models of the two articulating bones, the femur and the acetabulum. Similar to the procedure described earlier for the ankle, this process involves segmenting the bones of interest (Figure 38) followed by 3D spatial filtering and interpolation to create .stl files representing the 3D geometry.

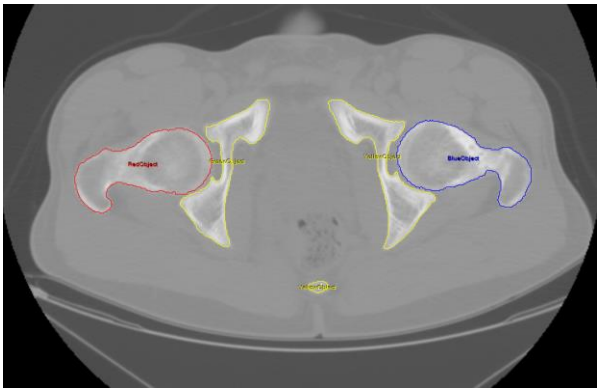

a) Example of the segmentation process used to obtain the contours of the bones in each 2-D slice

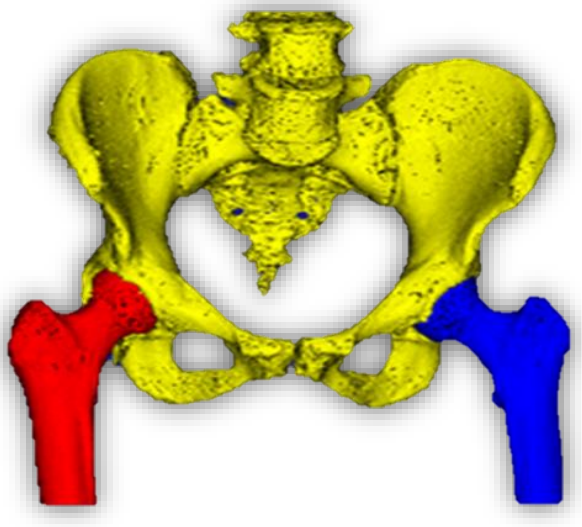

b) 3D model of bones after rending process

Figure 38. Image processing of hip joint CT image

Step 2: Post Processing

The rendered data obtained from Analyze™ is processed using Geomagic Studio™ to filter scanned artifacts, to fit the surface with polygons, to remove rough contours using a 3D smoothing algorithm, and to reduce model size so that the resulting geometry can be

efficiently handled by the dynamic simulation program (Figure 39). The center of rotation of the hip joint, assumed to be fixed, is then identified using the following procedure. First, a spatial least square error optimization algorithm is used to optimally fit a sphere to the femoral head and to the acetabulum (Figure 40). The center of rotation is assumed to be half-way between the centers of the two spheres.

One communally used algorithm to fit 3D sets of points to a sphere is the least squares minimization [84].

$$\boldsymbol{E(a,b,c,r) = \sum_{i=1}^{m}(L_i - r)^2} \qquad \textbf{Equation 5}$$

$(x-a)^2+(x-b)^2+(x-c)^2 = r^2$ is the sphere to be fitted by the points $\{(x_i, y_i, z_i)\}_{i=1}^{m}$, m>4 and $L_i = \sqrt{(x-a)^2 + (y-b)^2+(z-c)^2}$

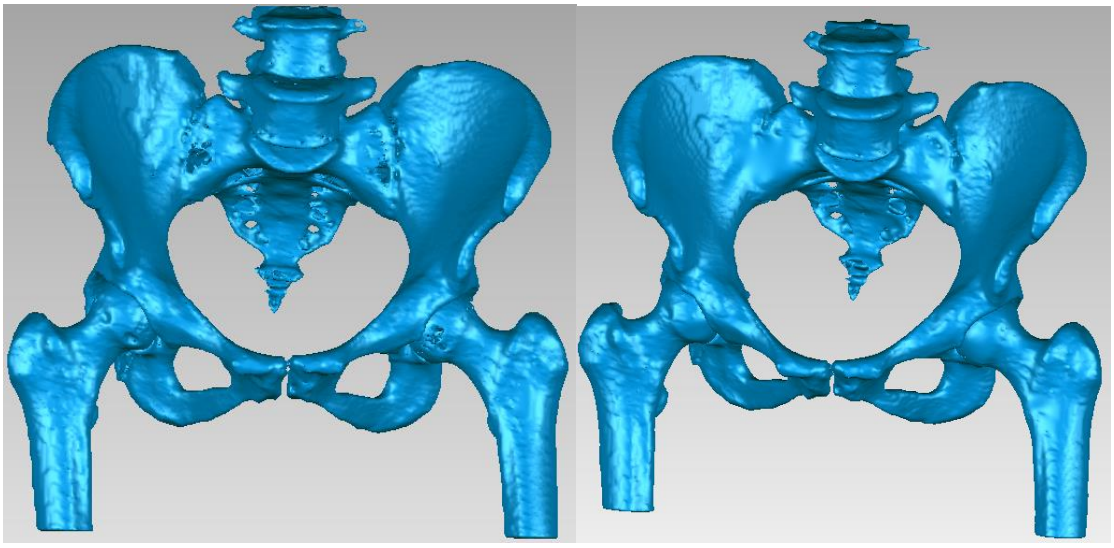

Before **After**

Figure 39. CAD model before and after smoothing and filling holes.

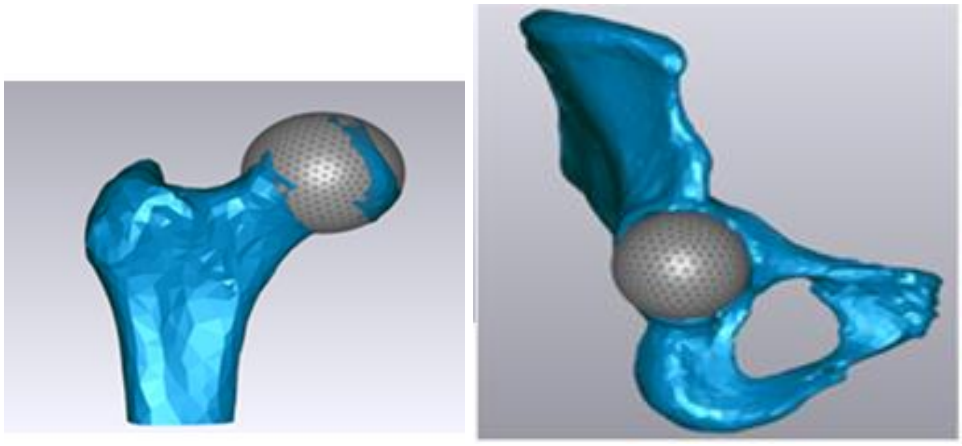

Figure 40. Hip joint center calculation
Fitting spheres to acetabulum and femoral head of hip joint to calculate the center of rotation of the hip joint.

A labrum is modeled in this stage by offsetting the rim of acetabulum by 2mm.

Step 3: Rigid Body Dynamic Model

The three dimensional morphology of the bones and the labrum is imported into a dynamic simulation software environment ADAMS^{TM} (Figure 41). A spherical joint with its center coincident with the previously identified center of rotation is established. Labrum is fixed to acetabulum. Boundary conditions consisting of a fixed acetabulum and a free femur are specified and moments are applied across the hip joint in various anatomical directions.

Contact Properties

An Interference Detection Algorithm (RAPID^{TM}) [78] is used to establish contact between the bones where the properties of the contact are defined by the material properties of cartilage. The contact force between articular surfaces is defined in equation 6 as a non-linear function of penetration depth, x, and penetration velocity,$\dot{x}$

$$\boldsymbol{Force = kx^{e} + c_2\dot{x}} \qquad \textbf{Equation 6}$$

The values of *k, e* and *c2* are considered as contact between rigid bodies. The stiffness parameter, k=10^5 N/mm^2, the exponent e=10 and penetration depth, x=0.1mm.

In addition to the bone interference patterns identified through the contact algorithm, distance maps were established for various hip positions. Distance maps are color coded maps drawn on top of either of the two articulating bones which show the distance between the two articulating surfaces (Figure 42).

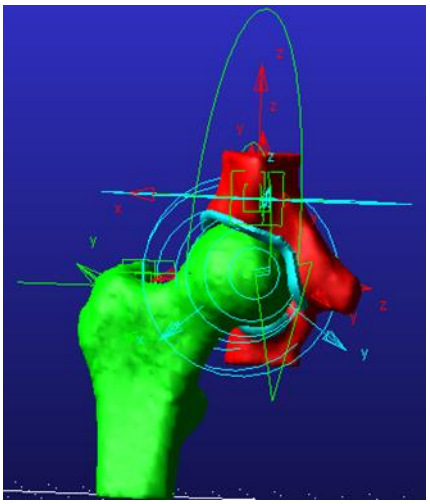

Figure 41. Rigid body dynamic model of hip joint in ADAMS™

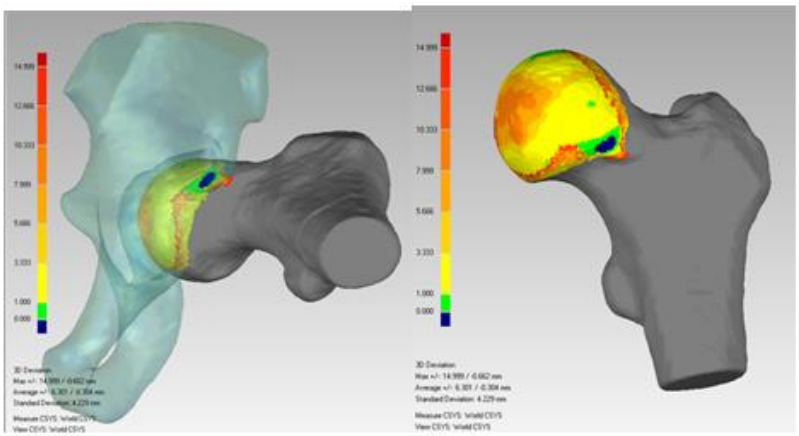

Figure 42. Distance map of hip joint obtained for one simulation position.
Blue region indicates the region of contact between femur and acetabulum.

Zone Method to Quantify Interference

In order to compare the patterns of interference acetabulum and femoral head are divided into several zones following similar but slightly modified procedure as in literature [85]. The acetabulum was divided into 6 different zones by use of the acetabular fossa as the

principal landmark. Two vertical lines are drawn by the use of the anterior and posterior notch walls as a reference. A horizontal line is drawn at the top of the acetabular notch. Numbers are assigned to each zone starting with number 1 at the anterior-inferior zone and ending with the number 6 at the acetabular notch (Figure 43).

The femoral head has been divided into 6 zones around the projection of the acetabular fossa. The area that corresponds to the acetabular fossa is positioned on the femoral head around the ligamentum teres, and the same imaginary lines are then positioned on the femoral head following the same pattern that was used for the acetabulum. Zone 1 is the anterior-inferior femoral head; zone 2, anterior-superior femoral head; zone 3, central superior femoral head; zone 4, posterior superior femoral head; zone 5, posterior-inferior femoral head; and zone 6, area around ligamentum teres . Further the zones are subdivided divided into Medial (M), Superior(S) and Lateral (L) from proximal to distal direction on femoral head. Anterior-inferior is always zone 1 for both right and left hips (Figure 44). The zone method was more reproducible than the clock-face method in the geographic description of intra-articular injuries on the acetabulum and the femoral head [85]. By using this zone method it is easy to compare the change in impingement at each simulation stage of hip joint (Figure 45).

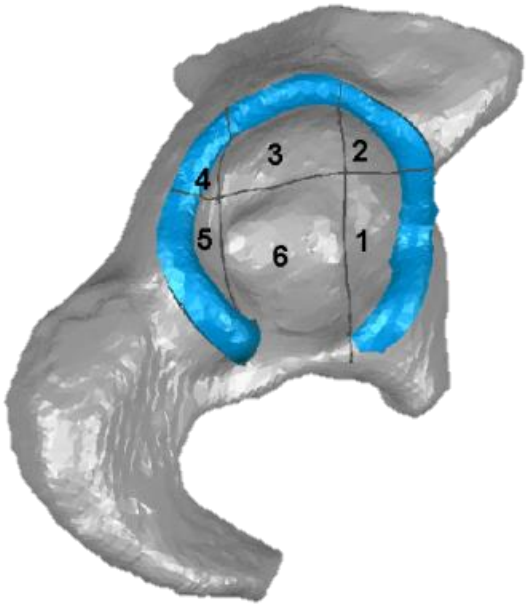

Figure 43. Zone Method - Divisions on acetabulum

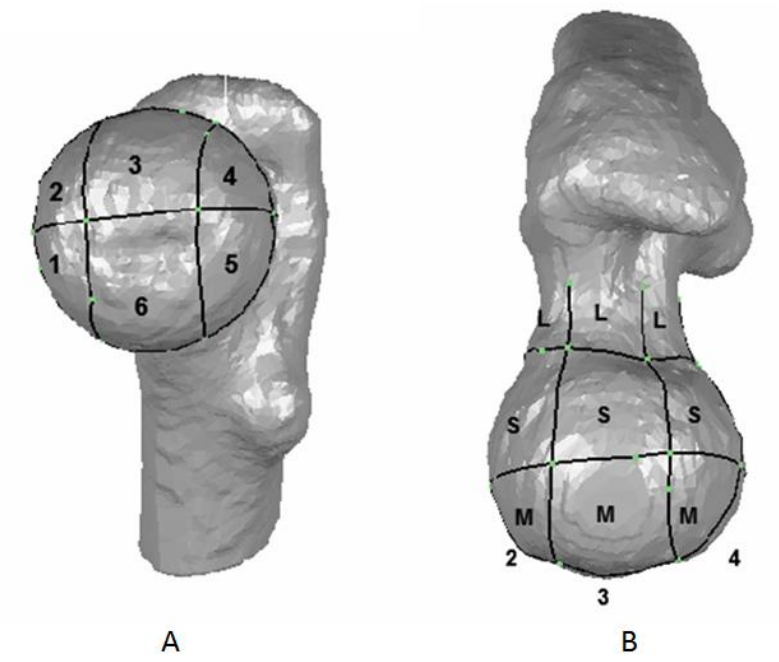

Figure 44. Zone Method - Divisions on femur.
(A) Front view of right proximal femur model. (B) Superior view of right proximal femur model.

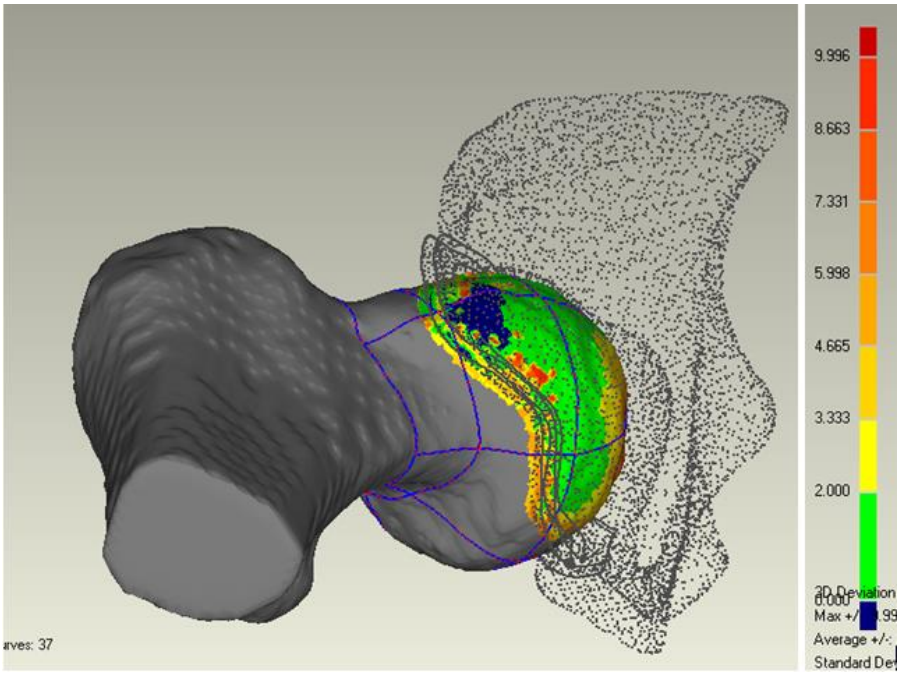

Figure 45. Distance map showing interference on femoral zones obtained at one simulated position
Interference is observed in zones 1S, 2S.

METHODOLOGY PART 2: EFFECT OF CHANGE IN MORPHOLOGY ON JOINT MECHANICAL BEHAVIOR

Using the numerical models developed in aim 1, the relationship between the morphology and the mechanical behavior of ankle and hip joints will be investigated. This will be achieved by systematically varying selected morphological parameters such as bone surface geometry and insertion sites of ligaments in the models. The effect of these variations on mechanical characteristics will then be identified through numerical simulations.

To achieve this goal the following steps are followed for the ankle and the hip joint separately.

Ankle Joint

Step 1: Selecting and Measuring the Morphological Parameters:

This step is divided into two steps first selecting the morphology (region of interest) and second measuring the morphological parameters of the selected morphology

1 a) Selecting the Parameters

To investigate the effect of change in morphology of the ankle joint complex on the mechanics the following parts of ankle are selected.

1. CFL ligament
2. Sustentaculum tali

The CFL ligament is selected because this ligament plays a major role in stability of ankle in inversion and the injury of this ligament may lead to chronic lateral ankle pain, chronic instability, and osteoarthritis. Sustentaculum tali is selected because it acts as a support relative to the talar facet.

1 b) Measuring the Morphological Parameters

The original orientation of CFL (Figure 46), Sustentaculum tali width, calcaneus width, ratio of Sustentaculum tali width to calcaneus width, Sustentaculum tali length, calcaneus length, ratio of Sustentaculum tali length to calcaneus length for six subjects are measured (Figure 47).

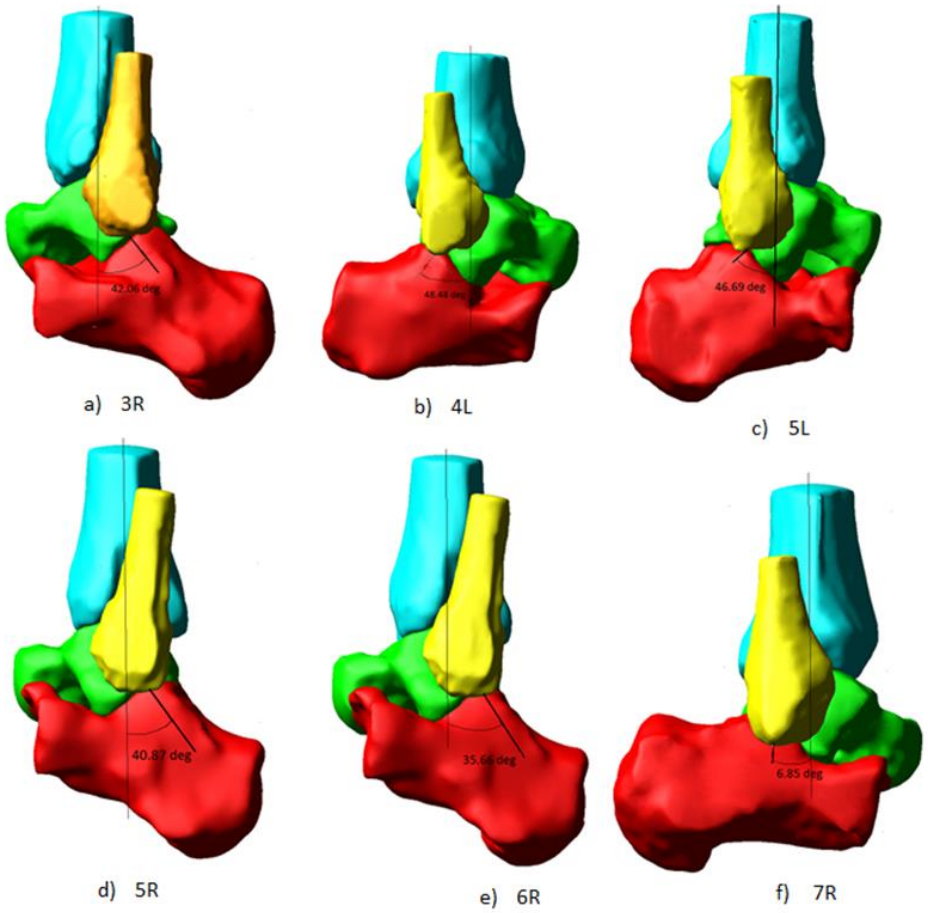

Figure 46. Orientation of calcaneofibular ligament in all the six subjects

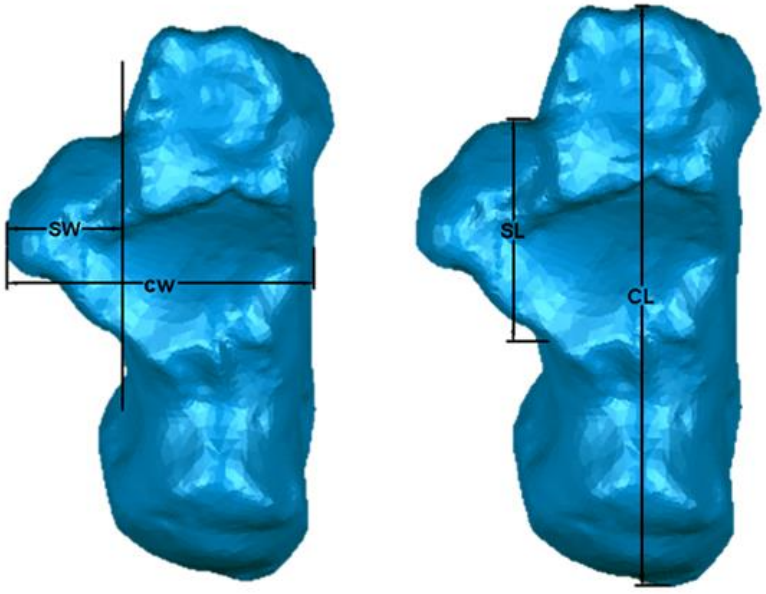

Figure 47. Width of Sustentaculum tali (SW), Width of Calcaneus (CW), Length of Sustentaculum Tali (SL) and Length of Calcaneus (CL)

Step 2: Changing Morphology of Bone and Ligament Insertion Sites and Comparing the Mechanical Behavior

2a) Changing the Orientation of CFL Ligament

The orientation of the ligament is measured in the sagittal plane with respect to the tibial axis for all the six subjects. The orientation of the ligament is altered by changing ligament insertion sites on the calcaneous such that the orientation of the ligament is 0 degrees, 30 degrees, 60 degrees and 90 degrees with respect to tibial axis (Figure 48). Passive mechanical properties such as range of motion, force in the CFL are calculated during plantar/dorsiflexion, inversion/eversion and internal/external motions at each orientation of the CFL.

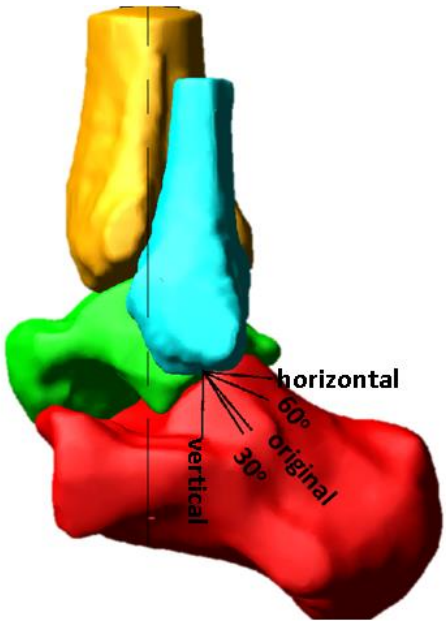

Figure 48. Change in orientation of calcaneofibular ligament from vertical to horizontal with respect to tibial axis

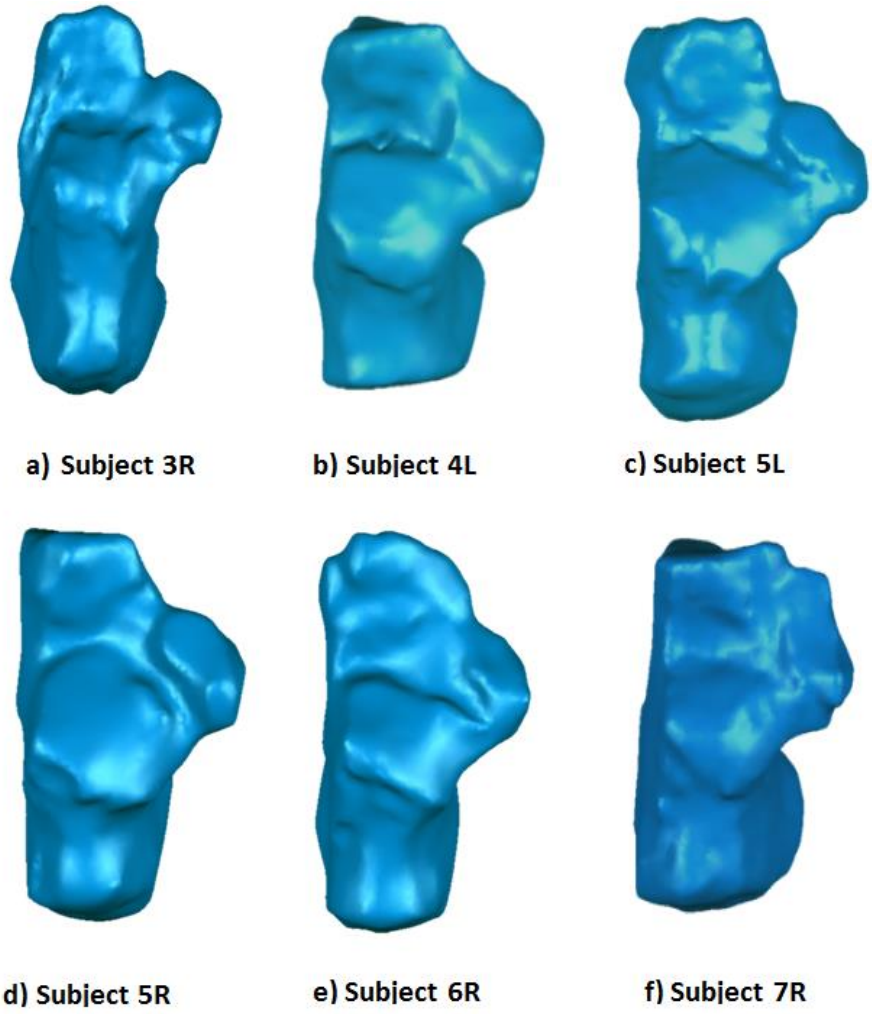

Figure 49. Morphology of the sustentaculum tali of the six subjects in neutral position.
In subjects 3R, 5L, 5R and 6R anterior and medial facets are separate. In subjects 7R and 4L anterior and medial facets are fused.

2b) Changing the Morphology Sustentaculum tali

Figure 49 shows the original morphology of sustentaculum tali of the 6 subjects. Subjects 3R, 5L, 5R, 6R have separate anterior and medial facets where are in subjects 7R and 4L the anterior and medial facets are fused (Figure 49). The effect of morphology of

sustentaculum tali on the passive mechanical properties of the ankle joint complex is studied by removing the sustentaculum tali in four stages.

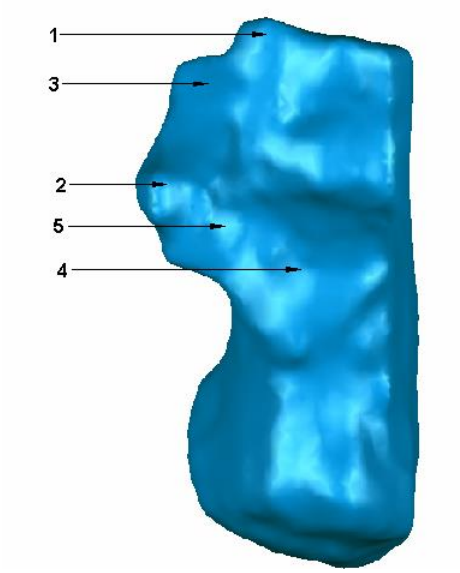

Figure 50. Calcaneus-Features.
1. Anterior talar articulating surface; 2. Middle talar articulating surface; 3. Fused anterior and middle talar articulating surface; 4. Posterior talar articulating surface; 5. Canalis tarsi.

In order to study the effect of morphology change of the sustentaculum tali on joint mechanics of the six subjects the morphology of sustentaculum tali is changed by following Alterations #1 through #4 of the sustentaculum tali by successively altering the supportive function of the middle articular facet on the talus (Figure 50).

Alteration 1: The fused anterior and middle facet supporting structure is removed. The talus remains supported deep in the canalis tarsi, posterior end of the middle articulating facet and on the medial side of the posterior articulating facet extension (Figure 50 and Figure 51).

Alteration 2: In this stage the elevation of sustentaculum tali is lowered by lowering the elevation of middle articulating facet (Figure 50 and Figure 51).

Through this process there is a loss of support in the canalis tarsi. The talus is supported mostly on the medial-side posterior articular facet extension (Figure 50 and Figure 51).

Alteration 3: The medial-side posterior articulating facet extension is removed by lowering its articulating surface elevation (Figure 50 and Figure 51).

Alteration 4: Sustentaculum tali is completely removed. After this alteration, the posterior articular facet is the primary supporting facet (Figure 50 and Figure 51).

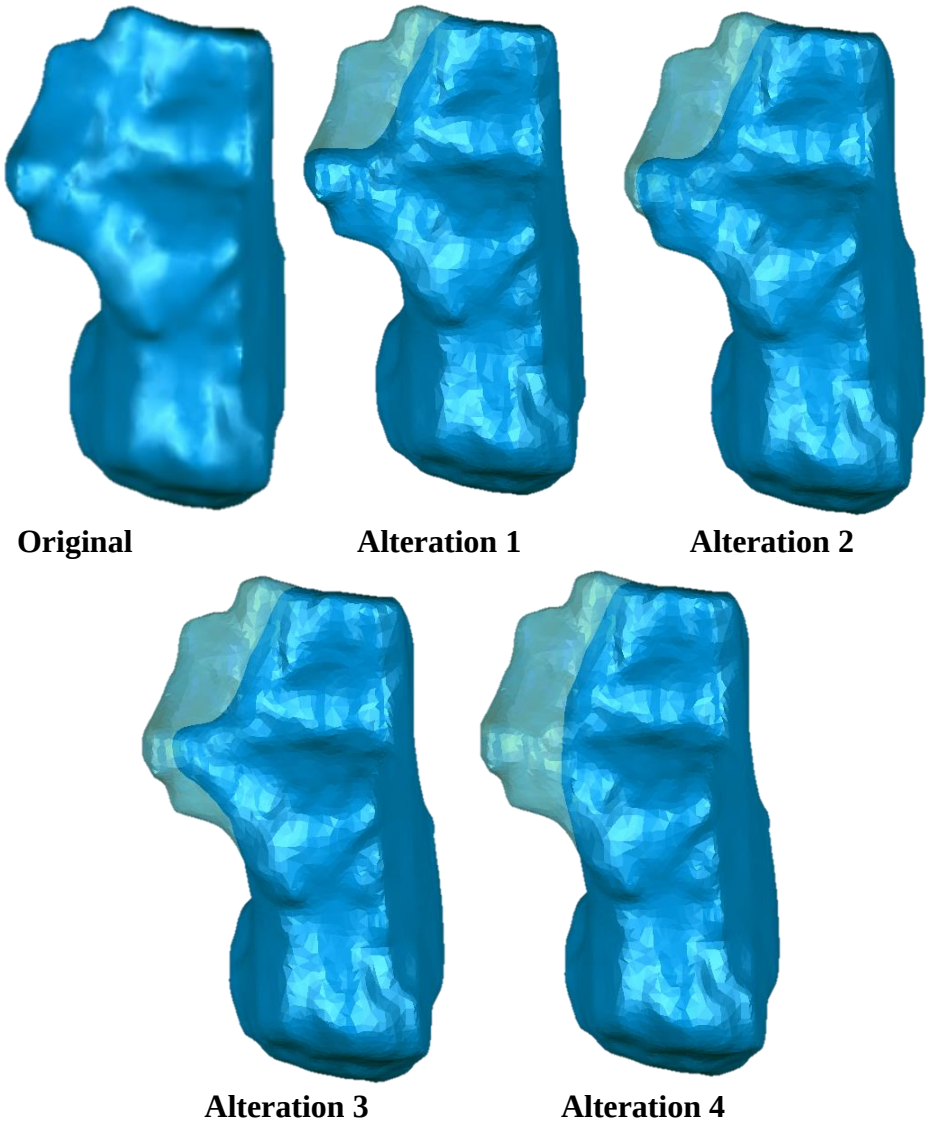

a) Sustentaculum tali after removing the bone in each alteration in top view. The transparent blue region shows original morphology and dark blue region shows the altered morphology.

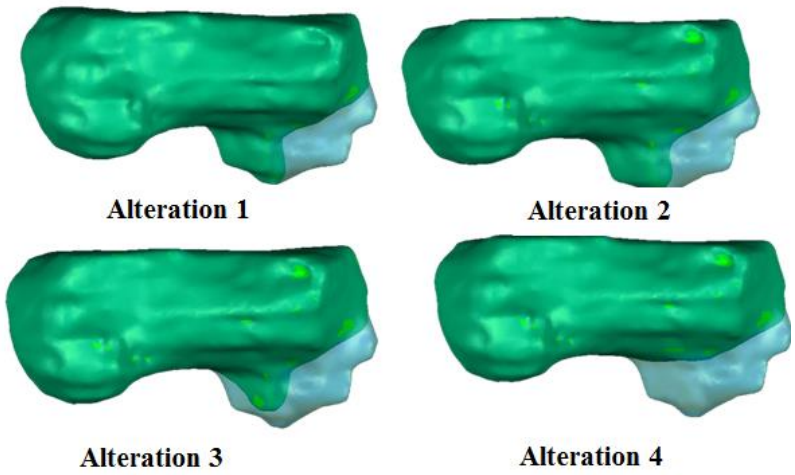

b) Sustentaculum tali after removing the bone in each alteration in bottom view. The transparent blue region shows original morphology and green region shows the altered morphology

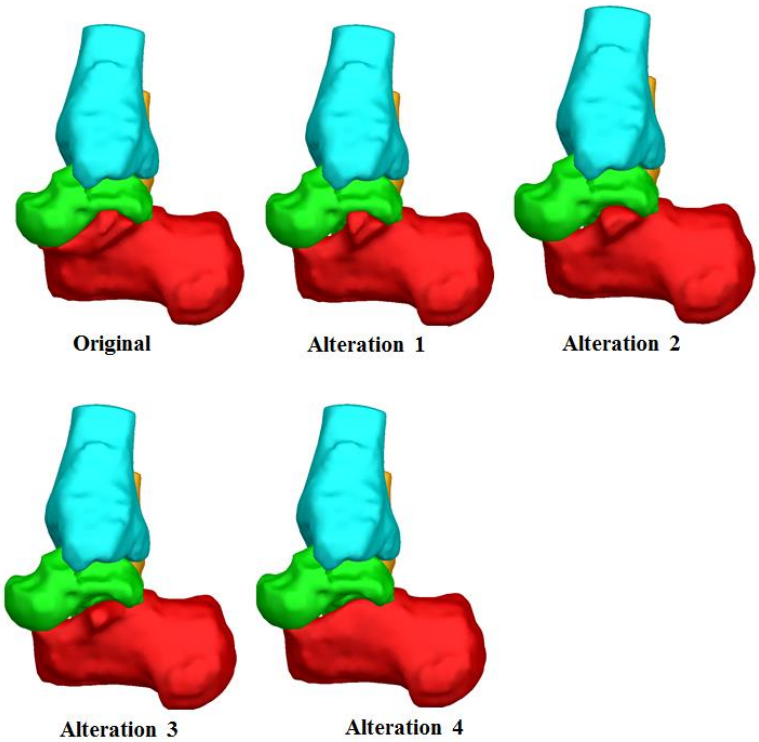

b) Sustentaculum tali in the ankle joint after each alteration

Figure 51. Process of removing the volume of sustentaculum tali

The morphology of sustentaculum tali is altered as discussed in Figure 51 and the effect of these changes on passive mechanical properties of ankle joint such as the range of motion and forces in CFL ligament are measured. Further, distance maps are calculated between talus and calcaneus after each morphological change in sustentaculum tali in order to evaluate the loss of contact support at each stage (Figure 52).

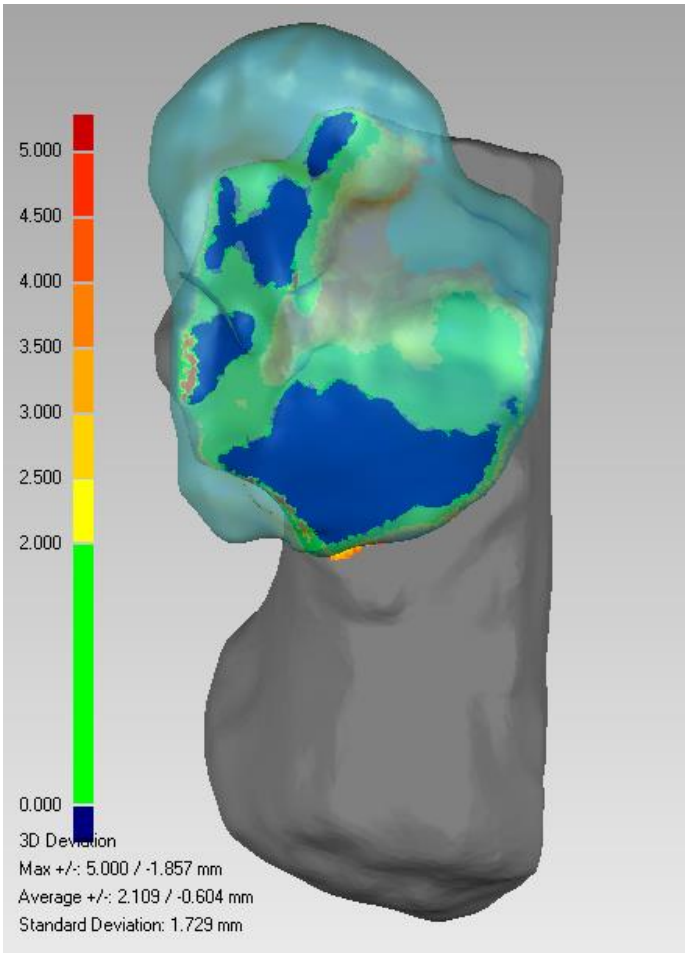

Figure 52. Distance map showing the distance between original calcaneus and talus.
Blue regions show contact regions.

Table 5. Percentage volume of bone retained after changing morphology of sustentaculum tali of all six subjects

SUBJECTS	ORIGINAL	ALTER1	ALTER2	ALTER3	ALTER4
CAD 3R	100	97.07875	96.79182	96.19357	95.12927
CAD 4L	100	96.94226	96.46665	94.82877	93.0333
CAD 5L	100	98.03287	97.73657	96.44864	95.26753
CAD 5R	100	98.00588	97.46217	96.28232	95.06531
CAD 6R	100	98.38405	97.93748	97.00045	96.00537
CAD 7R	100	96.93309	96.48294	95.49769	94.16573

Measuring Mechanical Properties

Flexibility of AJC

Early Flexibility of AJC is calculated by fitting a line on the load-displacement curve in the region of initial motion. The slope of the line gives the flexibility of the curve (Figure 53).

Range of Motion of AJC

Range of motion of AJC is the Maximum angle rotated by applying moment about each coordinate of AJC (Figure 54).

Force in CFL

The force in CFL is defined as the force measured in CFL at Maximum ROM (Figure 55).

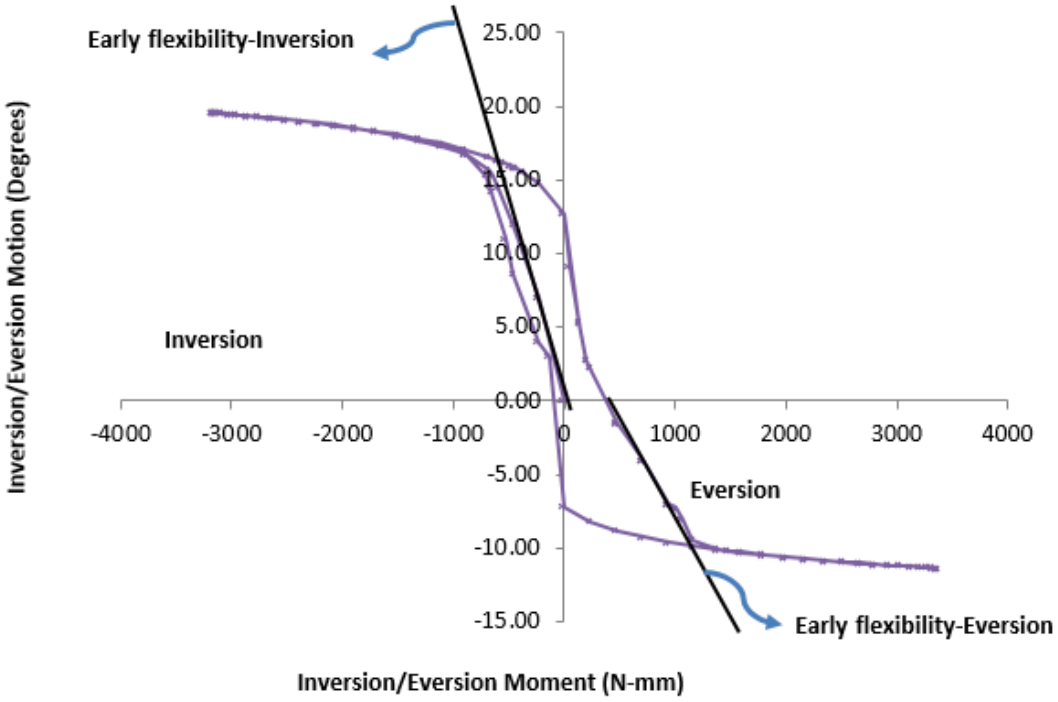

Figure 53. Calculating flexibility of AJC from load-displacement plot

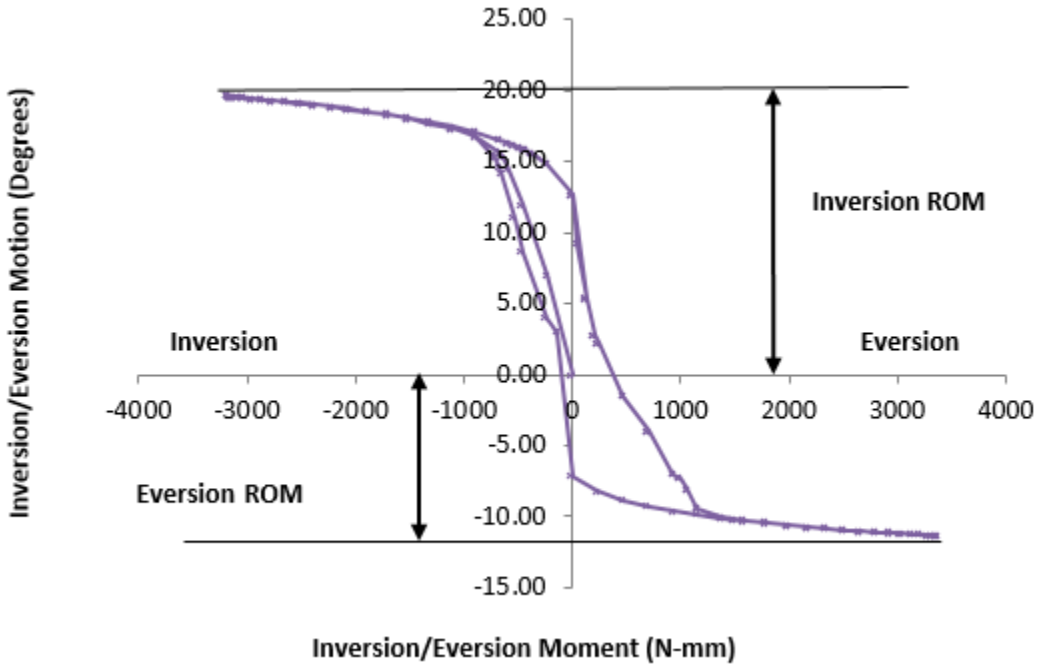

Figure 54. Calculating range of motion of AJC from load-displacement plot.

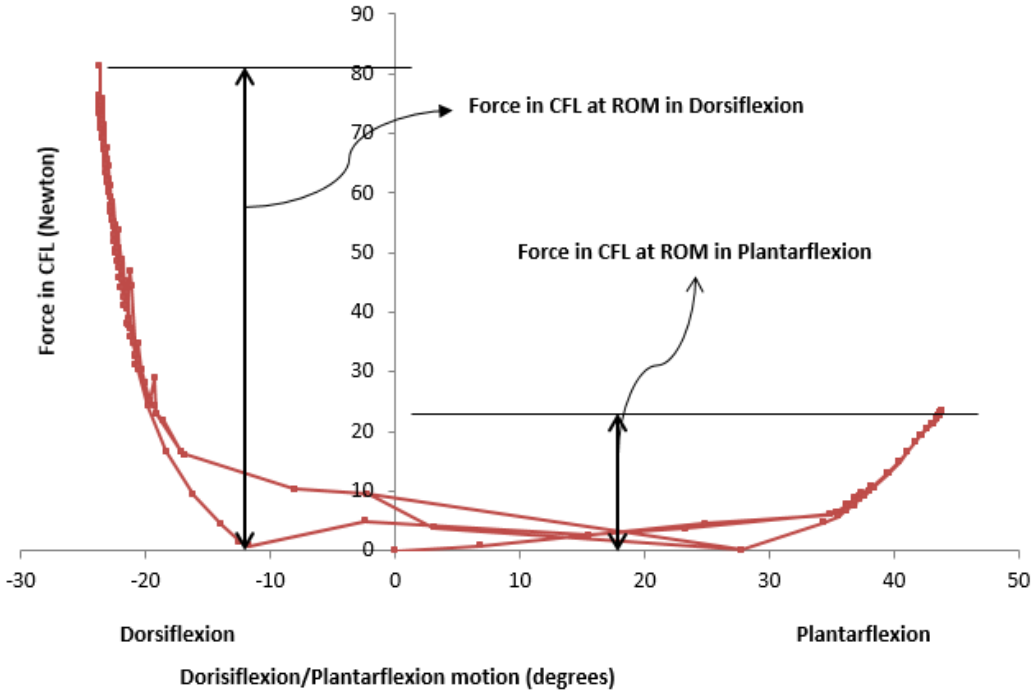

Figure 55. Calculating force in CFL from ligament Force versus Motion plot

STATISTICAL ANALYSIS

In this study the morphology of bone is changed following four alterations and the oriantations of CFL is changed to four different orintations and the effect of these changes on mechanical behaviour of the ankle joint is calculated using dynamic simulations. To findout if there is any significant change in the mechanical behavior of the joint after changing the morphology of the bone and orientation of CFL, one-way repeated measures ANOVA is used using the software SPSS^{TM} by IBM. This particular statistical method is chosen because the same entities take part in all the simulations [86]. A significance value p=0.05 is chosen for the statistical analysis. Greenhouse and Geisser method is used to calculate the signicance of the changes in the values and to test the

violation of the assumption of sphericity. Inorder to determine particularly between which changes in morphology there is a significant change in mechanical behavior of joint a post-hoc procedure known as Fishers Least Square Difference (LSD) method is followed.

Repeated measures ANOVA is a powerful tool and provides significance for smaller subjects than population based analysis. Each subject is model based, all the properties are identical and this decreases variability. Further, changes are done in a very controlled manner. Loading conditions are same after each change unlike experimental studies.

Hip Joint

Step 1: Selecting and Measuring Morphological Parameters

The morphological parameters such as femoral neck-shaft angle, femoral anteversion/retroversion, alpha angle, neck offset angle, pistol grip deformity are considered as crucial parameters for femoroacetabular impingement [51] (Figure 56). These parameters are measured for all the subjects and are compared.

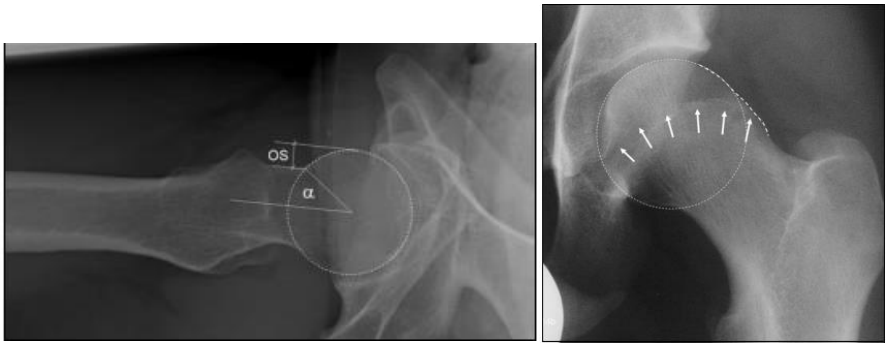

a) Alpha angle and head neck offset

b) Pistol grip deformity [51]

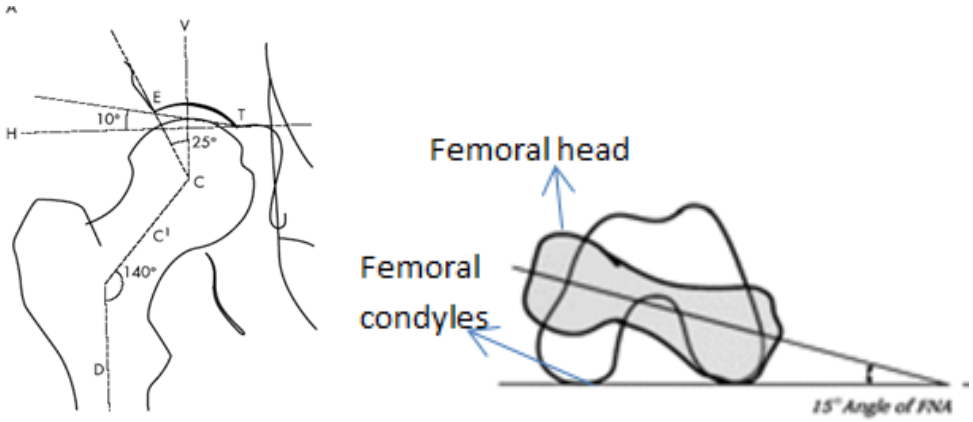

c) Femoral neck-shaft angle CC'D [87]

d) Femoral neck anteversion [88]

Figure 56. Morphological parameters of hip joint that are crucial for Femoroacetabular Impingement.

Step 2: Changing Morphology of Normal Hips and Comparing the Joint Mechanical behavior

The morphology of normal hip joints is changed to abnormal morphology by changing each clinical parameter in step 1 from normal range to abnormal range. Then the simulation is performed with 100 degrees flexion followed by 20 degree adduction and 40 degree internal rotation so as to imitate the physical FAI test and the impingement is plotted and compared to that of normal hip

2a) Changing Femoral Neck-shaft angle: The normal range of femoral neck-shaft angle is 126 degrees-139 degrees [65, 66]. The condition with neck-shaft angle greater than 140 degrees is called as Coxavalga and less than 125 degrees is called as Coxavara. The morphology of the femur is changed so as to decrease the neck-shaft angle less than 125 degrees. This is done by following the procedure of intertrochanteric osteotomy [69, 70] where a wedge is cut in the femoral shaf. This process of osteotomy is discussed in Appendix B. Figure 57 shows the femur after changing the neck-shaft angle. The simulation is performed with 100 degrees flexion followed by 20 degree adduction and 40 degree internal rotation and so as to imitate the physical FAI test and the interference at hip joint is calculated through distance maps and compared to that of normal hip (Figure 58).

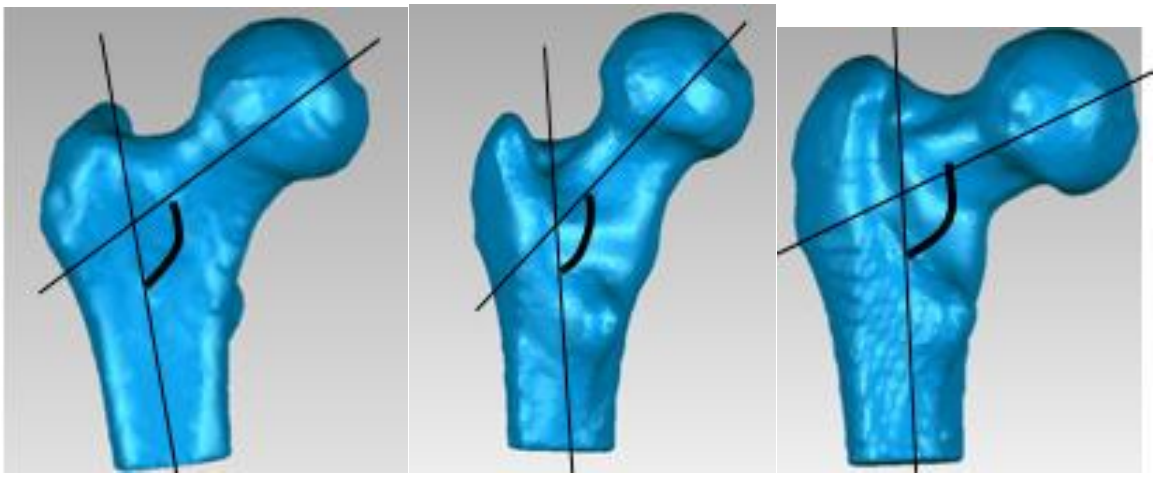

a) Normal, angle= 130^{o} b) Coxavara , angle = 110^{o} c) Coxavalga, angle = 150^{o}

Figure 57. Morphology of femur after decreasing and increasing the neck-shaft angle by 20 degrees

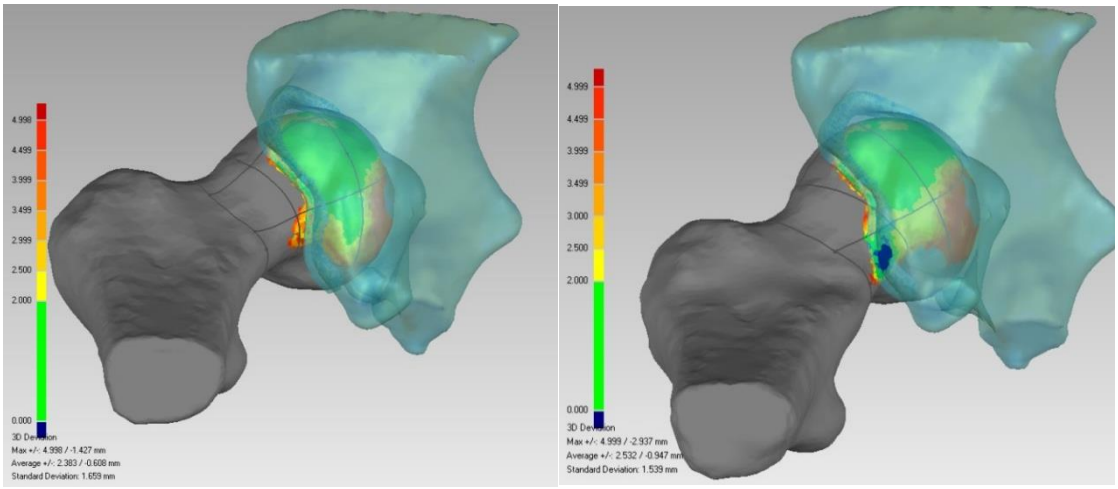

a) Normal, no interference b) Coxavalga, interference in zone 6L

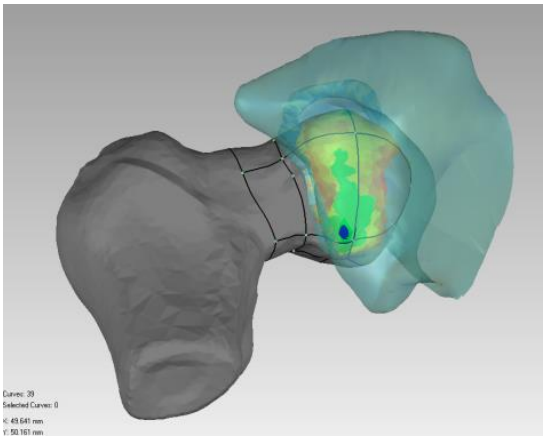

c) Coxavara, interference in zone 1S

Figure 58. Interference pattern observed on femur by changing femoral neck-shaft sngle.
At simulation position 100 degree flexion, 20 degree adduction and 40 degree internal rotation, interference is observed on a) Normal hip joint b) Increasing neck-shaft angle by 20 degrees (Coxavalga) c) Decreasing the neck-shaft angle by 20 degrees (Coxavara).

2b) Anteversion/Retroversion

The normal value of femoral anteversion is 15º-20º [72]. The morphology of femoral anteversion angle is increased by 20 degrees to create excessive anteversion and retroversion is created by decreasing anteversion angle by 20 degrees (Figure 59). The simulation is performed with 100 degrees flexion followed by 20 degree adduction and

40 degree internal rotation and so as to imitate the physical FAI test and the interference at hip joint is calculated through distance maps and compared to that of normal hip (Figure 60). This morphology change of changing anteversion angle is performed imitating surgical procedure derotational osteotomy [72] where the femoral shaft is cut and rotated. This process of osteotomy on the femur model is discussed in Appendix B.

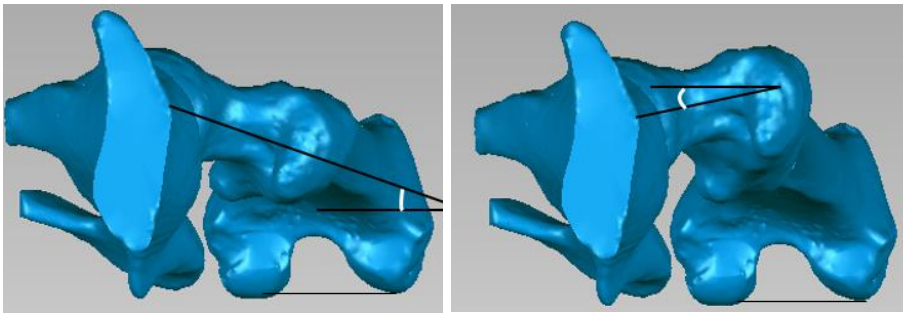

a) Normal, angle = 15°-20° b) Retroversion, angle < 15°

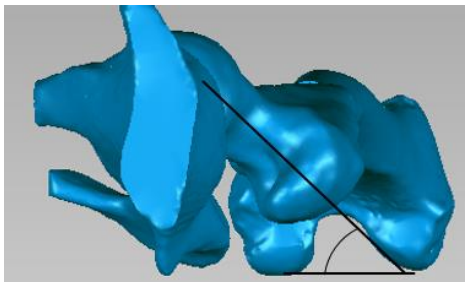

c) Excessive Anteversion, angle >20°

Figure 59. Morphology of femur after changing anteversion angle

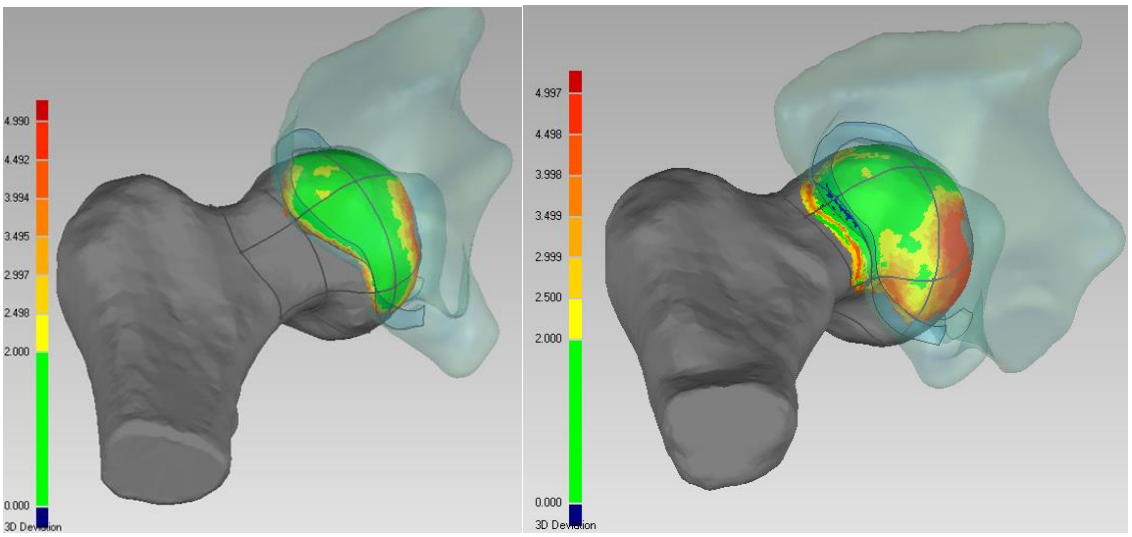

b) Normal, no interference b) Retroversion, Interference in zones 1L, 2L

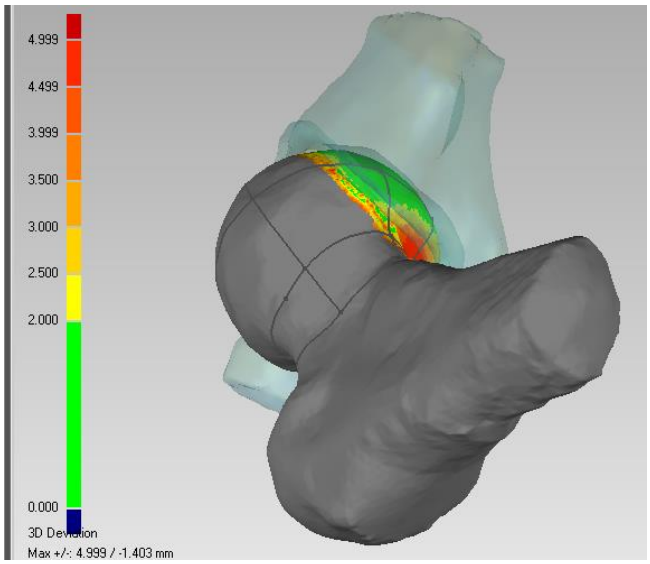

c) Excessive Anteversion, no interference

Figure 60. Interference pattern observed on femur by changing angle of anteversion.
At simulation position 100 degree flexion, 20 degree adduction and 40 degree internal rotaion interference is observed on a) Normal hip joint b) Decreasing anteversion angle by 20 degrees (Retroversion) c) Increasing the anteversion angle by 20 degrees (Excessive Anteversion).

2c) Alpha Angle

Alpha angle is normal if it is less than 55 degrees. Morphology of Alpha angle is increased to greater than 55 degrees. This process of increasing alpha angle is performed by adding material around the femoral head neck junction so that alpha angle is greater than 75 degrees (Figure 61). Interference pattern at simulated position 100 degree flexion combined with adduction and internal rotation is calculated after changing alpha angle and compared to normal hip (Figure 62).

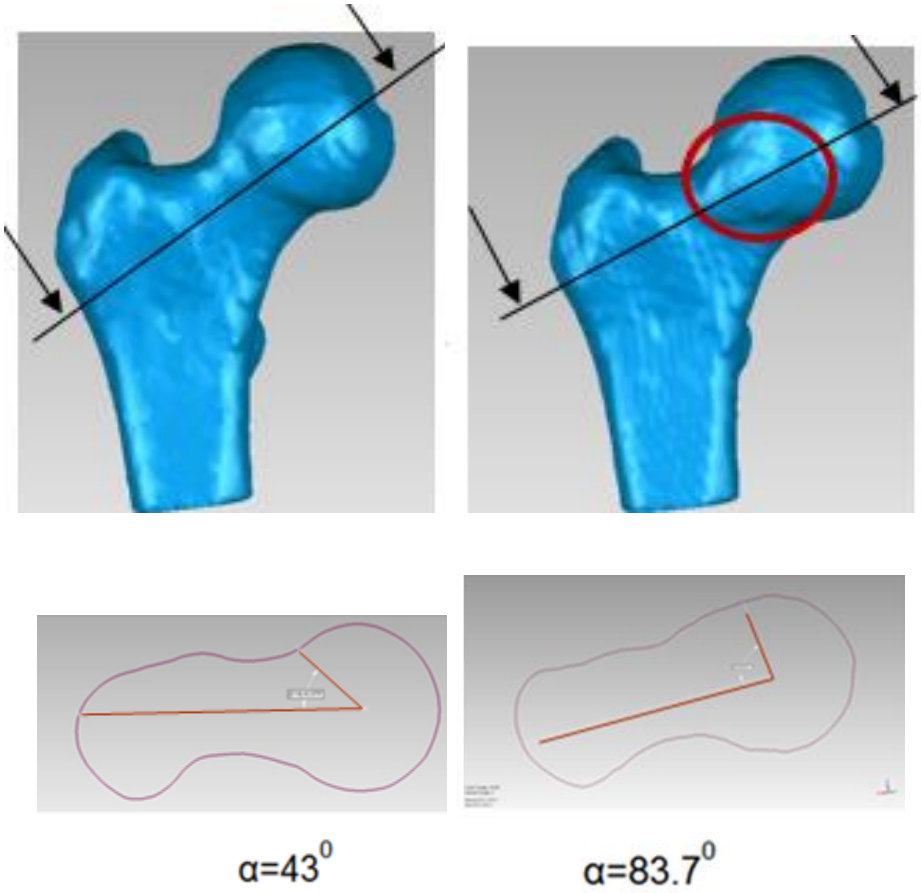

a) Alpha angle of normal hip b) After increasing alpha angle to 83.7 degrees

Figure 61. Before and after increasing the alpha angle of normal hip

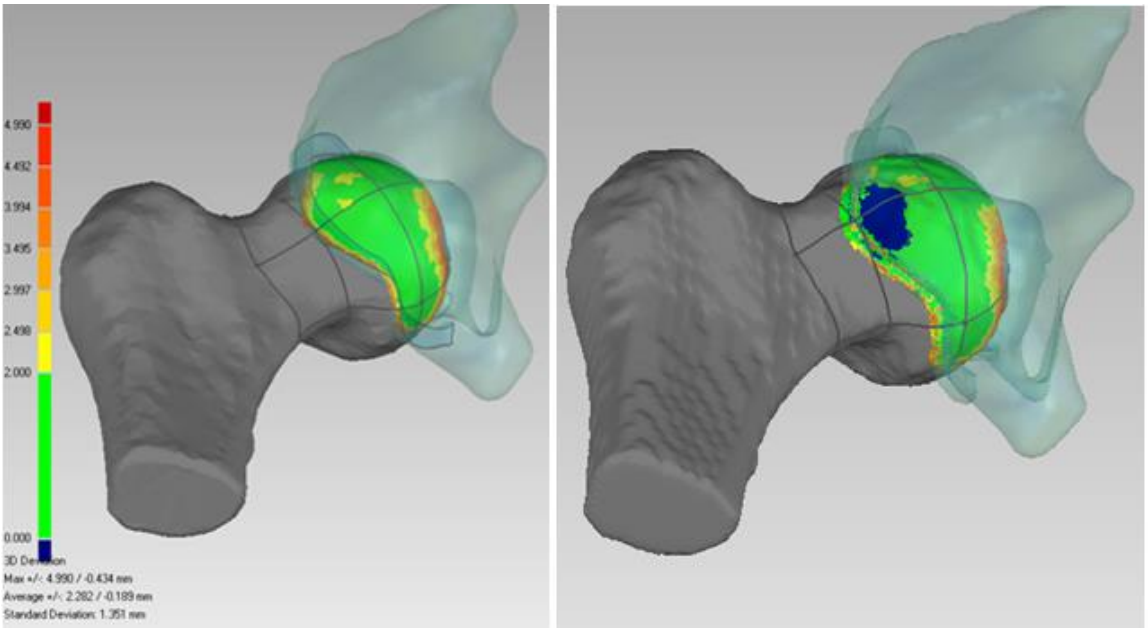

a) Normal, alpha =46 degrees, no interference. b) Alpha =86 degrees, interference in zones 1s, 2s

Figure 62. Interference pattern observed by increasing alpha angle to 86 degrees at position 100 degree flexion, 20 degree adduction and 40 degree internal rotation

2d) Pistol Grip Deformity

Pistol grip deformity is induced in the femur by adding material on the superior femoral neck at the head-neck junction (Figure 63). Interference pattern at simulated position 20 degree adduction is calculated after inducing pistol grip deformity and compared to normal hip (Figure 64).

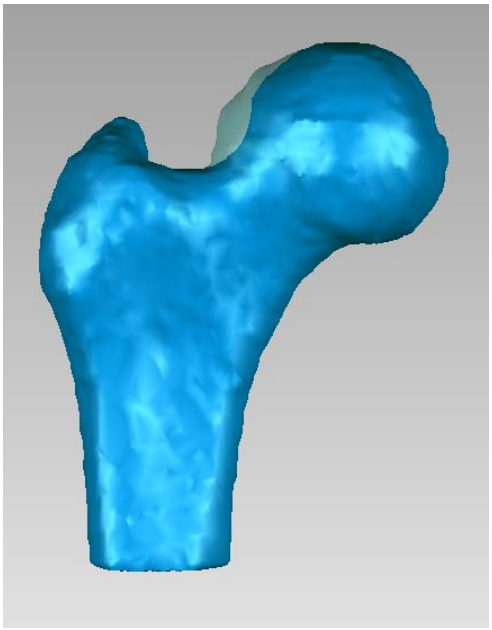

Figure 63. Changing the morphology of normal femur (solid blue) to femur with pistol grip deformity (transparent blue).

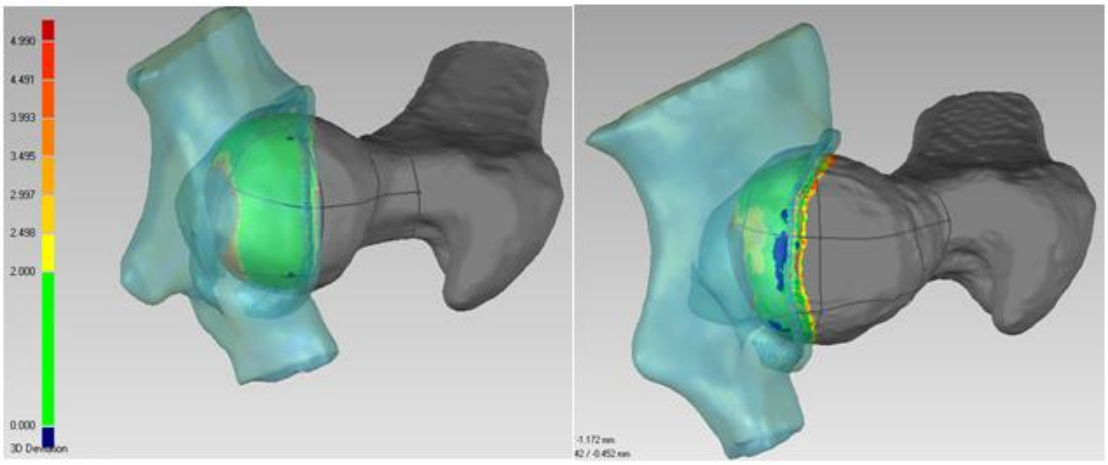

a) Normal femur b) Femur with pistol grip deformity.

Figure 64. Interference pattern observed at the stance of 100 degrees flexion and 20 degrees adduction before (left) and after (right) introducing the pistol grip deformity.

This process of changing the morphology of femur and inducing several deformities will help to identify if there are any other morphological parameters leading to pathological condition FAI and the surgeon should correct these parameters before performing the native surgical process.

CHAPTER 4: RESULTS

The results demonstrate the effects of change in morphology of the ankle and the hip joints on their corresponding joint mechanics.

MODEL DEVELOPMENT

Ankle Joint

Step 1: Image Processing

Magnetic Resonance (MR) images are obtained from six non-pathological cadaveric feet. These MR images are then processed using ANALYZE^{TM} software to produce 3D numerical models of the articulating bones and the regions of insertion of surrounding ligaments.

Step 2: Post Processing

The surfaces of 3D models of the ankle joints are smoothened and the number of polygons are reduced to be compatible with the dynamic analysis software.

Step 3: Rigid Body Dynamic Model

Rigid Body dynamic models of the six ankle joints are developed using the three dimensional bone morphology and ligament insertion sites measured in the post processing step. The model is then loaded through cyclic three dimensional moments and forces which are applied across the ankle joint complex in various anatomically significant directions (dorsiflexion/plantarflexion; inversion/eversion; internal

rotation/external rotation). Average model predictions of ROM were found to be in close agreement with values reported previously (20º–50º plantarflexion; 13º–33º dorsiflexion; 15º–20º inversion; 10º–17º eversion; and 24º external rotation).Range of motion of AJC are compared between all the subjects (Figure 65) and it is observed that subjects 4L and 7R with fused medial and anterior facets on calcaneus have less Range of motion in Inversion and internal rotations compared to other subjects with distinct facets. Subject 4L has less ROM in other motions too.

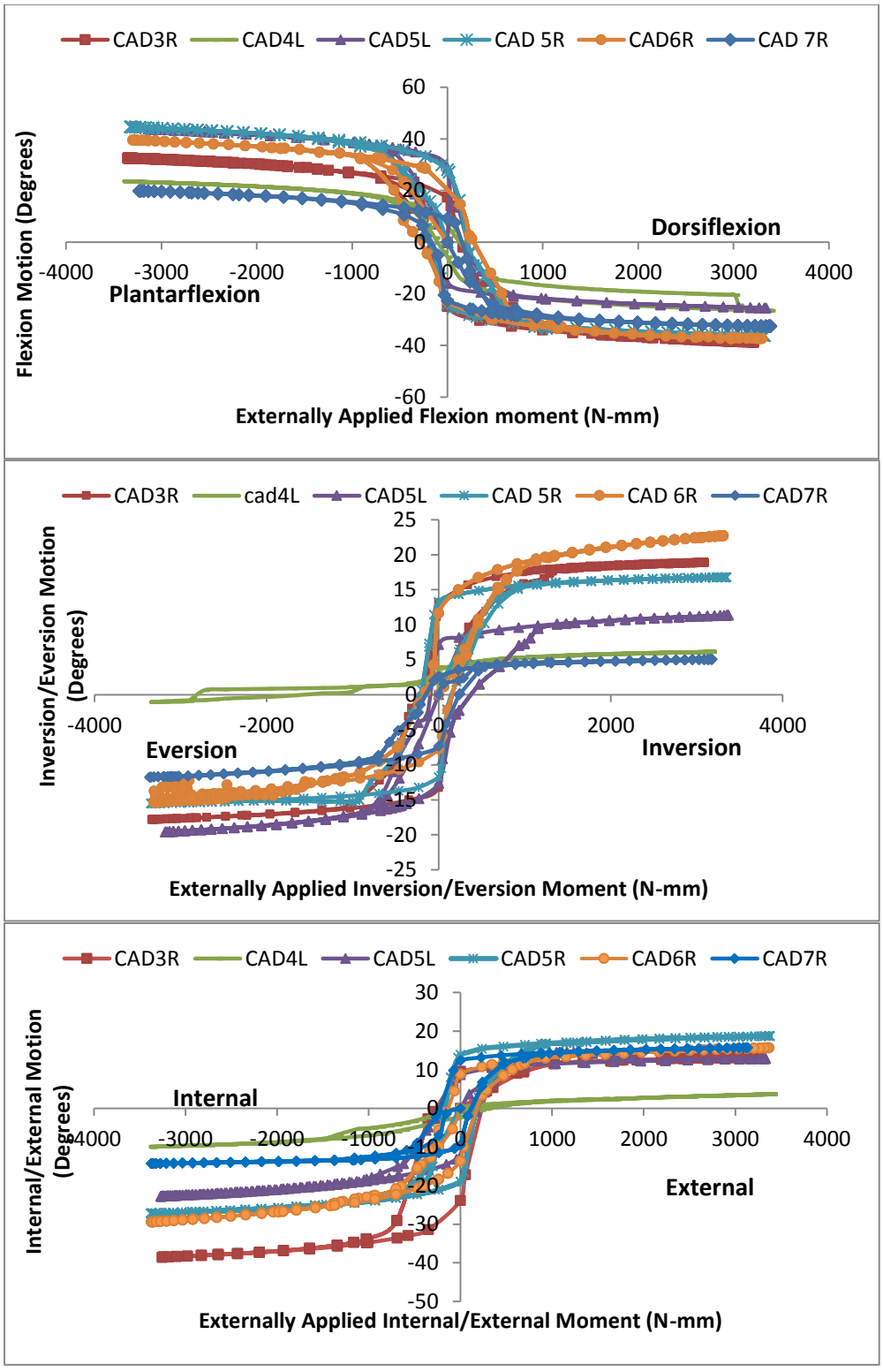

Figure 65. Comparing the motion of AJC of the six subjects by applying torque about the three axis dorsiflexion / plantarflexion, inversion / eversion, internal / external rotation.

MODEL DEVELOPMENT

Hip Joint

Step 1: Image Processing

Computer Tomography (CT) images obtained from seven healthy asymptomatic subjects and ten patients diagnosed with a condition referred to as Femoro Acetabular Impingement (FAI) are acquired. These CT images are then processed using ANALYZE^{TM} software to produce 3D numerical models of the two articulating bones, the femur and the acetabulum.

Step 2: Post Processing

The surface of 3D models of the hip joints is smoothened and the number of polygons is reduced to be compatible with the dynamic analysis software. The center of rotation of the hip joints is calculated as the average of the centers of the spheres fitted to the femoral head and acetabulum.

Step3: Rigid Body Dynamic Model of Hip Joint

Rigid body dynamic models of 4 normal and 4 FAI hips are developed and the interference patters are identified through distance maps. The interference patterns between FAI and healthy subjects are compared (Figure 66). The results indicated early interference in the hip models obtained from the FAI subjects as compared to healthy ones.

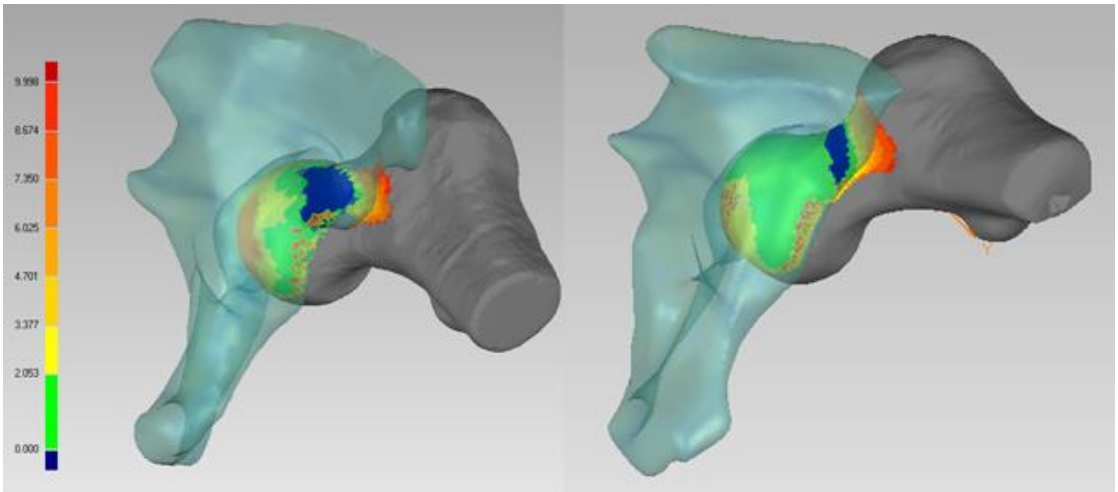

a) FAI hip b) Normal hip

Figure 66. Comparing distance maps between FAI and normal hips

EFFECT OF CHANGE IN MORPHOLOGY ON JOINT MECHANICAL BEHAVIOR

Ankle Joint

Step 1: Selecting and Measuring Morphological parameters

Orientation of CFL, width of sustentaculum tali and calcaneus, length of sustentaculum tali and calcaneus are measured in the six ankle joints as shown in Table 6.

Table 6. CFL orientation, Sustentaculum tali Width (SW), Calcaneus Width (CW), ratio of Sustentaculum tali Width to Calcaneus Width (SW/CW) , Sustentaculum tali Length (SL), Calcaneus Length (CL), ratio of Sustentaculum tali Length to Calcaneus Length (SL/CL)

Subject	Age	Sex	CFL orientation in degrees	SW in mm	CW in mm	SW/CW	SL in mm	CL in mm	SL/CL
3R	67	F	42.06	17.12	42.6	0.40	27.67	82.9	0.33
4L	86	M	48.48	17.61	42.98	0.41	39.6	80.39	0.492

5L	89	M	46.69	15.85	40.50	0.39	29.7	74.3	0.39
5R	72	M	40.871	15.33	43.65	0.35	28.8	75.78	0.38
6R	72	F	35.66	13.47	37.54	0.36	25.5	83.1	0.30
7R	47	M	6.85	14.5	41.83	0.35	41.67	83.97	0.496

It is observed that orientation of CFL in subject 7R is almost closer to tibial shaft axis which may make the joint stiffer in inversion motion. Ratio of Sustentaculum length to Calcaneus length for subjects 4L and 7R are higher than other subjects and this is due to the fused anterior and medial facets of calcaneus.

Step 2: Changing the Morphological Parameters

Effect of change in orientation of CFL on mechanical behavior

Effect of change in orientation of CFL from vertical to horizontal on mechanical function such as Range of motion of AJC, flexibility of AJC and force in CFL are measured. A moment of 3400N-mm is applied in cycles to produce dorsiflexion/ plantarflexion, inversion/eversion and internal/external rotations one after the other. The statistical analysis to find the significance in the chaNges in mechanical behavior of AJC by changing orientation of CFL is calculated using Repeated measures ANOVA as described earlier under methodology section. All the data from the simulations is found to be normally distributed using Shapiro-Wilk test using SPSS^{TM} software.

Inversion/Eversion motion

Flexibility of AJC increased in inversion when the orientation of CFL is changed from vertical to horizontal (Figure 67). Using repeated measures ANOVA, flexibility of AJC

in all the subjects of AJC increased significantly with p=0.009 (p<0.05) by changing the orientation of CFL from vertical to horizontal with average value 0.0101 deg/N-mm (min 0.0055, max 0.0156) to 0.0187 deg/N-mm (min 0.0095, max 0.0279) (Figure 70). There is a significant change in flexibility between these orientations-vertical and original (p=0.034), vertical and 60 degrees (p=0.003), vertical and horizontal (p=0.034) and between 30 degrees and 60 degrees (p=0.002).

Inversion Range of motion increased gradually by changing the orientation of CFL from vertical to horizontal (Figure 67). Using repeated measures ANOVA, inversion ROM in all the subjects of AJC increased significantly with p=0.002(p<0.05) by changing the orientation of CFL from vertical to horizontal (Figure 73) with a mean difference of 9.16^{o} (min 4.05^{o}, max 14.27^{o}). Statistically except between orientations-original and 60^{o} and between orientations 60^{o} and horizontal, there is statistical significance in change in inversion ROM between all other orientations. There is significance between-vertical and 30 degrees (p=0.036), vertical and original (p=0.012), vertical and 60 degrees (p=0.015), vertical and horizontal (p=0.006), 30 degrees and original (p=0.032), 30 degrees and 60 degrees (p=0.019), 30 degrees and horizontal (p=0.013) and between original and horizontal (p=0.044).

By applying inversion motion force in the CFL decreased significantly with p=0.04 (p<0.05) as the orientation of ligament changed from vertical to horizontal (Figure 76) with a mean difference of 27.2 N (min 5.7N, max 48.7N) (Figure 79). Statistically there is a significant change in force between orientations-vertical and horizontal (p=0.023), vertical and 60 degrees (p=0.035), 30 degrees and original (p=0.036) and 30 degrees and horizontal (p=0.036).

By applying eversion motion there is no significant change in Eversion ROM, flexibility or force in CFL with change in orientation of CFL (Figure 67, Figure 70, Figure 73, Figure 76 and Figure 79).

Internal Rotation

In all the six subjects there is a slight increase in ROM of AJC with p=0.04 in internal rotation by changing the orientation of CFL from vertical to horizontal by a mean difference of 3.6^o (min 0.32^o, max 6.93^o) (Figure 68). Statistically there is significance in the change in ROM between vertical and horizontal orientations (p=0.037) and between vertical and 60^o orientation (p=0.043) (Figure 74).

By applying internal motion Forces in the CFL decreased significantly with p=0.011 ($p<0.05$) as the orientation of ligament changed from vertical to horizontal with a mean difference of 32 N and standard error (min 8.7N, max 55.5N) (Figure 76). Statistically there is a significant change in force between the following orientation of CFL-vertical and 30 degrees (p=0.035), vertical and original (p=0.027), vertical and 60 degrees (p=0.023) and vertical and horizontal (p=0.017) (Figure 80). There is no significant change in flexibility of AJC with change in orientation of CFL in internal rotation (Figure 68 and Figure 71).

External Rotation

In all the subjects there is a slight decrease in ROM of AJC with p=0.023 in external rotation by changing the orientation of CFL from vertical to horizontal by a mean difference of 5.8^o (min 0.483N, max 11.19N) (Figure 68). Statistically there is

significance in the change in ROM between the following orientations- vertical and original (p=0.044), vertical and 60 degrees (p=0.037), vertical and horizontal (p=0.038), 30 degrees and 60 degrees p=p=0.037), 30 degrees and horizontal (p=0.046) and original and 60 degrees (p=0.035) (Figure 74).

By applying external motion forces in the CFL increased as the orientation of ligament changed from vertical to horizontal with a mean difference of 39.8 N (min 20.22N, max 59.44N) (Figure 77) with p=0.011. Statistically there is a significant change in force between orientations vertical and 60 degrees (p=0.01) and vertical and horizontal (p=0.003) (Figure 80). There is no significant change in flexibility of AJC with change in orientation of CFL in External rotation.

Dorsiflexion/Plantarflexion

Statistically there are no significant difference in ROM of AJC, Flexibility of AJC and force in CFL ligament in Dorsiflexion or Plantarflexion with change in the orientation of CFL from vertical to horizontal (Figure 69**,** Figure 72, Figure 75, Figure 78 and Figure 81).

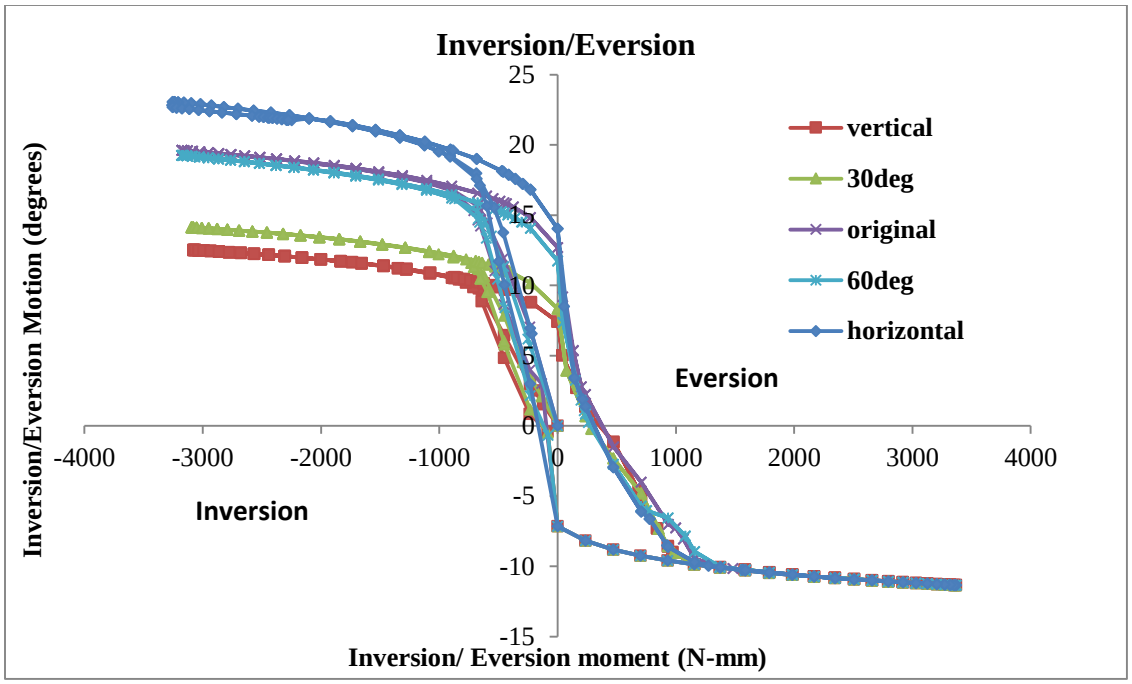

Figure 67. Change in load-displacement characteristics of AJC in inversion / eversion with change in orientation of CFL for subject 5L

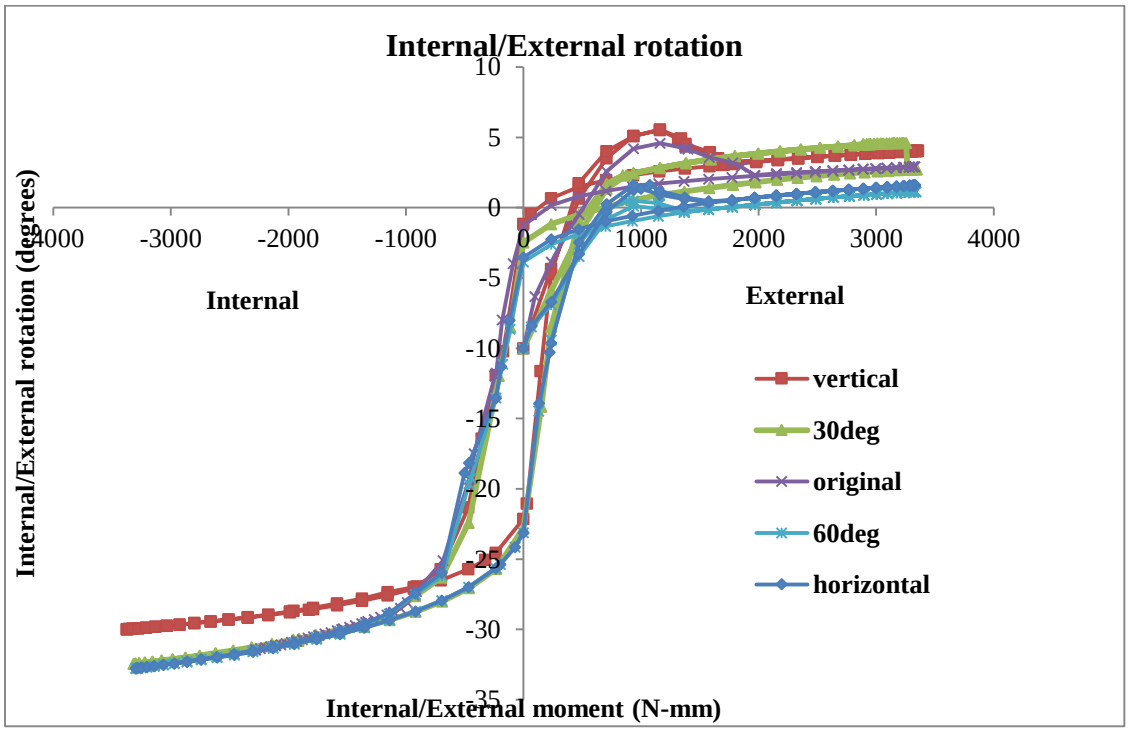

Figure 68. Change in load-displacement characteristics of AJC in internal / external rotation with change in orientation of CFL for subject 5L

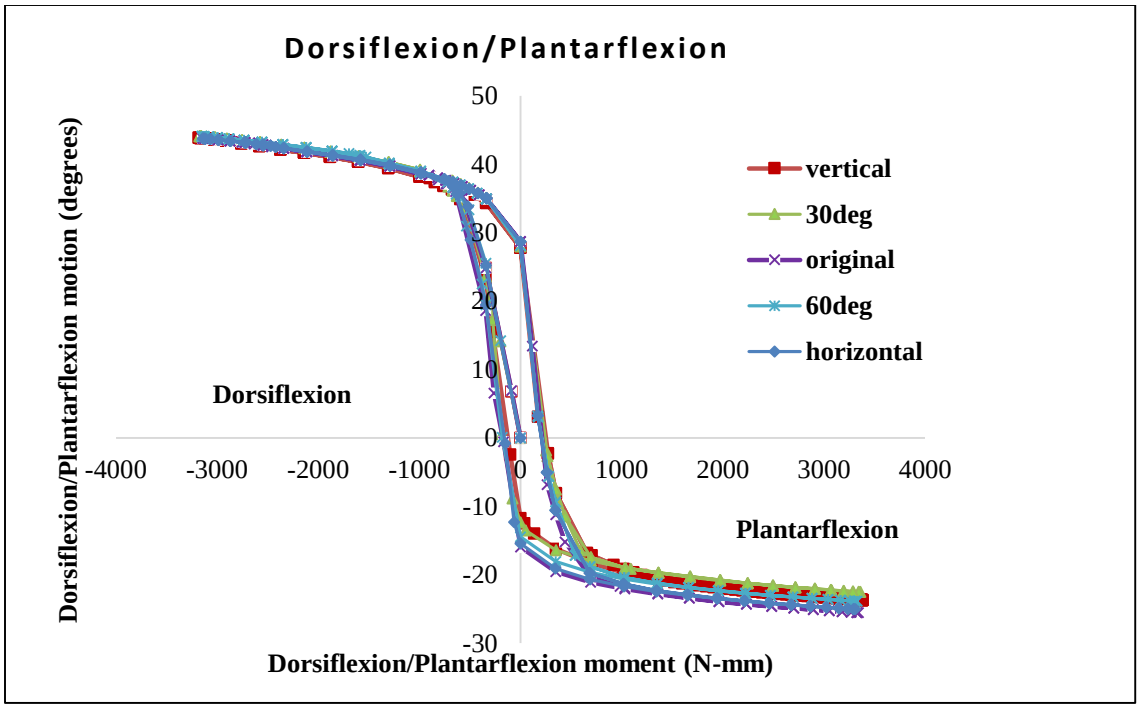

Figure 69. Change in load-displacement characteristics of AJC in dorsiflexion / plantarflexion with change in orientation of CFL for subject 5L

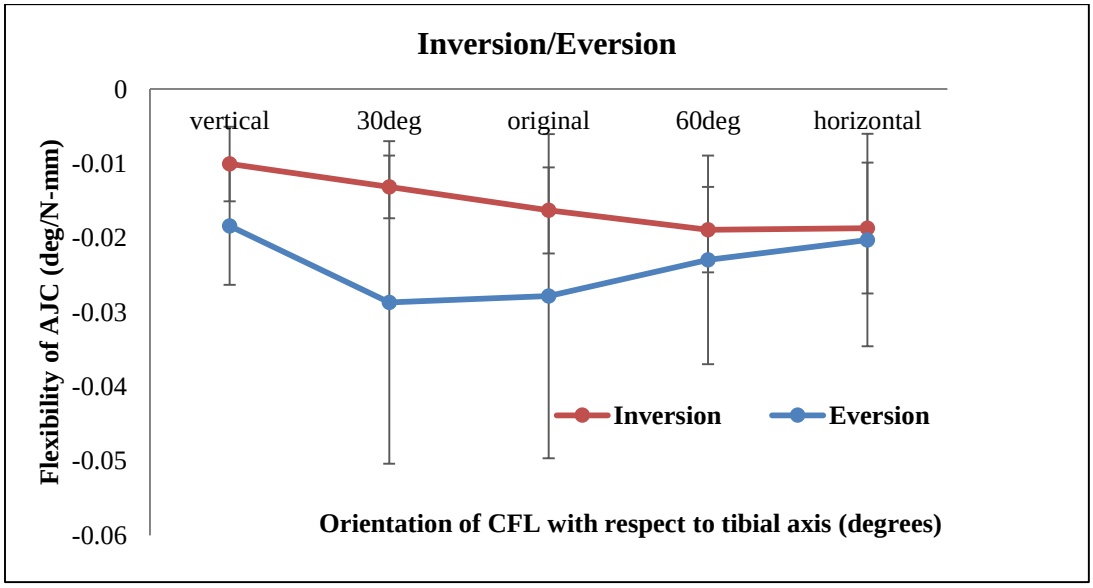

Figure 70. Change in load-displacement characteristics of AJC in inversion / eversion in all subjects

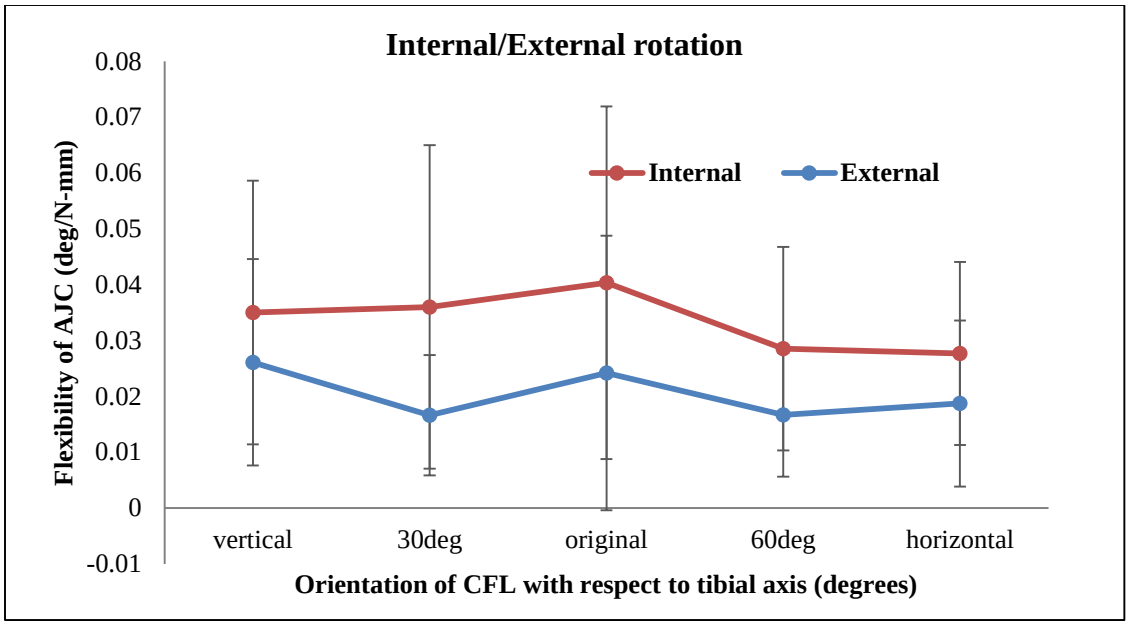

Figure 71. Average change in flexibility of AJC in internal / external rotation in all subjects

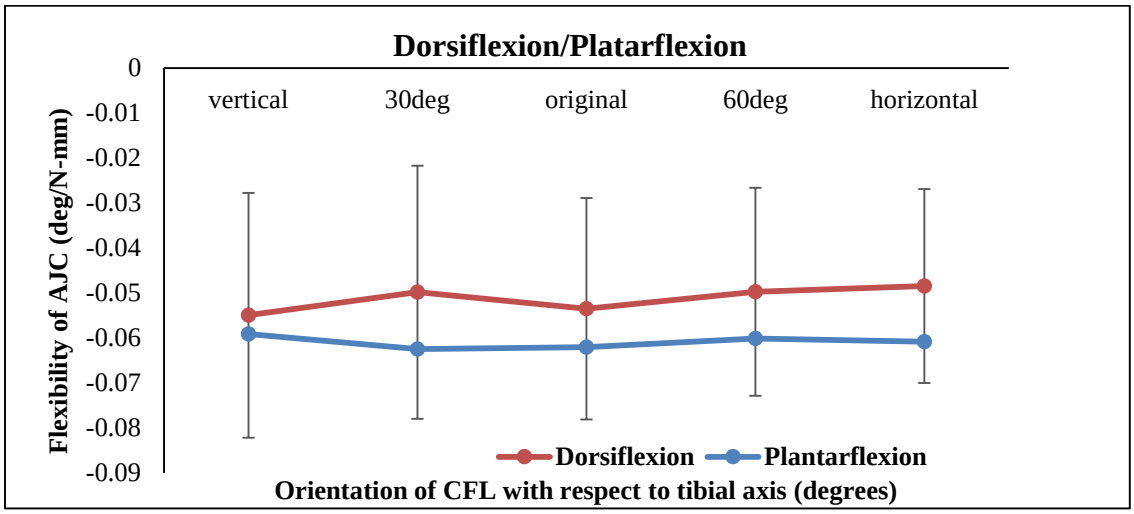

Figure 72. Average change in flexibility of AJC in dorsiflexion / plantarflexion in all subjects

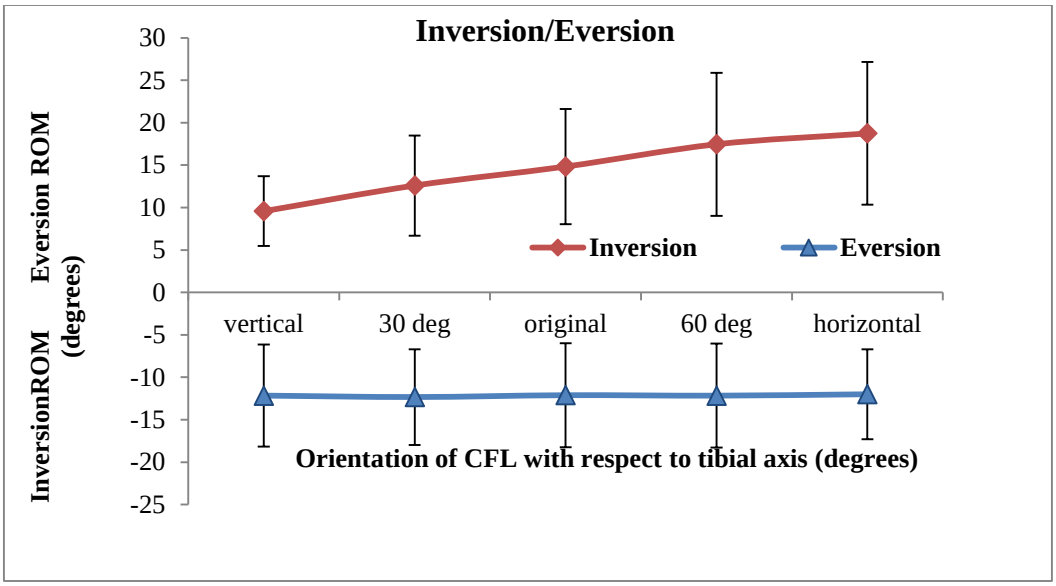

Figure 73. Average change in ROM of AJC with change in orientation of CFL in inversion / eversion in all subjects.

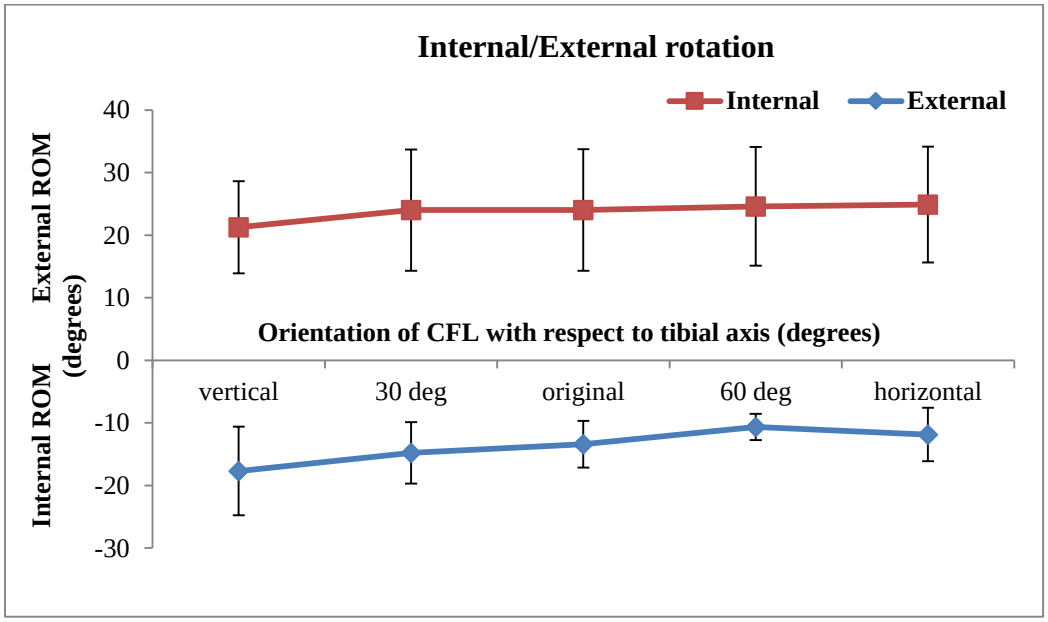

Figure 74. Average change in ROM of AJC in internal / external rotation in all subjects.

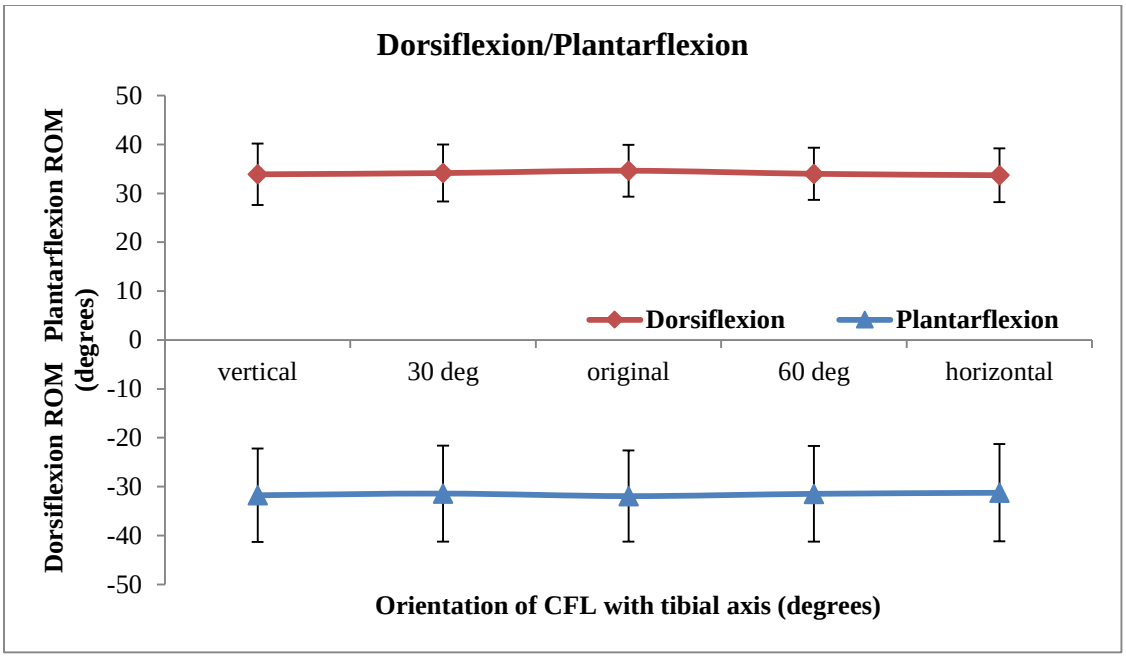

Figure 75. Average change in ROM of AJC in dorsiflexion / plantarflexion in all subjects.

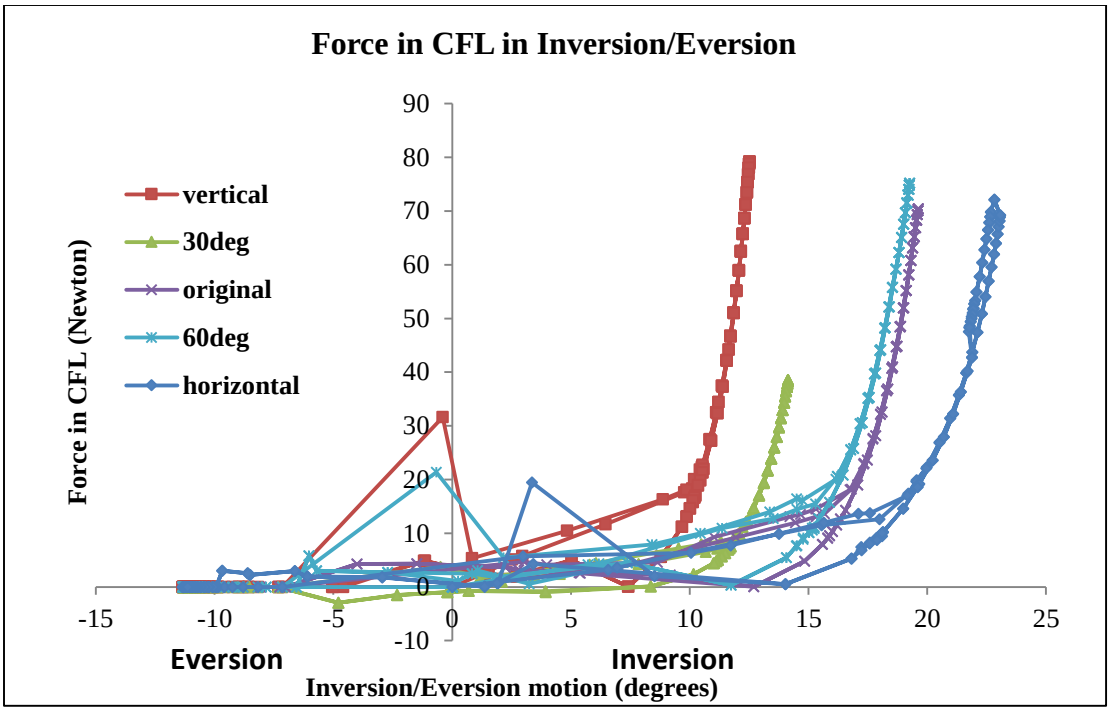

Figure 76. Change in force in CFL in inversion / eversion motion with change in orientation of CFL for subject 5L

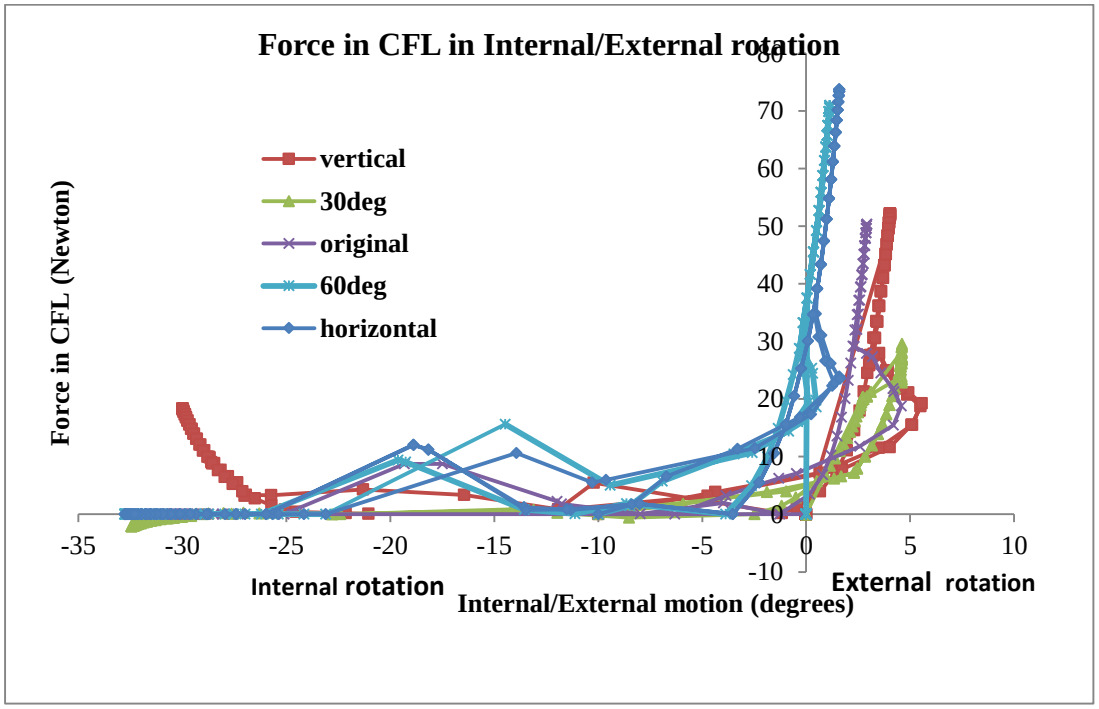

Figure 77. Change in force in CFL in inversion / eversion motion with change in orientation of CFL for subject 5L

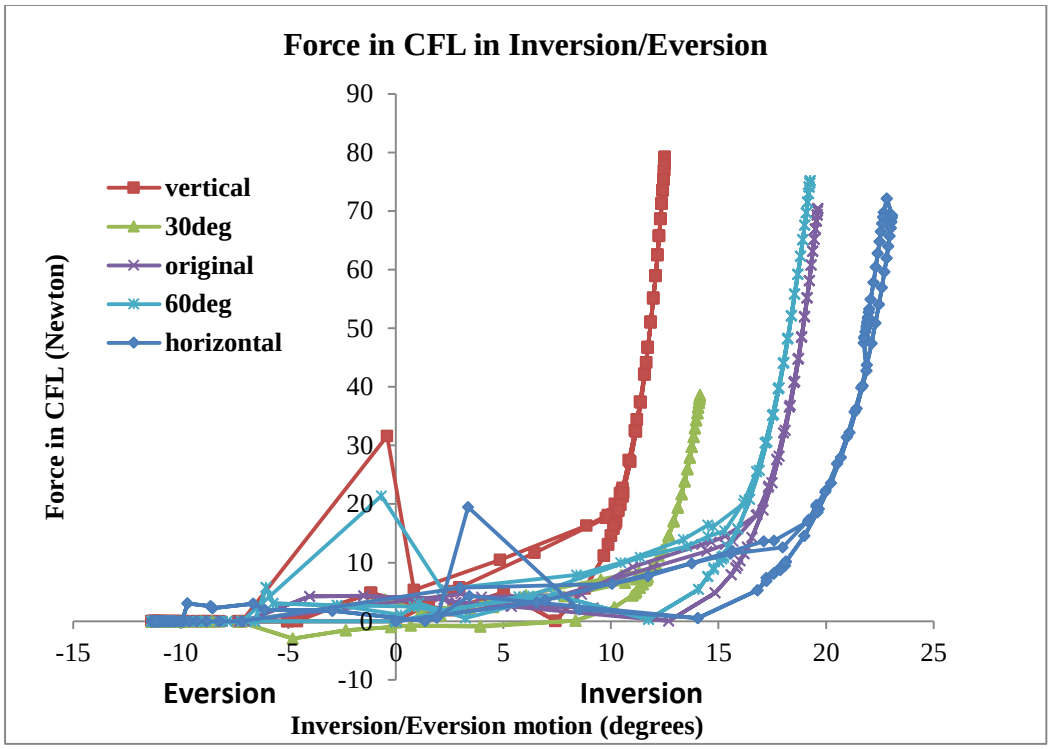

Figure 78. Change in force in CFL in inversion / eversion motion with change in orientation of CFL for subject 5L

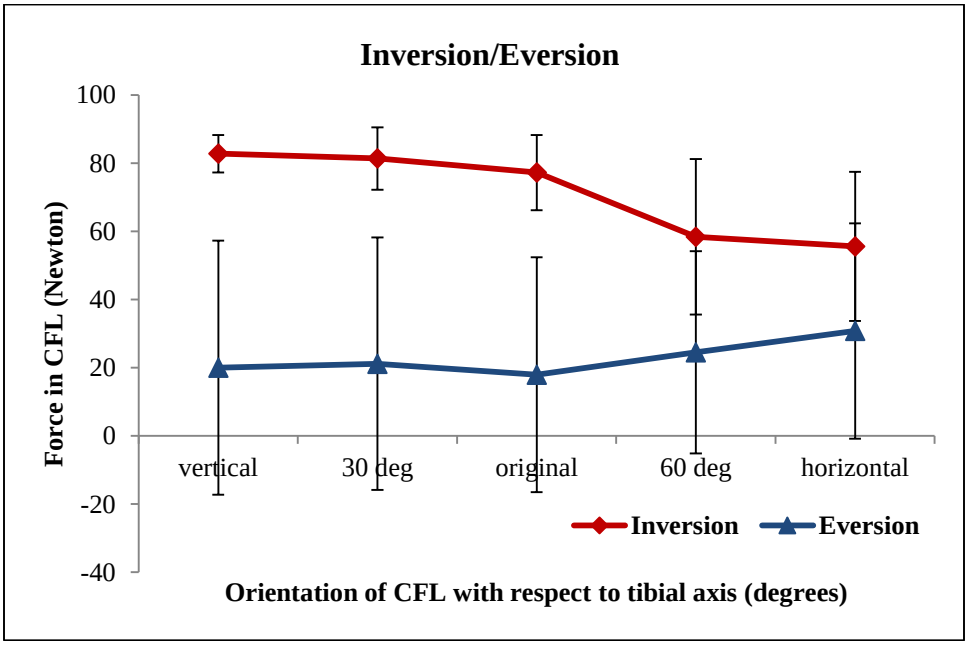

Figure 79. Average change in force in CFL with change in orientation of CFL at ROM in inversion / eversion in all subjects

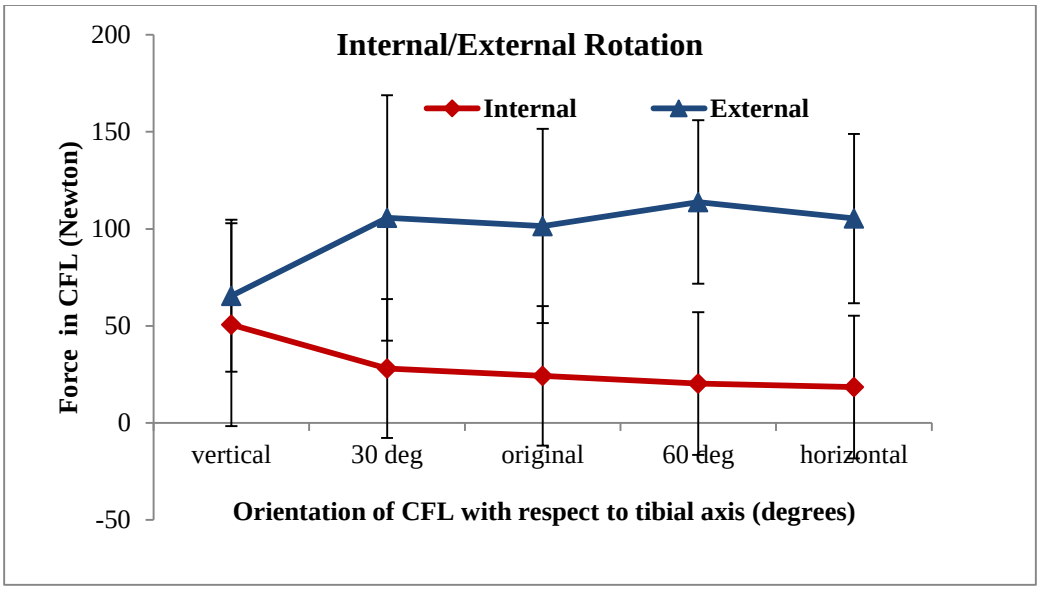

Figure 80. Average change in force in CFL with change in orientation of CFL at ROM in internal / external rotation in all subjects

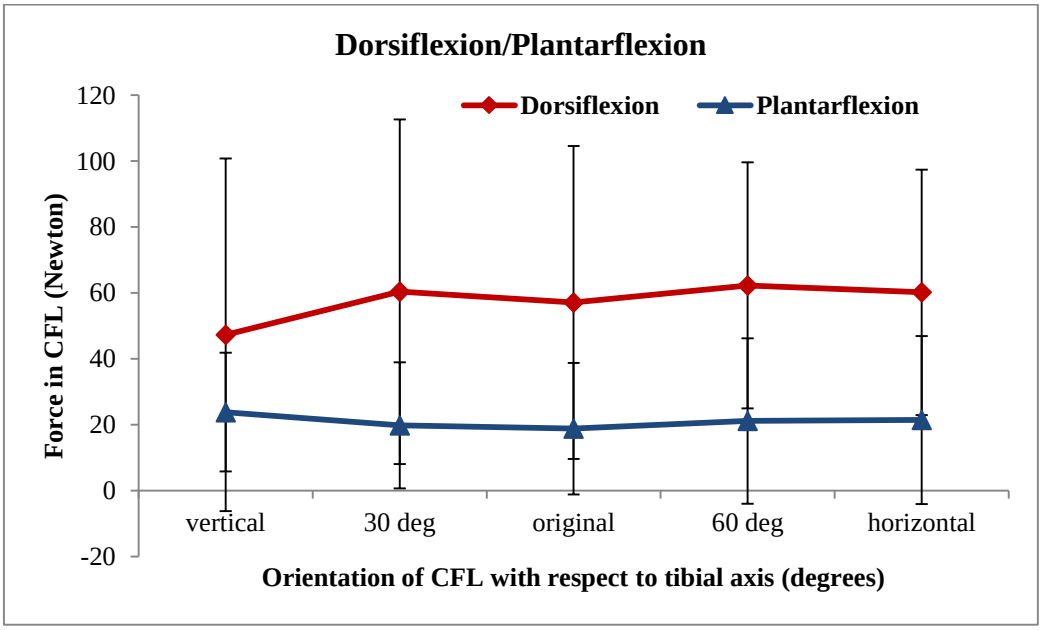

Figure 81. Average change in force in CFL with change in orientation of CFL at ROM in dorsiflexion / plantarflexion in all subjects

Effect of Change in Morphology of Sustentaculum Tali on Joint Mechanical Behavior

The morphology of sustentaculum tali is changed by reducing volume in 4 stages as described in Chapter 3. The effect of this change on mechanical function such as flexibility of AJC, ROM of AJC and force in ligament is calculated by applying moment of 3400 N-mm in inversion/eversion, internal/external and dorsiflexion/plantarflexion. The statistical analysis to find the significance in the chnages in mechanical behavior of AJC by changing morphology of sustentaculum tali is calculated using Repeated measures ANOVA as described earlier under methodology section. All the data from the simulations is found to be normally distributed using Shapiro-Wilk test using SPSS^{TM} software.

Inversion/Eversion Motion

By applying inversion motion there is decrease in average flexibility of AJC for all the subjects after the sustentaculum tali is removed but this is not a statistically significant change (Figure 82 and Figure 85). The inversion ROM is increased at AJC by removing the sustentaculum tali (Figure 82). In subject 7R, alteration 1 has approximately 1 degree increase in inversion ROM. There is a rise in inversion ROM from alteration 1 to 2 by 5 degrees. Alteration 3 has 2 degrees increase in inversion ROM after alteration 2. Alteration 4 has no more effect than alteration 3. Statistically, in all the six subjects inversion ROM of AJC increased significantly with $p=0.002$ ($p<0.05$) by removing the sustentaculum tali (Figure 88) with a mean difference of 4.5^{o} (min 2.84^{o}, max 6.3^{o}). There is no significant change in inversion ROM by following alterations 1 and 2. There is a

significant increase by following alteration 3 (p=0.004) by removing the medial-side posterior articulating facet extension. There is no further change by alteration 4 where sustentaculum tali is fully removed.

There is increase in force in CFL at ROM in some subjects and decrease in others but on overall there is decrease in average force in CFL for all the subjects by removing the sustentaculum tali but it is not statistically significant (Figure 91 and Figure 94). There is no significant change in eversion ROM, flexibility of AJC or the forces in CFL by removing sustentaculum tali during eversion (Figure 82, Figure 85, Figure 88, Figure 91 and Figure 94).

Dorsiflexion/Plantarflexion Motion

In dorsiflexion, there is increase in average flexibility of AJC of all the subjects by removing sustentaculum tali but this change is not statistically significant (Figure 87).

In dorsiflexion there is a significant increase in ROM by removing sustentaculum tali. Figure 85 shows the change in ROM of AJC in dorsiflexion for subject 7R. Statistically, in all six subjects average ROM during Dorsiflexion increased significantly (p=0.006) by removing the sustentaculum tali with a mean difference of 11^{o} (min 3.33^{o}, max 18.8^{o}). There is a significant change in dorsiflexion ROM by following alterations 1 where the ROM increased by mean value of 8.12^{o} (min 1.82^{o}, max 14.41^{o}). The significant change ($p<0.05$) is seen between original and all other alterations but not between each alteration (Figure 90). Also it is observed that there is a significant change in forces of CFL by removing sustentaculum tali (p=0.047) (Figure 94). Forces in CFL increased during

dorsiflexion by removing sustentaculum tali with a mean value of 79.8N (min 9N, max 150.7N). The significance is only between original and final alteration of removing sustentaculum tali completely (p=0.034) (Figure 96). There is no significant change in plantarflexion ROM of AJC, flexibility of AJC or Force in CFL by removing sustentaculum tali (Figure 84, Figure 87, Figure 90, Figure 93 and Figure 96).

Internal/External Motion

There are no statistically significant changes in ROM of AJC, flexibility of AJC or Force in CFL during internal and external motions by removing the sustentaculum tali (Figure 83, Figure 86, Figure 89, Figure 92, Figure 95).

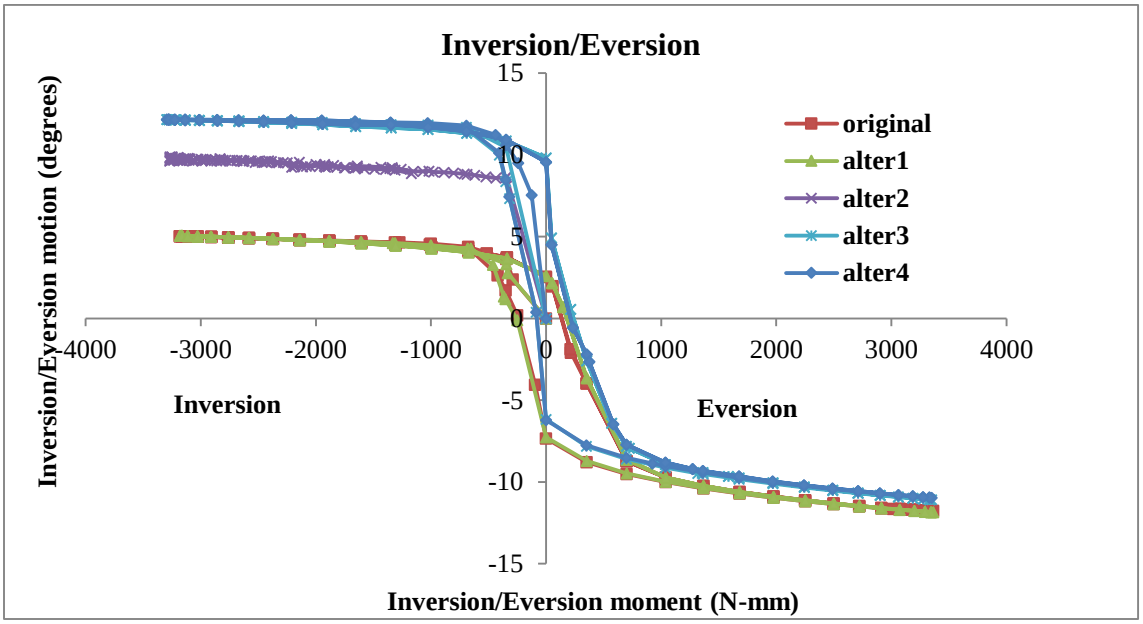

Figure 82. Change in load-displacement characteristics of AJC in inversion / eversion with change in morphology of sustentaculum tali for subject 7R.

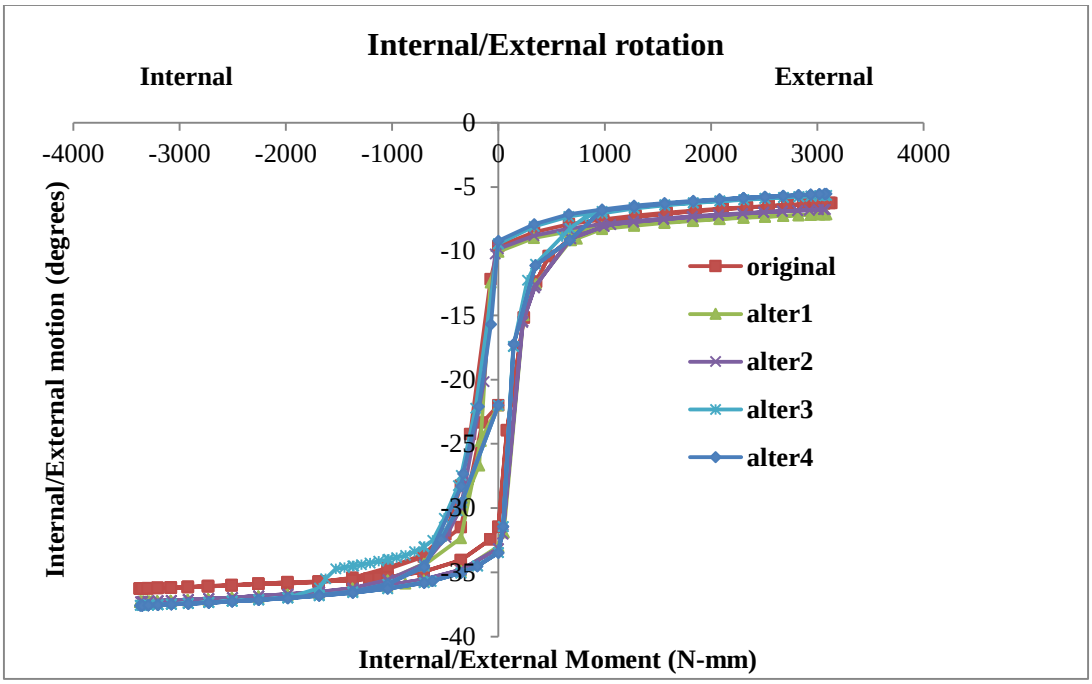

Figure 83. Change in load-displacement characteristics of AJC in internal / external rotation with change in morphology of sustentaculum tali for subject 7R

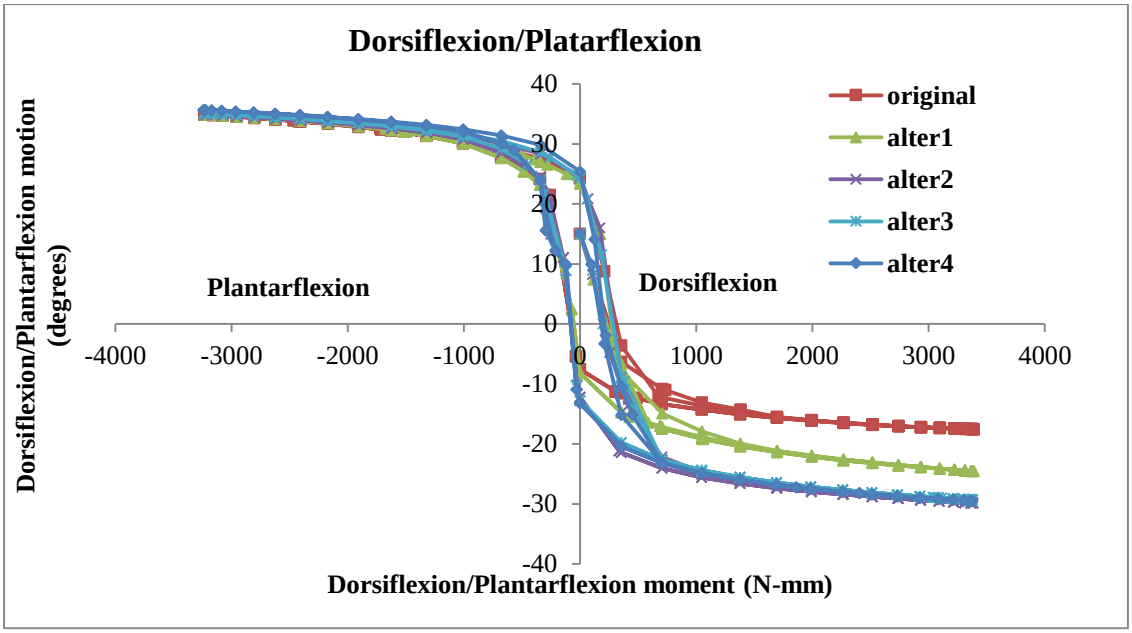

Figure 84. Change in load-displacement characteristics of AJC in dorsiflexion / plantarflexion by changing the morphology of sustentaculum tali for subject 7R

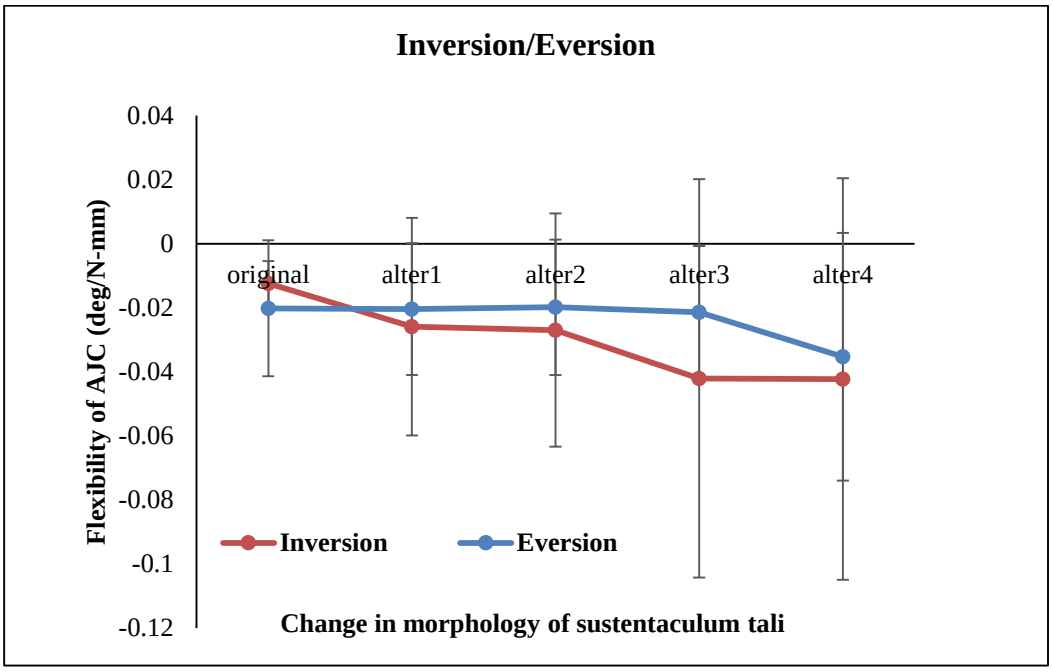

Figure 85. Average change in flexibility of AJC with change in morphology of sustentaculum tali in inversion / eversion in all the subjects

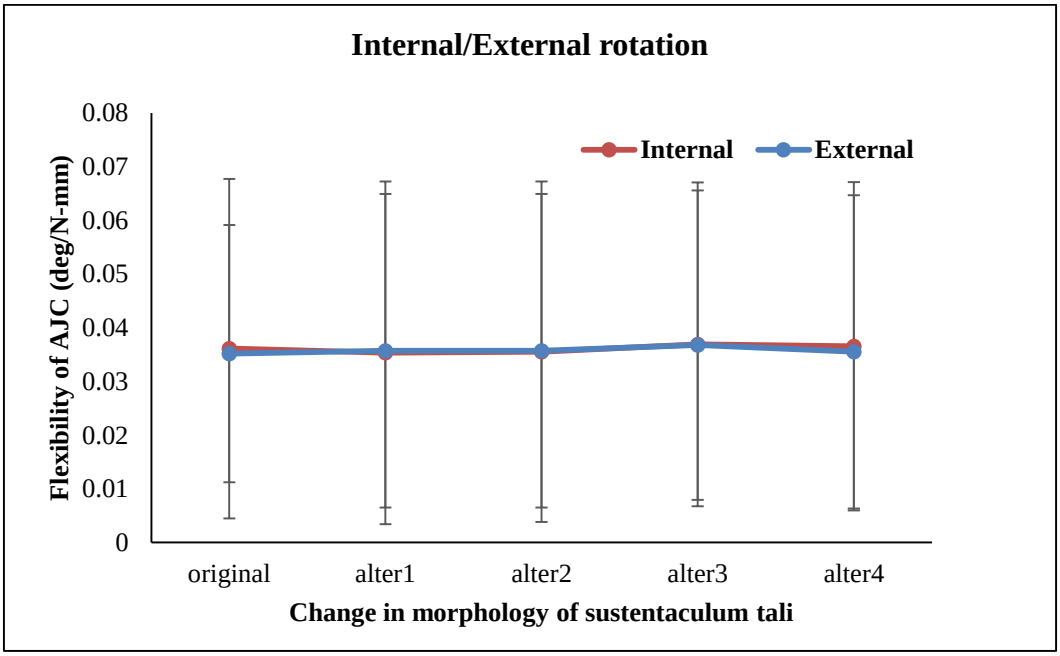

Figure 86. Average change in flexibility of AJC with change in morphology of sustentaculum tali in internal / external rotation in all the subjects

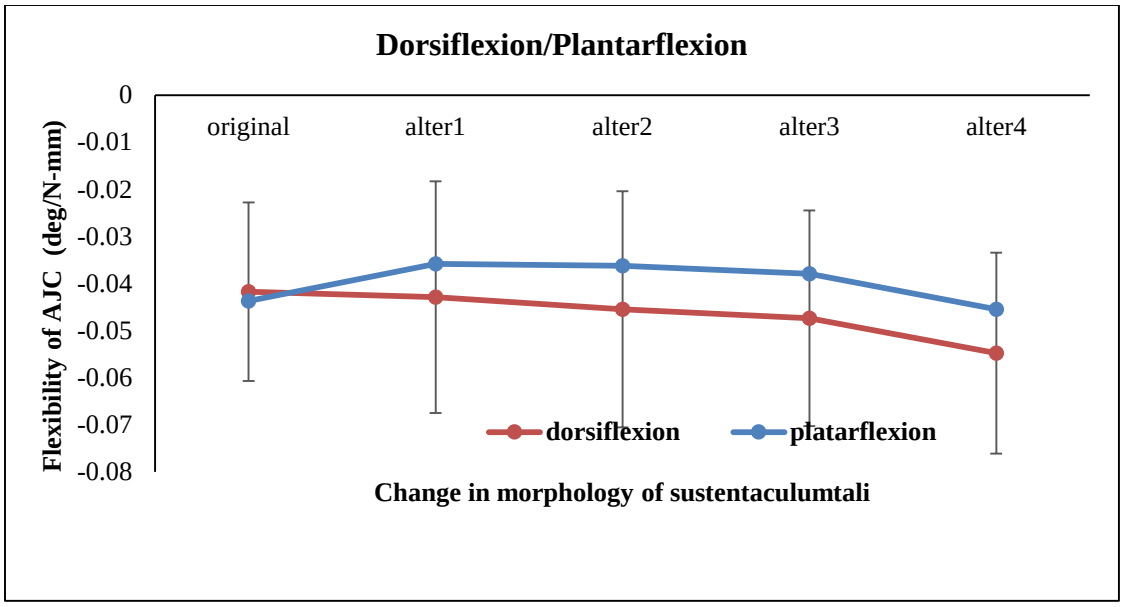

Figure 87. Average change in flexibility of AJC with change in morphology of sustentaculum tali in dorsiflexion / plantarflexion in all the subjects

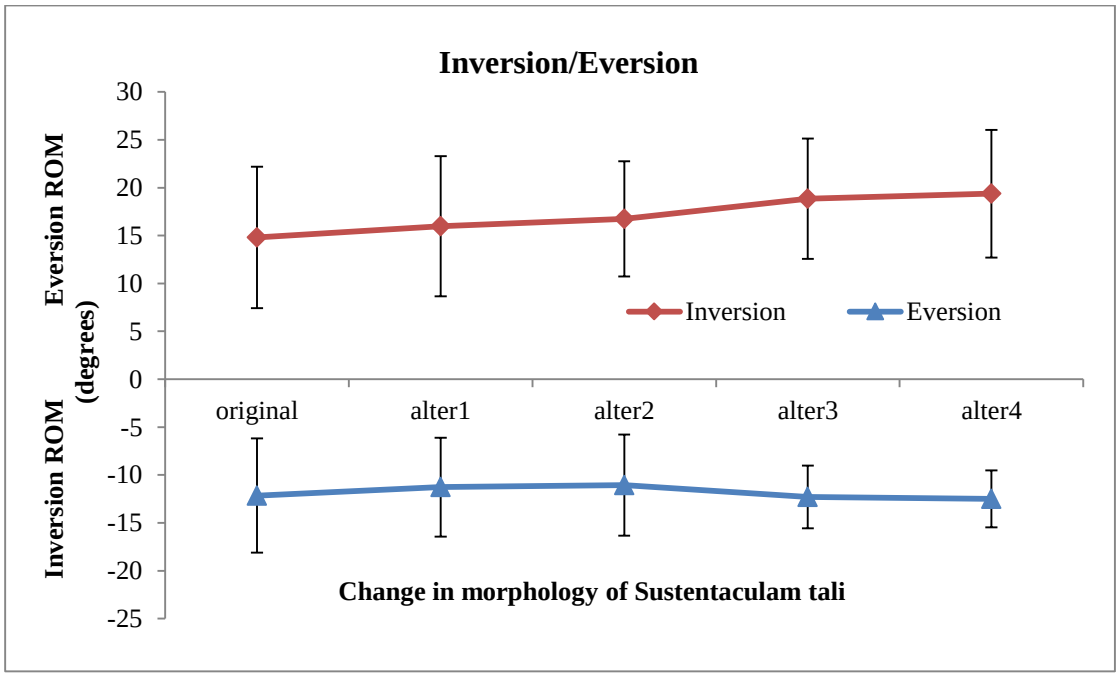

Figure 88. Average change in ROM of AJC with change in morphology of sustentaculum tali in inversion / eversion in all the subjects

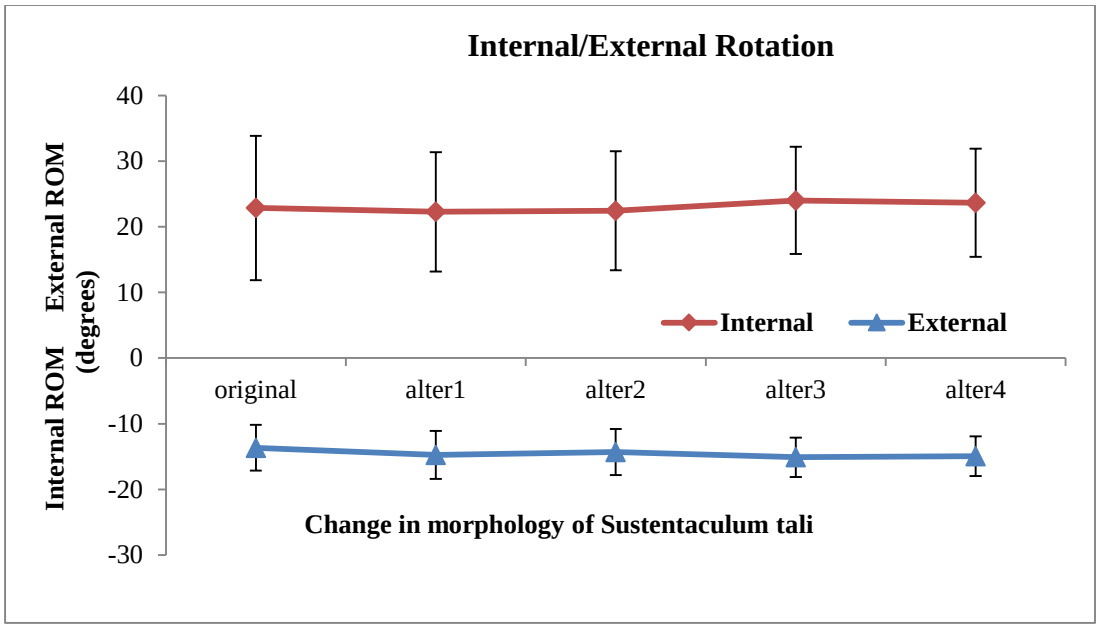

Figure 89. Average change in ROM of AJC with change in morphology of sustentaculum tali in internal / external rotation in all the subjects.

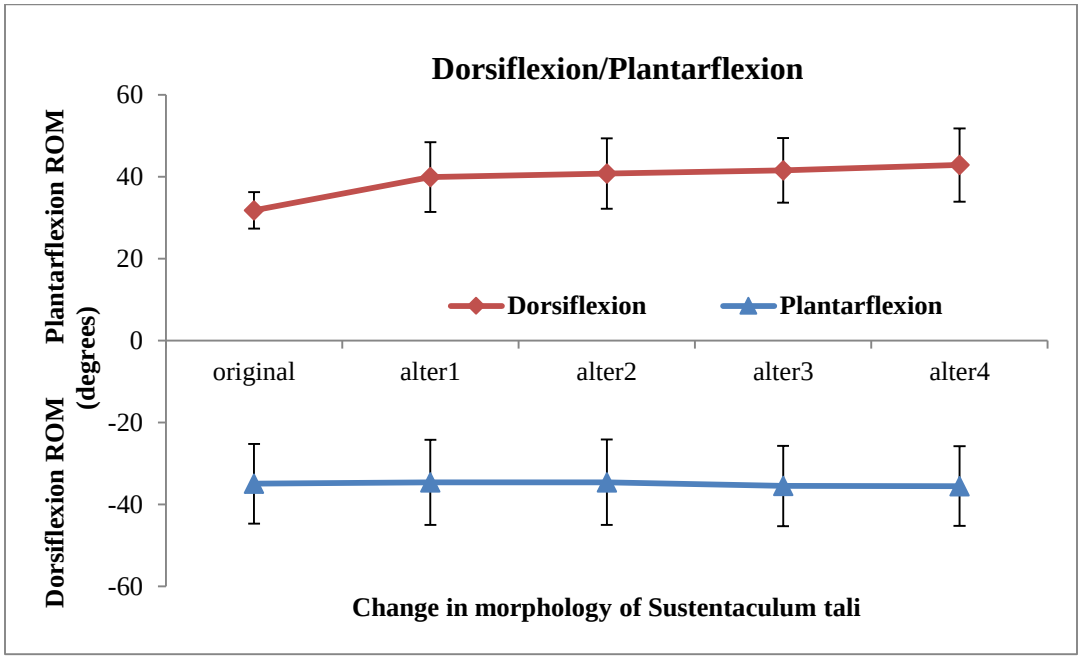

Figure 90. Average change in ROM of AJC with change in morphology of sustentaculum tali in dorsiflexion / plantarflexion in all the subjects

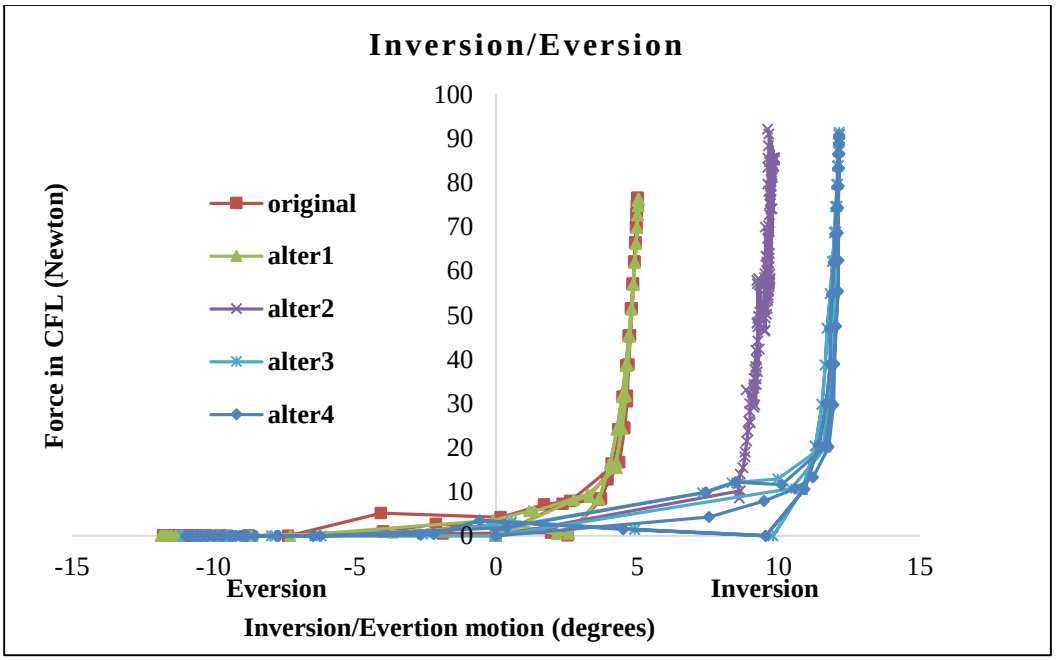

Figure 91. Change in force in CFL in inversion / eversion by changing the morphology of sustentaculum tali for subject 7R

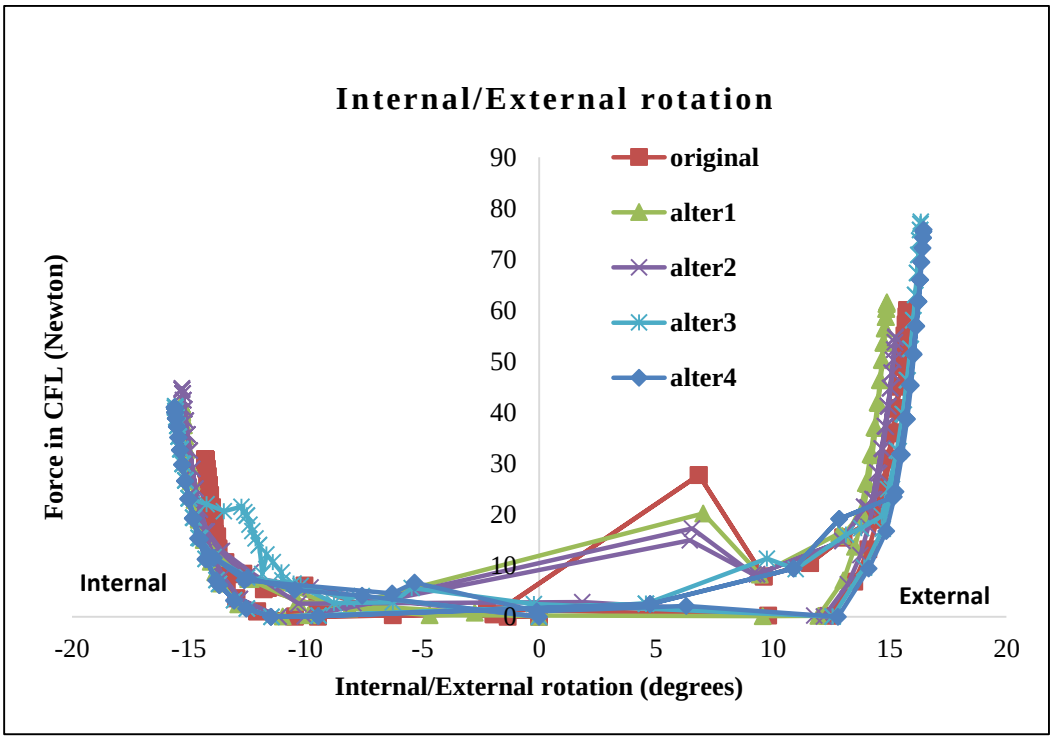

Figure 92. Change in force in CFL in internal / external rotation by changing the morphology of sustentaculum tali for subject 7R

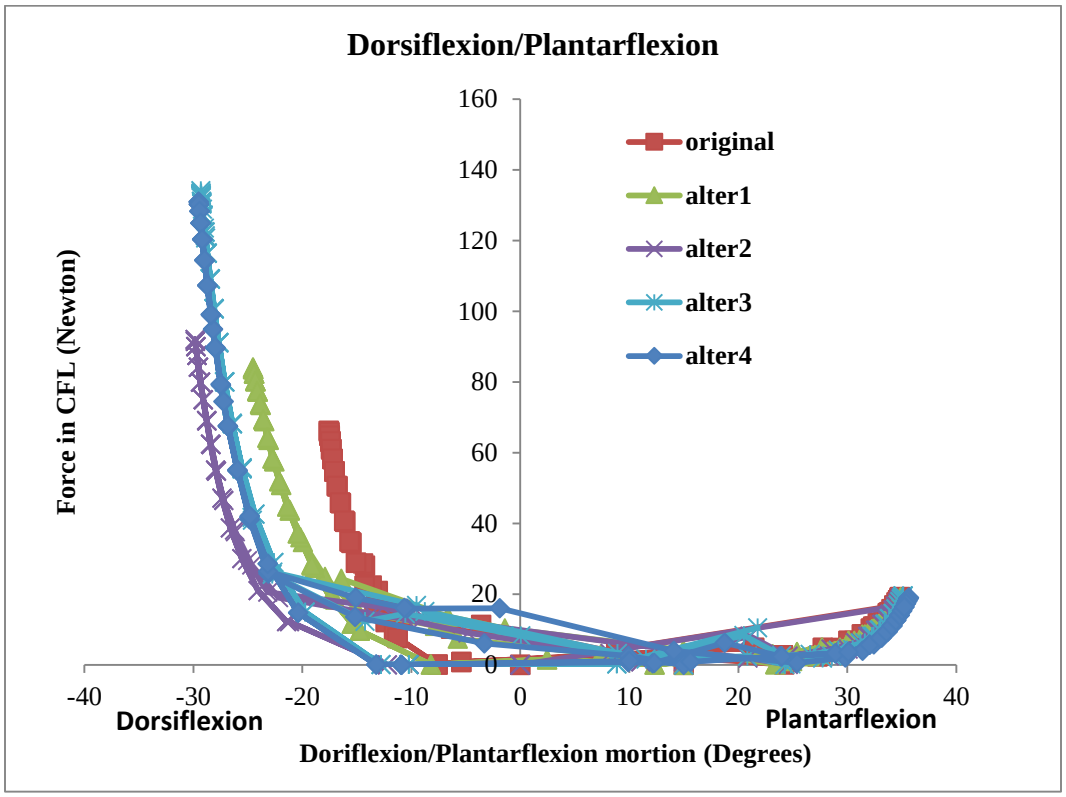

Figure 93. Change in force in CFL in dorsiflexion / plantarflexion by changing the morphology of sustentaculum tali for subject 7R

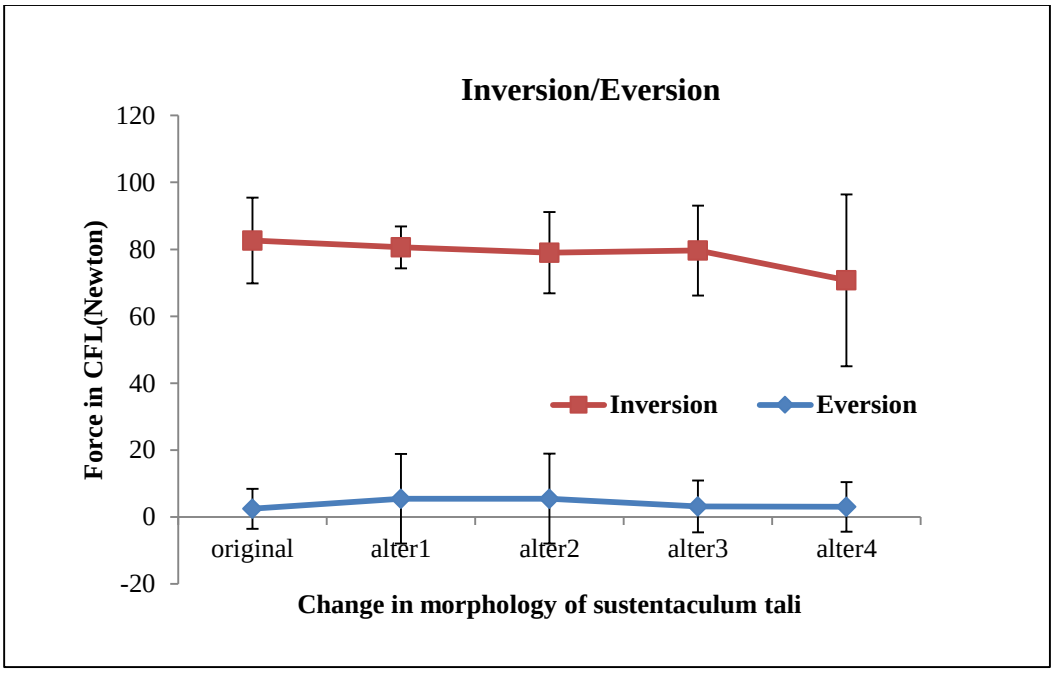

Figure 94. Average change in force in CFL with change in morphology of sustentaculum tali in inversion / eversion in all the subjects

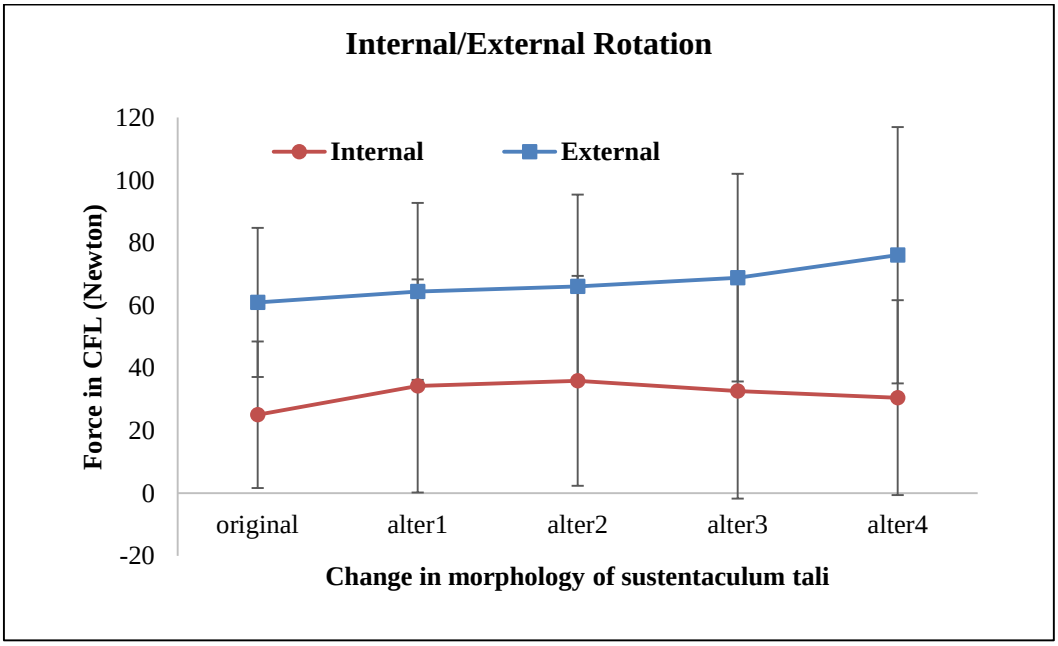

Figure 95. Average change in force in CFL with change in morphology of sustentaculum tali in internal / external rotation in all the subjects

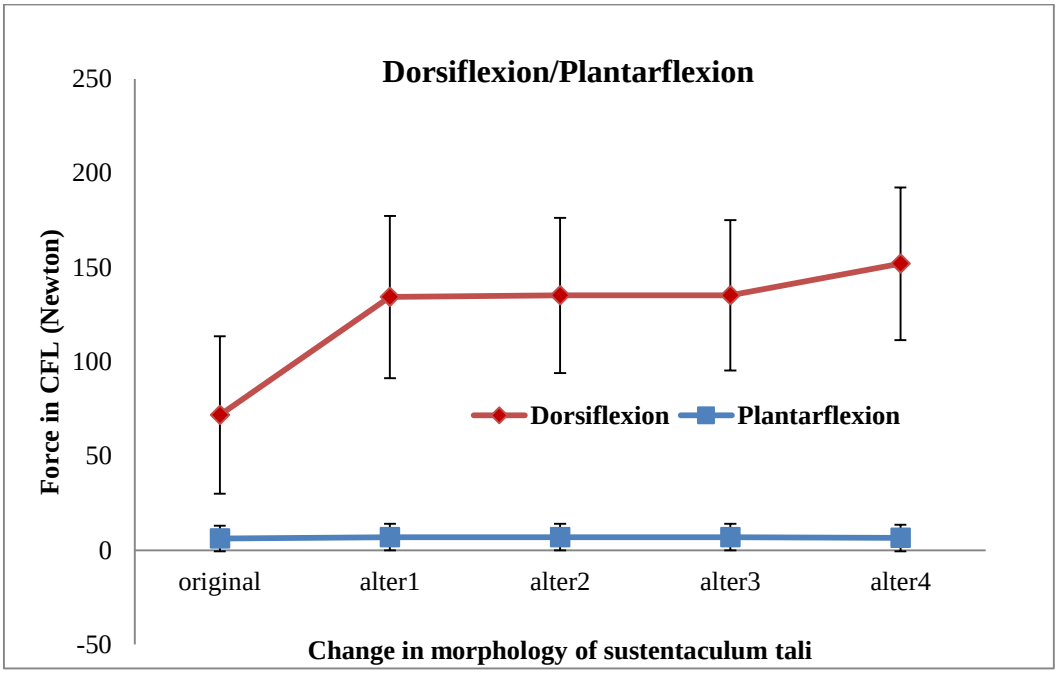

Figure 96. Average change in force in CFL with change in morphology of sustentaculum tali in dorsiflexion / plantarflexion in all the subjects

Variations in Regions of Contact between Talus and Calcaneus after Change in Morphology of Sustentaculum tali

Distance maps are calculated to determine the change in contact region between talus and calcaneus after each morphological change in calcaneus as described in Figure 48. The following conclusions are made from the results (Figure 97).

Alteration 1: There is a loss of support at the anterior talar articulating facet of calcaneus after alteration 1. Talus is supported mainly at the posterior side of middle articulating facet and medial side of posterior articulating facet.

Alteration 2: There is loss of support at the posterior side of middle articulating facet and the talus is supported mainly by medial side of posterior articulating facet.

Alteration 3: There is a loss of support at the medial side of posterior articulating facet. The talus is completely supported by the posterior articulating facet.

Alteration 4: There is no much change with this alteration.

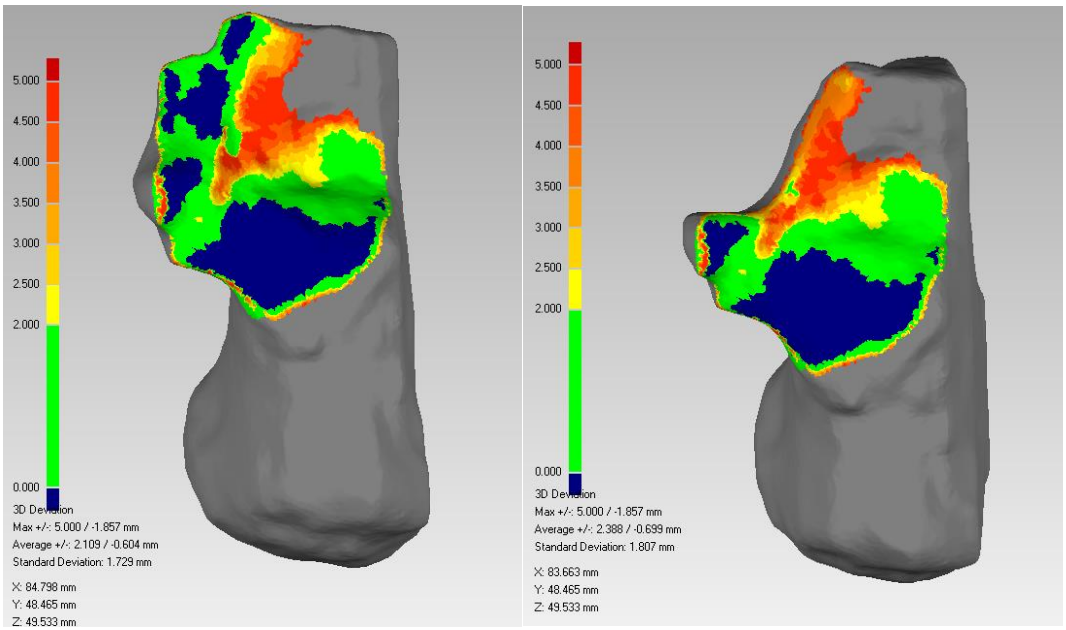

Original **Alteration1**

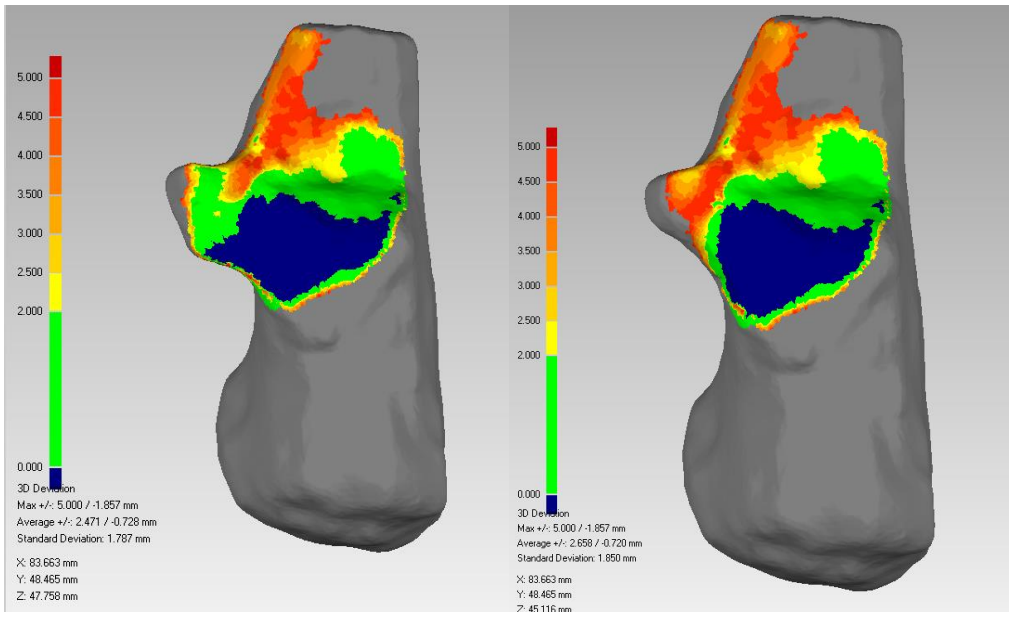

Alteration 2 **Alteration 3**

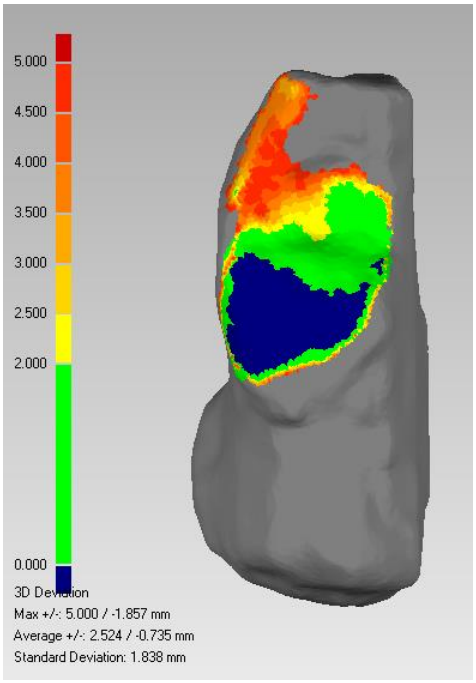

Alteration4

Figure 97. Variations in regions of contact between talus and calcaneus after change in morphology of sustentaculum tali. Blue regions indicate the regions of contact between talus and calcaneus.

Hip Joint

Step 1: Comparing Morphological Parameters between FAI and Normal hips

Twenty seven morphological parameters representing common clinical parameters for the acetabulum, femur, and acetabulum-femur relations were measured from the 3D bone models. These parameters are compared using statistical analysis as described below.

Statistical Analysis

A correlation analysis is used to find if any of these parameters are correlated and it is found that acetabular depth and acetabular index, acetabular diameter and femoral head diameter, spherical index of femur and femoral head neck offset, extrusion index and index of femoral head coverage, femoral neck width and femoral head diameter the correlation is significant at 0.01 level, between alpha angle and femoral head diameter, alpha angle and femoral head neck offset, peak edge distance and acetabular diameter the correlation is significant at 0.05 level (<0.02). A one way ANOVA is performed to determine which clinical parameters are significantly different between normal and FAI hips (Table 7).

Table 7. Variations in morphological parameters between FAI and normal subjects

Table:			Mean	Std. Deviation	Sig.
Acetabulum	Apparent acetabular depth	FAI	19.4296	5.02468	0.073
		NORMAL	23.5633	3.06703	
		Total	21.1317	4.7039	
	Ace Width	FAI	53.8806	5.24483	0.032
		NORMAL	47.4309	5.96774	
		Total	51.2248	6.28763	
	Acetabular index	FAI	0.3634	0.09835	0.006
		NORMAL	0.5006	0.06639	
		Total	0.4199	0.10924	
	ACM angle	FAI	50.9839	4.14272	0.355
		NORMAL	48.1556	8.04219	
		Total	49.8193	5.99718	
	Acetabular roof angle	FAI	14.1925	3.03868	0.995
		NORMAL	14.1824	2.85052	
		Total	14.1884	2.87071	
	Sharp angle	FAI	41.889	3.42979	0.547

		NORMAL	40.5593	5.50861	
		Total	41.3415	4.29549	
	Peak to edge distance	FAI	18.8493	4.31084	0.029
		NORMAL	14.5456	2.22876	
		Total	17.0772	4.13311	
	Femur neck length	FAI	105.5074	6.00844	0
Femur		NORMAL	67.5284	21.43228	
		Total	89.869	23.74378	
	Femur neck width	FAI	35.8887	5.05409	0.004
		NORMAL	28.4977	3.45029	
		Total	32.8454	5.73506	
	Trochanteroarticular distance	FAI	19.3888	9.68724	0.786
		NORMAL	18.1987	7.10071	
		Total	18.8988	8.48873	
	Neck neck-shaft angle	FAI	125.8877	3.5087	0.539
		NORMAL	127.1051	4.4952	
		Total	126.389	3.85797	
	Spherical index of head of femur	FAI	0.4716	0.0387	0.185
		NORMAL	0.5113	0.07844	
		Total	0.4879	0.05963	
	Alpha angle	FAI	65.6048	14.68423	0.006
		NORMAL	39.9873	18.70105	
		Total	55.0564	20.52628	
	Beta angle	FAI	50.9819	14.51004	0.236
		NORMAL	43.9029	4.77781	
		Total	48.067	11.82736	
Pelvis	Distance between two teardrops	FAI	112.5986	7.16922	0.036
		NORMAL	128.558	4.52265	
		Total	117.1584	9.91553	
	Distance between two head centers	FAI	179.9646	16.31918	0.652
		NORMAL	175.3565	11.82535	
		Total	177.9166	13.83821	
	Distance between ischialtuberosites	FAI	137.119	9.04015	0.454
		NORMAL	131.467	4.42225	
		Total	135.5041	8.08383	
	Pelvic height	FAI	205.7928	21.28005	0.407
		NORMAL	196.061	14.18464	

		Total	201.3693	18.24093	
Relation between acetabulum and femur	Lateral subluxation	FAI	6.2359	1.73984	0.78
		NORMAL	6.0096	1.39841	
		Total	6.1427	1.565	
	Superior subluxation	FAI	-6.5904	2.98028	0.526
		NORMAL	-5.3024	5.21253	
		Total	-6.0601	3.9512	
	Center edge angle	FAI	38.1658	5.56474	0.877
		NORMAL	38.5747	4.79162	
		Total	38.3342	5.10602	
	MZ distance	FAI	4.6826	1.77278	0.99
		NORMAL	4.6961	2.82364	
		Total	4.6882	2.18121	
	Articulotrochanteric distance	FAI	19.3888	9.68724	0.786
		NORMAL	18.1987	7.10071	
		Total	18.8988	8.48873	
	Extrusion index	FAI	31.2744	11.07502	0.242
		NORMAL	25.6602	5.92688	
		Total	28.9627	9.50151	

All distances are in mm and angles are in degrees.

Morphological parameters such as acetabular index, acetabular head diameter, femoral head diameter, femoral neck width, femoral neck length and alpha angle have significant differences between normal and FAI hips with significance $p(<0.05)$.

Comparing Interference Pattern between FAI and Normal

Distance maps are calculated for all FAI and normal subjects and are compared (Figure 98). The average distances are measured in zones that have contact throughout the simulation using distance maps and are plotted to compare the values (Figure 99 and

Figure 100). Further, percentage area of impingement is calculated and compared in each zone between FAI and normal subjects (Figure 101 and

Figure 102).

The FAI subjects had interference as early as 80^{o} flexion in some subjects and going through 100^{o} flexion combined with 20^{o} adduction and 40^{o} internal rotation (Figure 99). For the normal subjects, out of 7, 3 subjects did not have impingement throughout the simulation. 2 subjects have impingement at extreme range of motion i.e., at 100 degree flexion, 20 degree adduction and 40 degree internal rotation and 2 subjects has impingement starting with 100 degree flexion with 10 degree adduction (Figure 100). Also plotting the frequency of subjects that has impingement in each zone (Figure 103) shows that for FAI subjects the contact is in zones 6L, 1L and 2L which shows the impingement occurred in anterior inferior region of femur. For normal subjects, the contact is in zones 6L, 1L and 2L which shows the impingement occurred in anterior inferior region of femur (Figure 104).

On an average FAI subjects have higher values of percentage area of impingement than the normal subjects (Figure 103 and Figure 104).

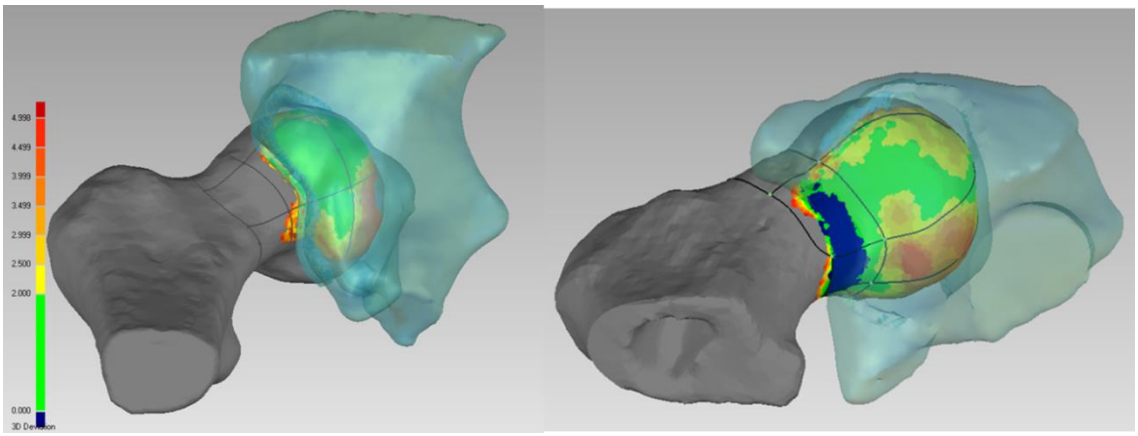

Figure 98. Interference in FAI hip (left) and normal hip (right) at the simulated position of 100º flexion combined with 20º adduction and 30º internal rotation. Blue region on FAI joint shows the region of contact.

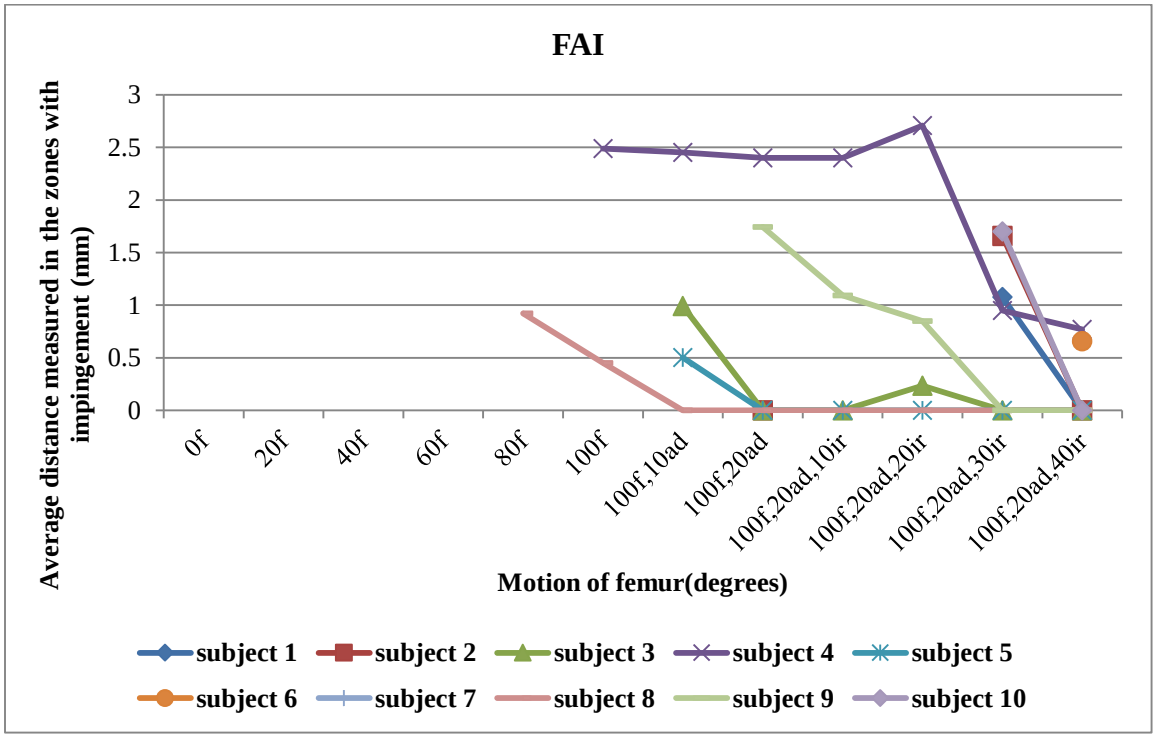

Figure 99. Average distance in the zones having contact during motion of femur in FAI subjects. f-flexion. ad-adduction, ir-internal rotation.

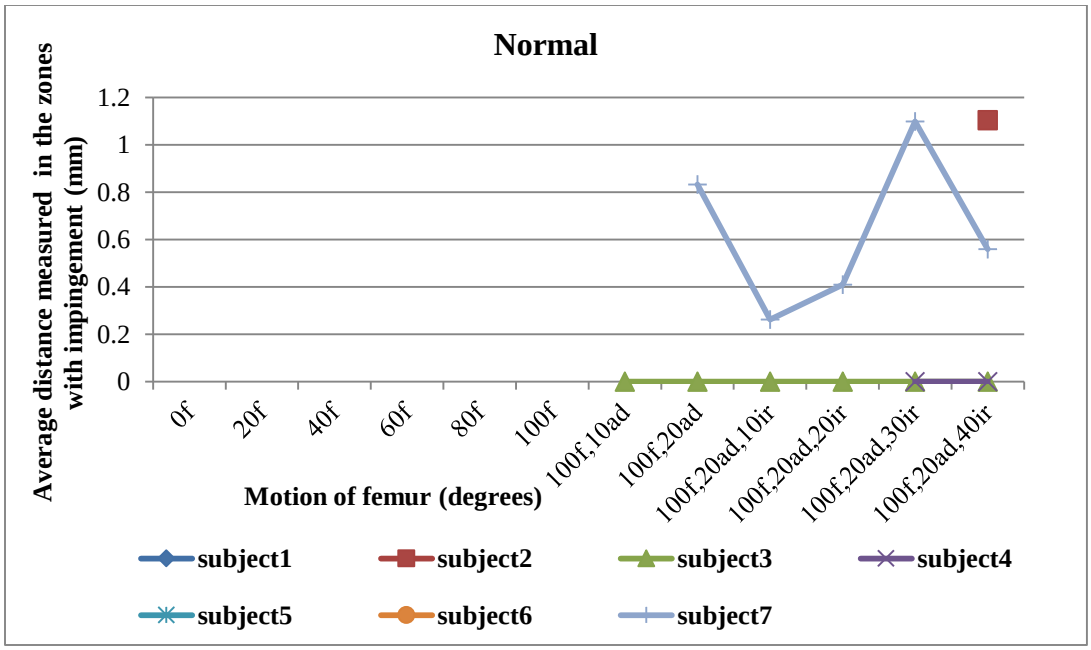

Figure 100. Average distance in the zones having contact during motion of femur in normal subjects

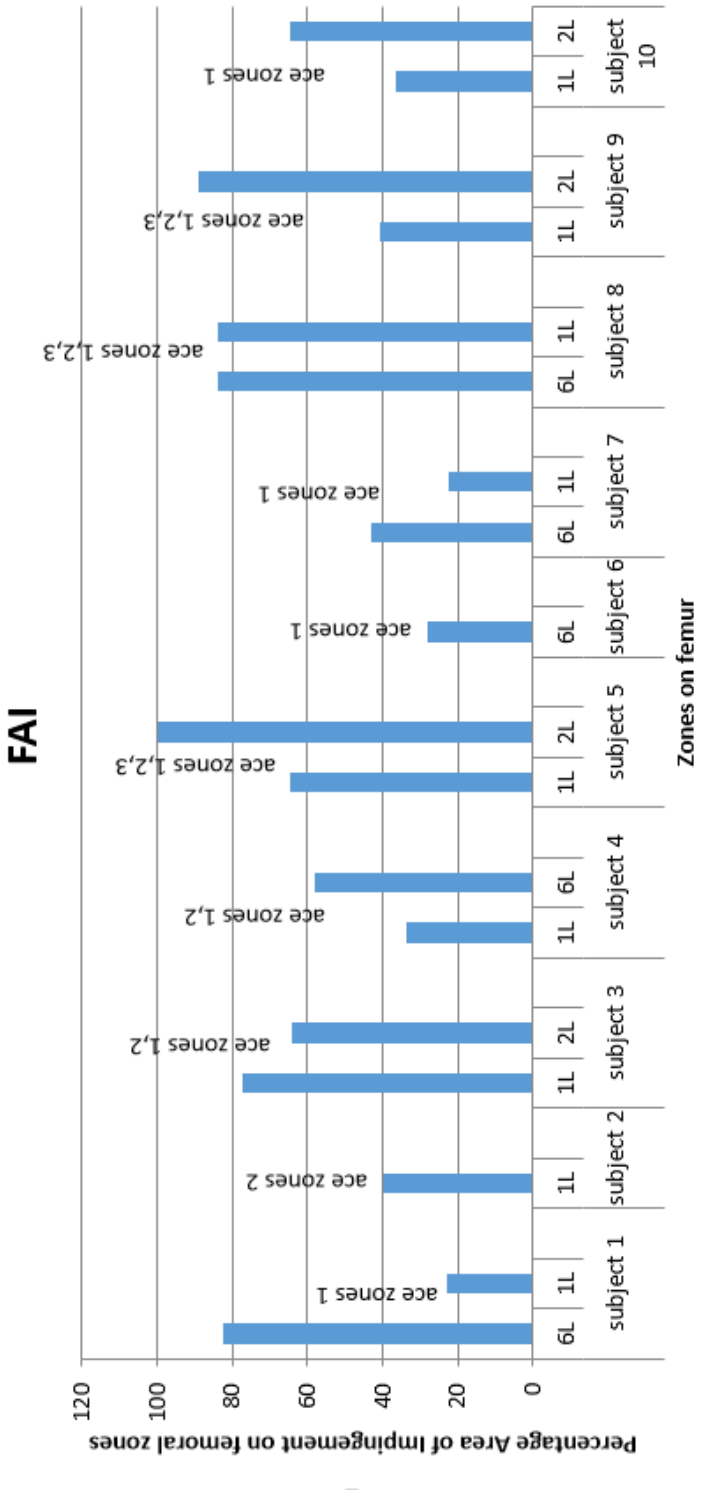

Figure 101. Percentage area of impingement in each zone on femoral head in FAI subjects

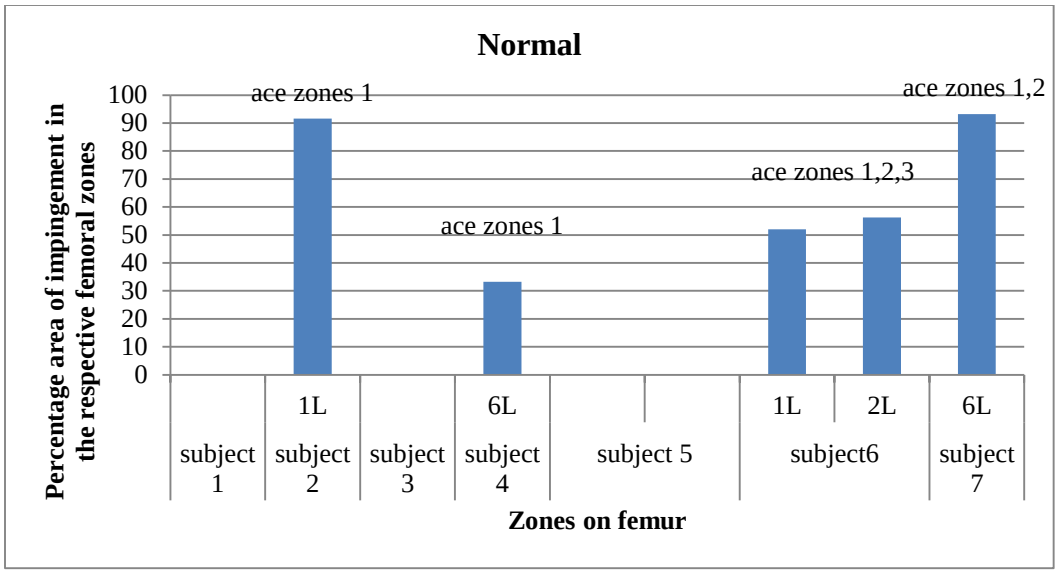

Figure 102. Percentage area of impingement in each zone on femoral head in normal subjects

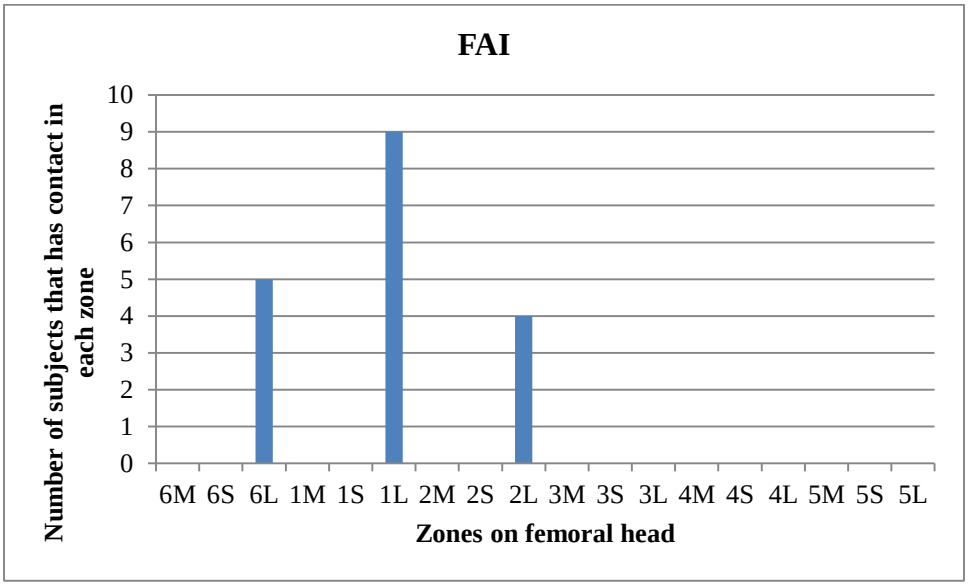

Figure 103. Number of FAI subjects that has contact in femoral head zones during simulation from neutral to 100º flexion, 20º adduction and 40º internal rotation.

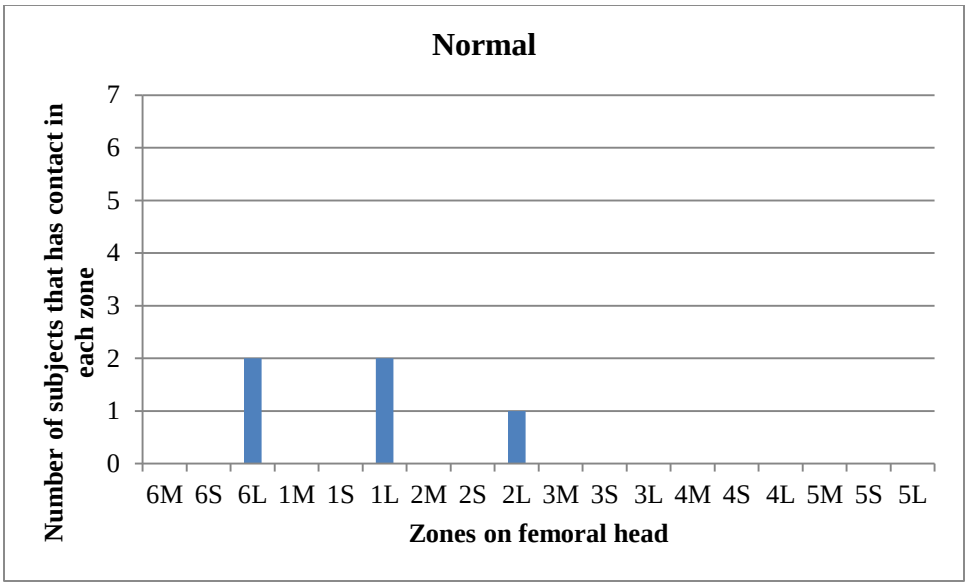

Figure 104. Number of normal subjects that has contact in femoral head zones during simulation from neutral to 100º flexion, 20º adduction and 40º internal rotation

Step 2: Changing the Morphological Parameters

Table 8 shows the values of the selected morphological parameters of normal subjects before changing the morphology

Table 8. Femoral Neck-shaft angle, femoral anteversion angle and alpha angle of the normal femurs. All angles are in degrees

Subject	Age	Sex	Neck-Shaft angle	Angle of anteversion	Alpha angle
1	22	F	129	14.5	49
2	22	F	126.5	15	44.5
3	28	F	130.96	10.5	41.75
4	32	F	124.4	10	46
5	27	F	119.3	16	39.4
6	30	F	126.3	11	44.6

The morphology of femurs from six normal subjects are changed from normal to abnormal by inducing coxavara, coxavalga, retroversion, anteversion, pistol grip deformity and increasing alpha angle as discussed in chapter 3, methodology. Table 9

gives the values of the morphological parameters after changing the morphology of normal hip subjects. Distance maps are calculated after changing femoral morphology throughout the simulation starting from neutral position to 100 degree flexion 20 degree adduction and 40 degree internal rotation. Figure 105 shows the number of subjects with each pathological condition that has impingement in each zone on femoral head during the entire simulation. Further, percentage area of impingement is calculated and compared in each zone between each morphological change and normal femur. Figure 106 shows the percentage area of contact on zones with impingement with each change in morphology and it is observed that by inducing conditions such as coxavara, coxavalga, retroversion and increasing alpha angle the % area of impingement increased to that of original femur.

Table 9. Morphological parameters after changing morphology of normal femurs. All angles are in degrees

Subject	Age	Sex	Neck-Shaft angle	Coxavalga	Coxavara	Angle of anteversion	Anteversion	Retroversion	Alpha angle	Increasein Alpha angle
1	22	F	129	149	109	14.5	34.5	-5.5	49	80
2	22	F	126.5	146.5	106.5	15	35	-5	44.5	78
3	28	F	130.96	150.96	110.96	10.5	30.5	-9.5	41.75	87.29
4	32	F	124.4	144.4	104.4	10	30	-10	46	81.66
5	27	F	119.3	139.3	99.3	16	36	-4	39.4	84
6	30	F	126.3	146.3	106.3	11	31	-9	44.6	77

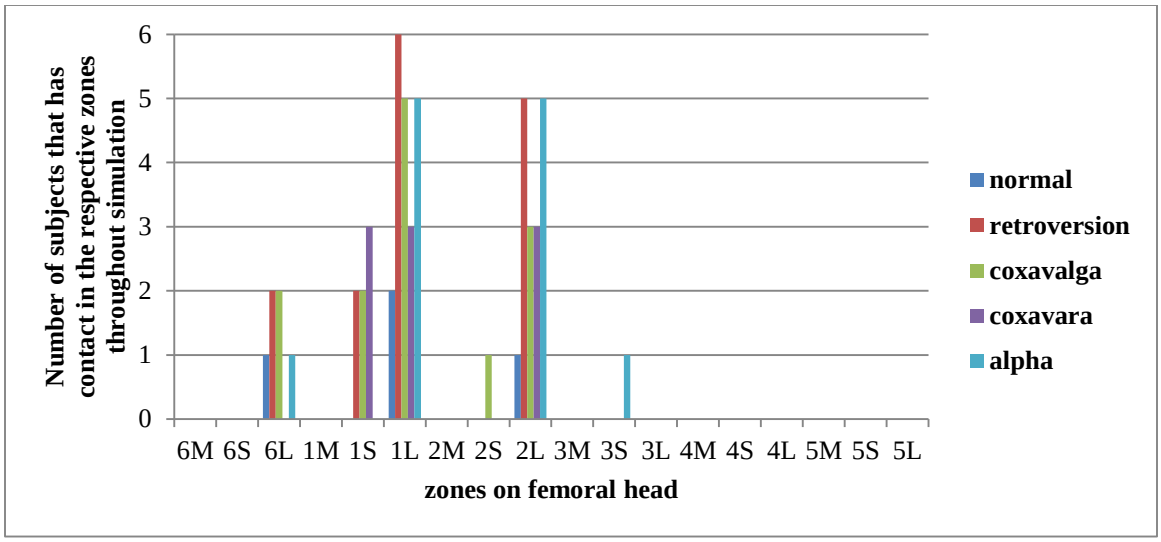

Figure 105. Number of subjects that has impingement in each zone during the entire simulation

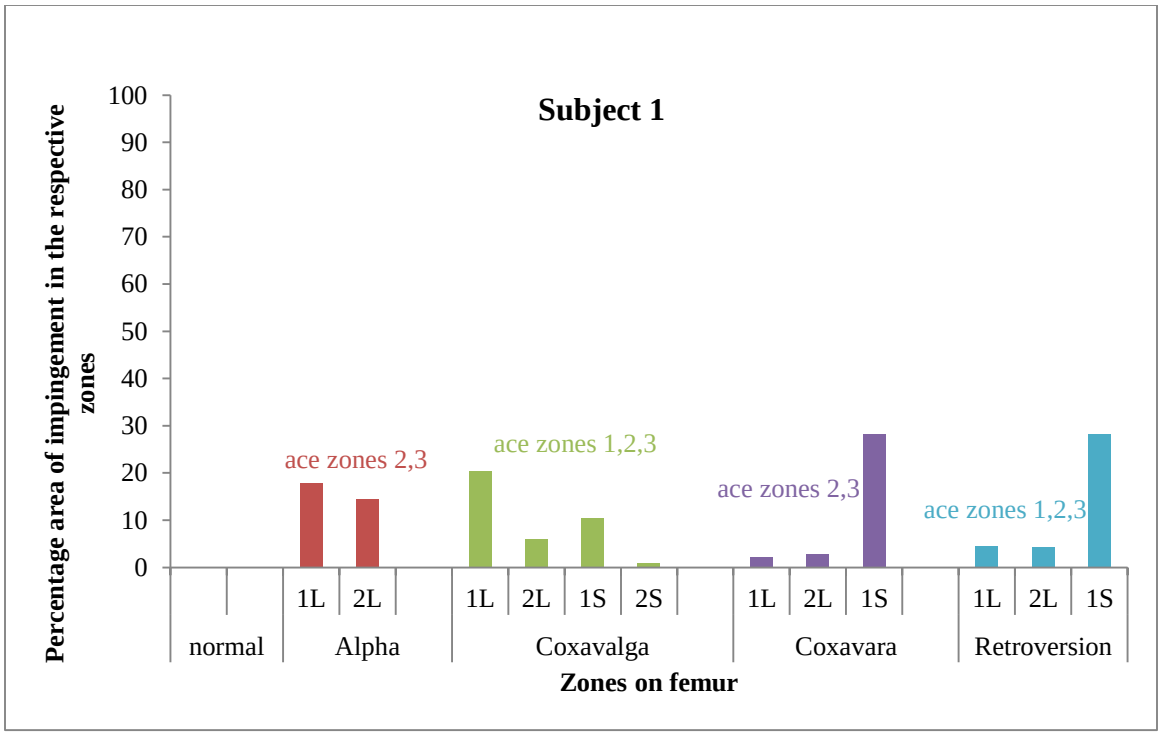

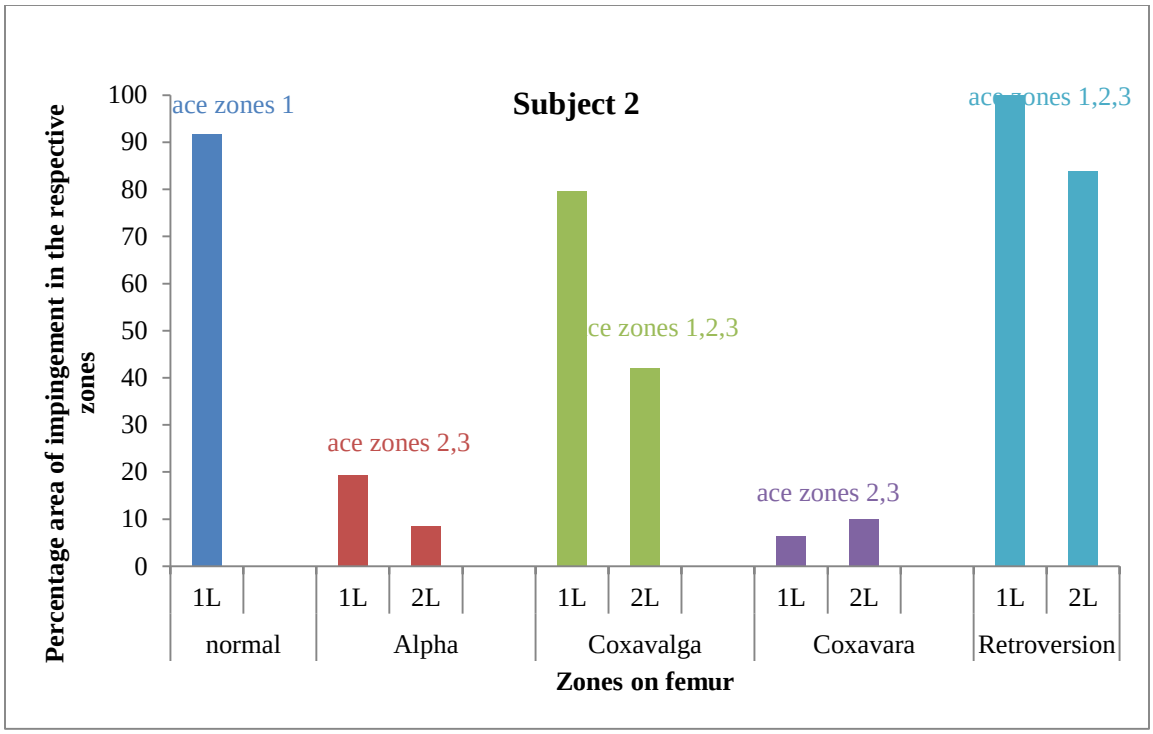
Subject 2
Percentage area of impingement in the respective zones
100
90
80
70
60
50
40
30
20
10
0
ace zones 1
ace zones 2,3
ce zones 1,2,3
ace zones 2,3
ace zones 1,2,3
1L
1L
2L
1L
2L
1L
2L
1L
2L
normal
Alpha
Coxavalga
Coxavara
Retroversion
Zones on femur

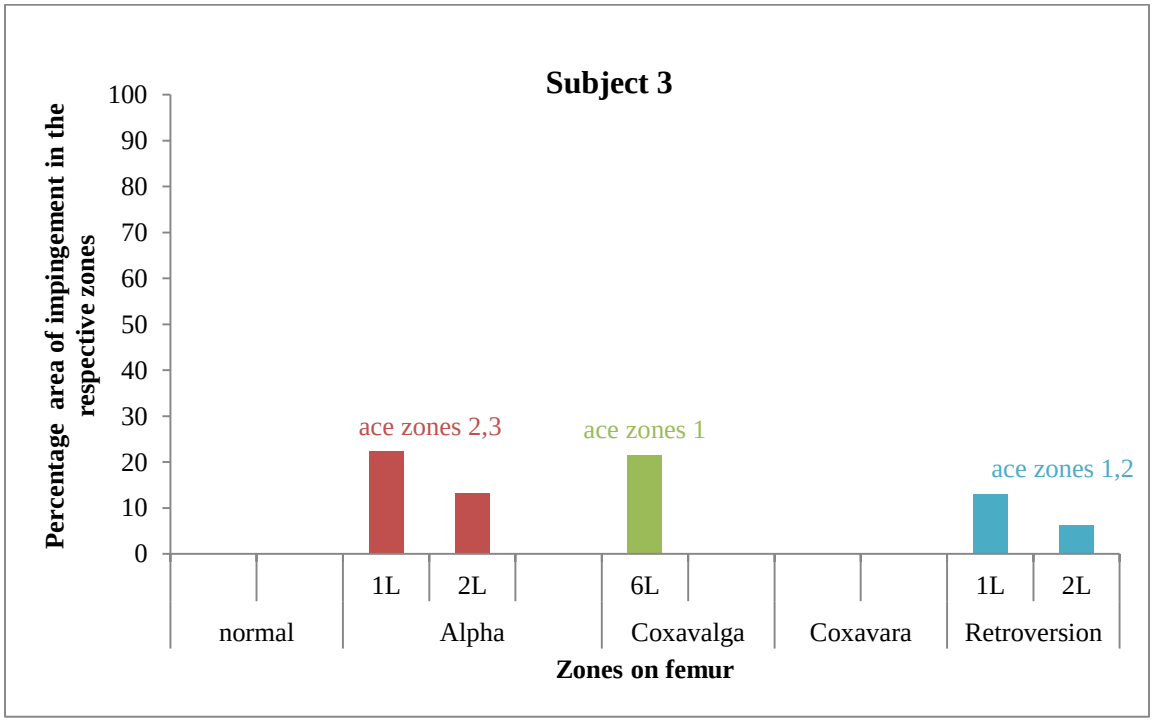
Subject 3
Percentage area of impingement in the respective zones
100
90
80
70
60
50
40
30
20
10
0
ace zones 2,3
ace zones 1
ace zones 1,2
1L
2L
6L
1L
2L
normal
Alpha
Coxavalga
Coxavara
Retroversion
Zones on femur

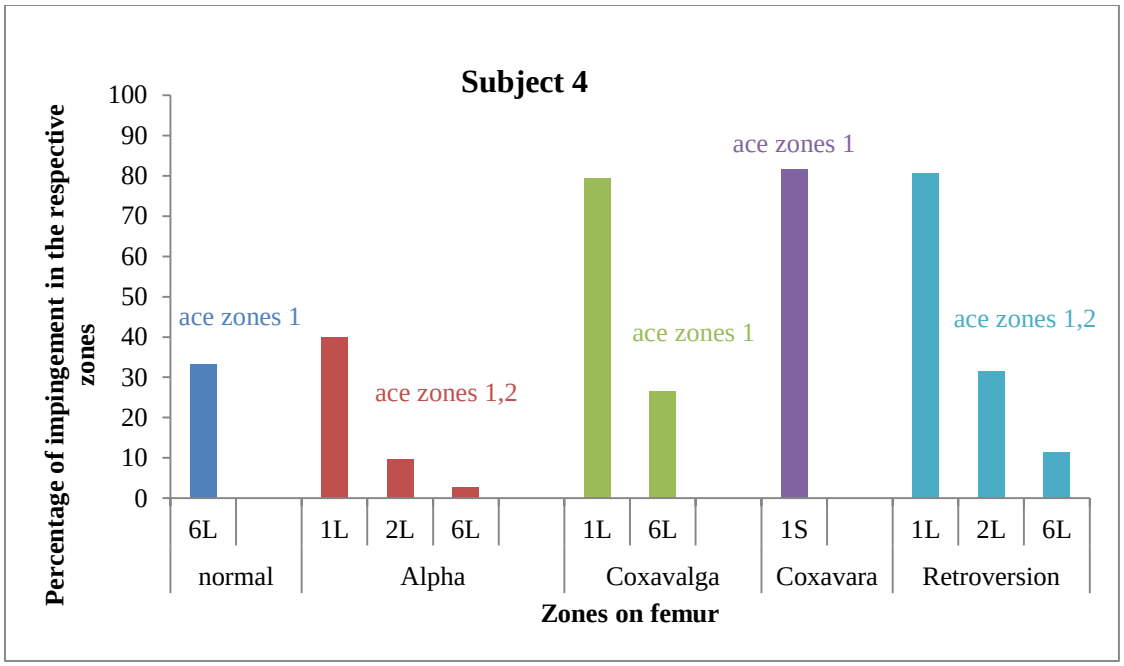
Subject 4
Percentage of impingement in the respective zones
100
90
80
70
60
50
40
30
20
10
0
ace zones 1
ace zones 1,2
ace zones 1
ace zones 1
ace zones 1,2
6L
1L
2L
6L
1L
6L
1S
1L
2L
6L
normal
Alpha
Coxavalga
Coxavara
Retroversion
Zones on femur

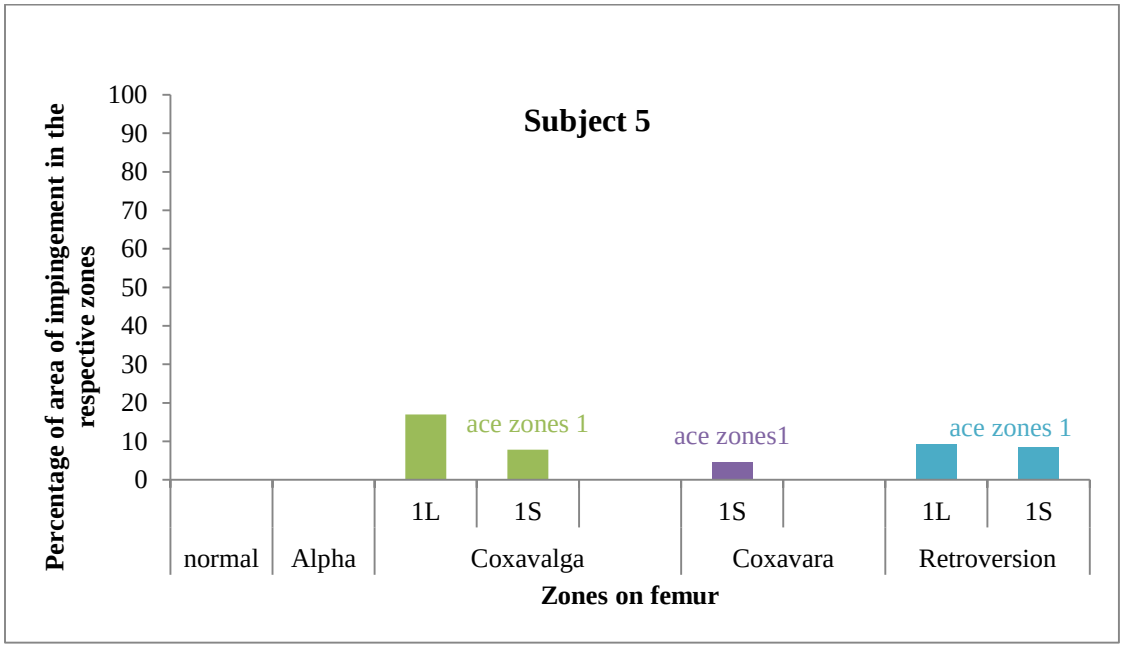
Subject 5
Percentage of area of impingement in the respective zones
100
90
80
70
60
50
40
30
20
10
0
ace zones 1
ace zones1
ace zones 1
1L
1S
1S
1L
1S
normal
Alpha
Coxavalga
Coxavara
Retroversion
Zones on femur

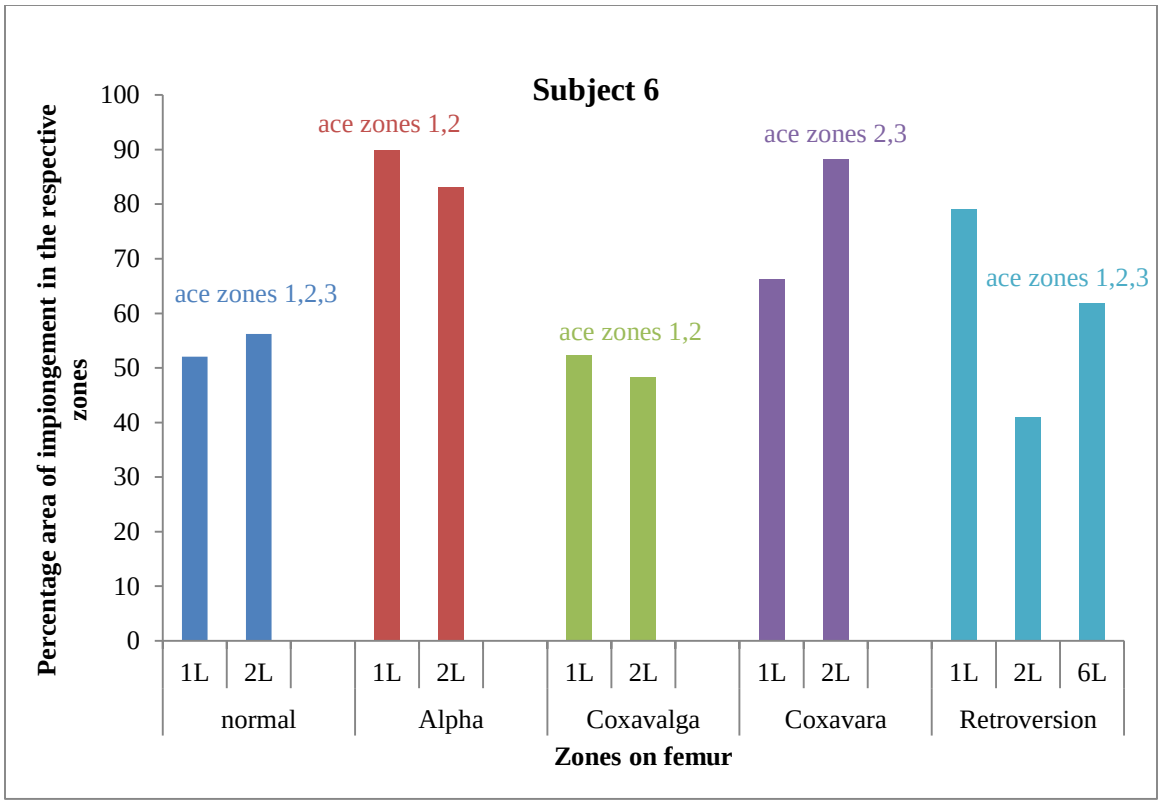

Figure 106. Percentage area of impingement in the zones of contact for subjects 1 to 6.

The average distances are measured in zones that have contact throughout the simulation using distance maps and are plotted to compare the values. The following section shows how the average distances changed by inducing each morphological change of femur.

Changing Femoral Neck-Shaft Angle

Coxavalga

After increasing the neck-shaft angle by 20 degrees all the normal hips fell in the range of coxavalga deformity greater than 140 degrees. It is observed that impingement increased

as the simulation increased from 100 degree flexion to 100 degree flexion combined with 20 degree adduction and 40 degree internal rotation (Figure 107). Percentage area of impingement increased in all the six subjects compared to that of their normal morphology (Figure 106) and the contact is in zones 6L, 1S, 1L, 2L for most of the subjects which shows the impingement occurred in anterior inferior region of femur (Figure 105).

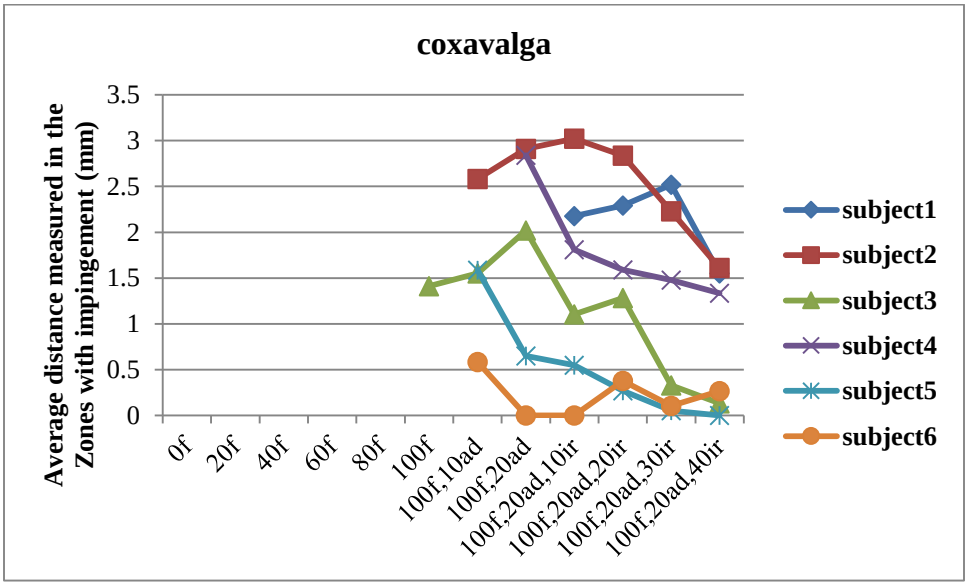

Figure 107. Average distance measured in the impingement zones during the entire simulation after increasing the femoral neck-shaft angle by 20 degrees

Coxavara

After decreasing the neck-shaft angle by 20 degrees all the normal hips fell in the range of coxavalga deformity greater than 140^{o}. It is observed that impingement occurred as the simulation increased from 100 degree flexion to 100 degree flexion combined with 20 degree adduction and 40 degree internal rotation. But there is no much increasing in the average values of contact calculated by distance map at extreme ranges of motion (Figure 108). Percentage area of impingement increased compared to normal in 4 subjects out of 6

subjects, no change in one subject and percentage area of impingement decreased in one subject compared to that of their normal morphology (Figure 106). The contact is in zones 6L, 1S, 1L, 2L for most of the subjects which shows the impingement occurred in anterior inferior region of femur (Figure 105).

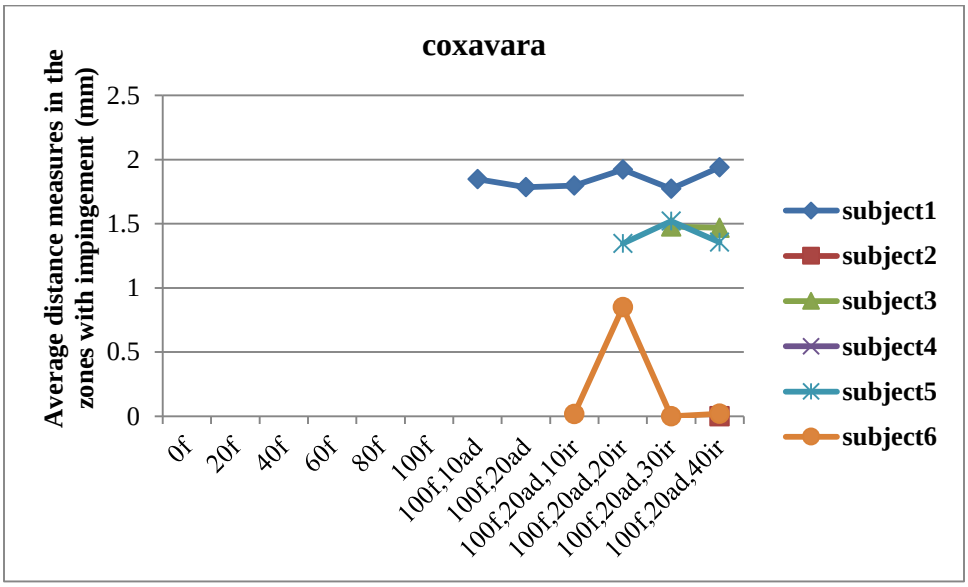

Figure 108. Average distance measured in the impingement zones during the entire simulation after decreasing femoral neck-shaft angle by 20 degrees

Changing Femoral Anteversion Angle

Retroversion

After decreasing the femoral aversion angle by 20 degrees all the normal hips fell in the range of retroversion deformity. It is observed that impingement increased as the simulation increased from 100 degree flexion to 100 degree flexion combined with 20 degree adduction and 40 degree internal rotation (Figure 109). Percentage area of

impingement increased in all the six subjects compared to that of their normal morphology (Figure 106). The contact is in zones 1S, 1L, 2L for most of the subjects which shows the impingement occurred in anterior inferior region of femur (Figure 105).

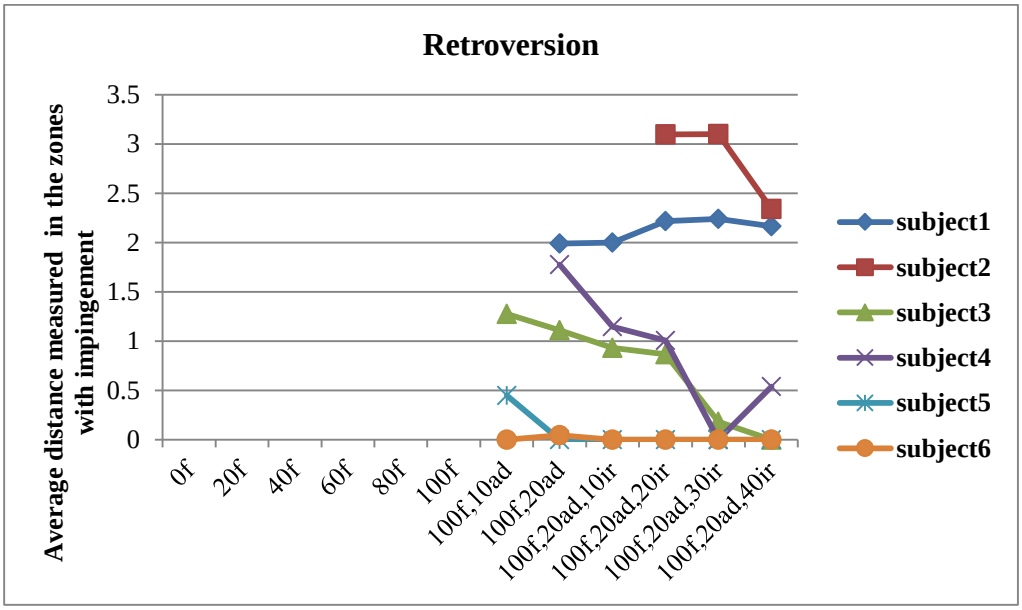

Figure 109. Average distance measured in the impingement zones during the entire simulation after decreasing the anteversion angle by 20 degrees

Excessive Anteversion

After increasing the femoral aversion angle by 20 degrees all the normal hips fell in the range of excessive anteversion. There is no impingement in any subject at any simulation position after increasing anteversion angle by 20 degrees.

Alpha Angle

After increasing the alpha angle greater than 70 degrees all the normal hips, it is observed that impingement increased as the simulation increased from 100 degree flexion to 100 degree flexion combined with 20 degree adduction and 40 degree internal rotation (Figure 110). Percentage area of impingement increased in all the six subjects compared to that of their normal morphology (Figure 106). The contact is in zones 1L, 2L for most of the subjects which shows the impingement occurred in anterior inferior region of femur (Figure 105).

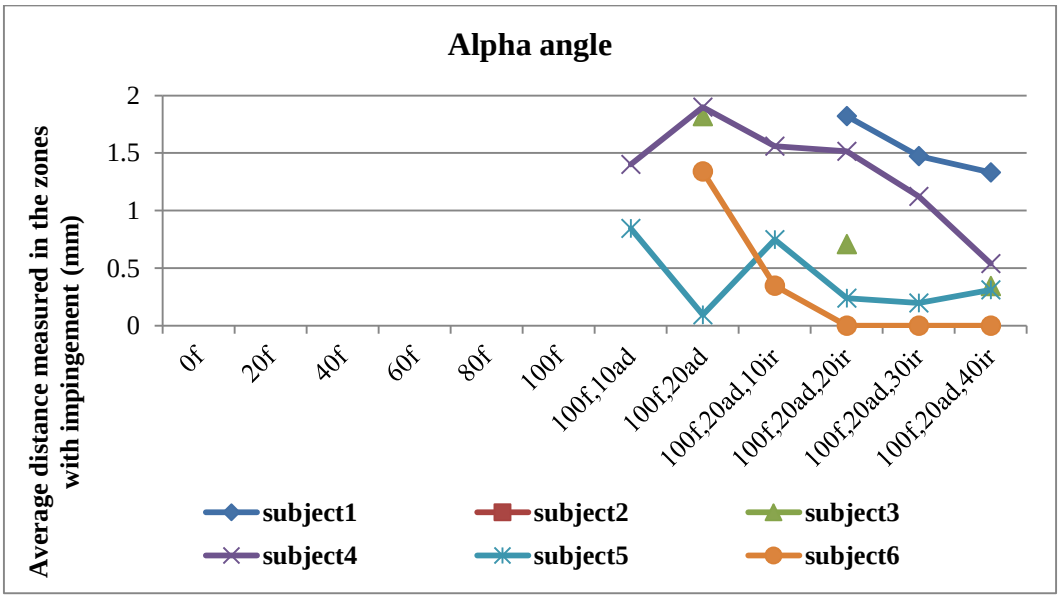

Figure 110. Average distance measured in the impingement zones during the entire simulation after increasing the alpha angle greater than 70 degrees

Pistol Grip Deformity

By inducing the pistol grip deformity, all the subjects has impingement with 100 degree flexion and 10 degrees adduction motion in zones 3M and 3S.

CHAPTER 5: DISCUSSION

This chapter discusses the results obtained in the process of model development and the variations in the mechanical behavior observed by changing the morphology of the ankle and hip joints.

MODEL DEVELOPMENT

Image Processing

Morphology of bones and ligament insertion sites of ankle joints are extracted from Magnetic Resonance Data. Morphology of bones of hip joints are extracted from Computer Tomographic images. MR data is used as it is possible to see the ligament insertion sites clearly in MR images and it is easier to extract bones with high quality using CT images.

Developing Dynamic Model

Previously developed models of ankle joint complex are used to simulate the motion of ankle joint complex [18] . Dynamic models are developed using the bones developed in previous step. These bones are stabilized by constructing ligaments from the ligament insertion sites coordinates from the previous step. The visco-elastic properties of ligaments are found in the literature [82]. The torque is applied about each axis dorsiflexion/plantar flexion, inversion/ eversion and internal/ external rotations of the anatomical coordinate system [42] and the output parameters such as joint flexibility,

ROM, kinematic coupling and the forces in ligaments are measured. In the case of hip joint, a simple spherical joint is established between the femur and acetabulum and motion is applied about the joint to produce motions such as flexion/extension, abduction/adduction and internal/external rotations.

EFFECT OF CHANGE IN MORPHOLOGY ON JOINT MECHANICAL BEHAVIOR

In order to study the effect of morphology on passive mechanical properties of ankle and hip joints the morphology of 3D models of bones are changed and the effect of this change in mechanics is measured and compared with that of normal subjects.

The initial Range of motion of AJC models vary between 5 to 22 degrees in inversion, 11to 18 degrees in eversion, 26 to 44 degrees in dorsiflexion, 19 to 45 in plantar flexion, 5 to 23 degrees in internal rotation and 6 to 18 degrees in external rotation. The lower values are subjected to subjects 4L and 7R in all the motions.

Changing the Orientation of Calcaneofibular Ligament

The initial orientation of CFL ligament varies between 35 to 49 degrees with respect to tibial axis except for subject 7R for which the orientation of CFL is 6.8 degrees. The orientation of CFL ligament is varied between horizontal to vertical with respect to tibial shaft axis with increments as 0 degrees, 30 degrees, 45 degrees, 60 degrees and 90

degrees and ROM, flexibility of AJC and forces in CFL ligament is calculated at each orientation of CFL. With the change in orientation of CFL from vertical to horizontal there is a significant increase in inversion an average of 9.1 degrees (min 4, max 14.2), a 95 % increase on an average and internal ROM an average of 3.62 degrees (min 0.32, max 6.9), a 17% increase and decrease in external ROM an average of 5.84 degrees (min 0.48, max 11.12), a 33 % decrease. There is significant increase in AJC flexibility in inversion an average of 0.09 degree/N-mm (min 0.001, max 0.016), a 90% increase. Also, with the change in orientation of CFL from vertical to horizontal there is a significant decrease in forces in CFL in inversion an average of 27.21 N (min 5.7, max 48.7), a 32.8% decrease and internal rotation an average of 32.15 N (min 8.72, max 55.59), a 63.4% decrease and increase in external rotation an average of 39.83N (min 20.22, max 59.44), a 61% increase. These results conclude that the joint is more stable when the ligament is vertical than it is horizontal. The inversion range of motion pattern is consistent with literature [3], a vertically oriented ligament is more restrictive because its tension is largest.

Changing the Morphology of Sustentaculum Tali

Morphology of sustentaculum tali is changed by removing sustentaculum tali in 4 stages as discussed in chapter 3. In alteration 1, the fused anterior and middle facet supporting structure is removed; in alteration 2, the elevation of sustentaculum tali is lowered by lowering the elevation of middle articulating facet; in alteration 3, The medial-side posterior articulating facet extension is removed by lowering its articulating surface elevation; in alteration 4, Sustentaculum tali is completely removed.

Mechanical function such as ROM, flexibility of joint and forces in CFL are measured after each alteration and compared to that of original morphology. Removing the sustentaculum tali shows a significant increase in inversion ROM a mean value of 4.757 degrees (min 2.84, max 6.3), a 31% increase and on an average major increase in ROM is noticed by alteration 3 in which the medial-side posterior articular facet extension is removed and shifts the contacting areas to the posterior articular facet and the sustentaculum tali no longer supports the talus. Also removing the sustentaculum tali shows that's there is a significant increase in dorsiflexion ROM a mean value of 11.08 degrees (min 3.33, max 18.84), a 35% increase. There is a 121% increase in force in CFL in dorsiflxion by removing volume of sustentaculum tali. There is an increase in flexibility of joint in inversion and dorsiflexion though statistically not significant. This shows that joint is more stable with sustentaculum tali and fused calcaneus joints have more stability than non-fused.

Changing the Morphology of Femur

The morphology of normal femur is changed by changing femoral neck-shaft angle, femoral anteversion angle, increasing alpha angle and inducing pistol grip deformity. The effect of this change in morphology is observed on interference at hip joint by simulating femur from neutral position to 100 degree flexion combined with 20 degree adduction and 40 degree internal rotation. The results show that by increase and decrease in neck-shaft angle to induce deformities such as coxavalga and coxavara increased impingement at anterior-inferior region of hip joint as the femur is simulated to 100 degree flexion combined with 20 degree adduction and 40 degree internal rotation. By inducing

coxavalga there is increase in early interference at hip joint in all six subjects mostly in the zones 1L, 2L, 6L on femoral head and in zones 1, 2, 3 on acetabulum. By inducing coxavara there is increase in impingement in four of six total subjects mostly in the zones 1L, 2L, 1S on femoral head and in zones 2, 3 on acetabulum, the impingement decreased in one subject and there is no change in one subject. Increase in femoral anteversion angle to induce excessive anteversion decreased impingement at hip joint and decrease in femoral anteversion angle to induce retroversion increased impingement at anterior-inferior region of hip joint as the femur is simulated to 100 degree flexion combined with 20 degree adduction and 40 degree internal rotation. The impingement is observed in zones 1L, 2L, 6L and 1S on femoral head and in zones 1, 2, 3 on acetabulum. With the increase in alpha angle impingement increased at anterior-inferior region of hip joint as the femur is simulated to 100 degree flexion combined with 20 degree adduction and 40 degree internal rotation. The impingement is observed in zones 1L, 2L on femoral head and in zones 1, 2, 3 on acetabulum. Inducing pistol grip deformity increased impingement on the top head of femur with adduction motion. This shows that other clinical parameters have effect on FAI and other parameters should be considered before performing the traditional surgery of removing the bone near the impingement area. Failure to correct these parameters to normal range might lead to post-surgical complications such as recurring FAI after the surgery.

CHAPTER 6: SUMMARY AND CONCLUSIONS

Main Goal

The goal of this study is to explore the casual relationship between the morphology and mechanics in two specific joints.

1. Ankle joint – irregular joint
2. Hip Joint- close to spherical joint

Model Development

Subject specific models are used to find the relation between the morphology and mechanics. Since all models used identical material properties and were subjected to identical loads and boundary conditions, it can be concluded that the observed variations in passive mechanical characteristics were due to variations in morphology. The three dimensional bones and ligament insertion sites are extracted from MRI data in case of Ankle joints. Previously developed dynamic model is used to study the mechanical function of the joints [18]. The three dimensional bones are extracted from CT data in case of hip joint. A spherical joint is used in the dynamic analysis software to produce ball and socket joint motion.

Effect of Morphology on Mechanical Behavior

Using computer models of bones it is feasible to change the morphology of bones and study the effect of the change in morphology on mechanical behavior.

Changing the Orientation of Calcaneofibular Ligament

Except for subject 7R, the initial orientation of CFL with respect to tibial axis lies between 35 to 50 degrees. For subject 7R the orientation is 6.85 degrees. By changing the orientation of CFL from vertical to horizontal with respect to tibial axis and measuring its effect of this change in mechanical function such as flexibility, ROM and force in CFL. The results show that with change in orientation of CFL from vertical to horizontal there is increase in flexibility of AJC in inversion, increase in ROM of joint in inversion and internal rotation and decrease in force in CFL in inversion and internal rotation which show that the joint is stiffer if the ligament is in vertical alignment. The effect of CFL on AJC is more in vertical direction than horizontal. This study shows AJC of subjects like 7R are stiffer than others whose ligaments are close to vertical.

Changing Morphology of Sustentaculum Tali

By observing the sustentaculum tali of all six subjects, subjects 4L and 7R as having long sustentaculum tali as the volume is continuous between medial and anterior facets of calcaneus. By changing the morphology of sustentaculum tali i.e., by removing the surface area of sustentaculum tali, it is observed that ROM of AJC increased in dorsiflexion and inversion. By following alteration 1, i.e., by removing the fused part between anterior and medial sides of calcaneus there is increase in dorsiflexion ROM. This shows that the fused part provides extra support in dorsiflexion motion. For subject 7R and 4L there is significant increase in inversion ROM by following alteration 2 i.e., by removing the middle talar articulating surface. On an average for all the subjects there is an increase in inversion ROM by removing posterior side of middle talar articulating

surface. This shows that the fused region acts as an extra support restricting additional dorsiflexion and inversion motion.

Changing the Morphology of Hip Joint

The morphological parameters of hip play a significant role in the interference of bones at the hip joints. Changing femoral neck-shaft angle by inducing both coxavara and coxavalga, decrease in anteversion angle i.e., retroversion, increase in alpha angle and pistol grip deformity increases early interference at the hip joint which shows that these parameters have to be considered while performing FAI surgery rather than just removing the bony bump on femoral head or acetabular rim.

SIGNIFICANCE

There is a strong relationship between the morphology and mechanical behavior of human joints. The outcome of the surgery and other treatments may vary. This results in success in some subjects and failure in others. It is possible that one clinical intervention which may succeed on one patient may fail on another patient with different morphology. Individualized subject-specific treatment procedures for ankle complex disorders may improve the clinical outcome.

In this study the results show that the ankle joint with fused medial-anterior facets in calcaneus morphologhas restricted motion than the calcaneus with two separate facets. Proceeding with surgical procedure of ankle fusion might make such ankles stiffer and may cause arthritis in the adjacent joints subtalar joint in the future. Patients with large

area of sustentaculum tali should be prioritized with TAR while those with smaller area may be good candidates for ankle fusion.

This study also shows that variations in the rientation of CFL produces variations in mechanical function of AJC. Therefore, the point of insertion during Ligament reconstruction surgeries should be optimized to produce normal jont motion, as the output mechanical function of the joint depends on the orientation of the ligament. The believed concept of CFL guided motion using as 4-bar mechanism in the literature may not be valid based on the finding that joint mechanics depend on the orientation of ligament.

This study also shows that the specific vartiations in femoral neck orientation produce early interference. Therefore, the orientation of femoral neck should be considered in the diagnosis and treatment of femoroacetabular impingement. For example, in this study the results show that femoral retroversion causes early interference at the hip joint. The surgeons should correct femoral retroversion before performing the Femoroacetabular impingement surgery of removing the excess bone. Correcting such parameters might help to solve the cause of the impingement rather than just correcting the problem and help to stop the problem to reoccur in the future. This may lead to the better diagnosis and treatment of this pathological condition.

ASSUMPTIONS AND LIMITATIONS

Exclusion of Cartilage Geometry

The geometry of cartilage is not physically present in the dynamic models of AJC. However the gaps between the bones are closed in the neutral position by translating bones by the sum of thickness of articular cartilage which introduces the assumption that the bone surfaces are articulating surfaces. The increased space between bones may cause small increases in joint rotations and translations.

Uniform Cartilage Thickness in AJC

Cartilage between all the joints of the AJC is assumed to be uniform. This assumption leads to constant contact stiffness across the articular surfaces, which is not physiological as the contact stiffness is a function of cartilage thickness and should vary across the articular surfaces [89].

Constant Contact Stiffness

The contact stiffness in AJC is derived by using the formula K= E*A/t, as defined in methodology and is a function of the modulus of elasticity of cartilage (E), an average surface polygon area (A) and the average tibiotalar cartilage thickness (t) [18]. The contact stiffness varies spatially as a function of cartilage thickness [89]. The contact areas and cartilage mechanical properties vary when moving the hind foot [90]. Therefore, the stiffness term should vary throughout the simulation. This feature is not available in the software and the cartilage stiffness only varies exponentially to report nonlinear viscoelastic behavior [18] .

Same Ligament Mechanical Properties

The mechanical properties of lateral collateral ligaments vary significantly from subject to subject in AJC [91]. Using the same load-displacement properties for the ligaments may be in adequate to use for all subjects. For example, the anterior talofibular ligament and calcaneofibular ligament elastic modulus may vary as 255.5 ±181.3MPa and 512.0 ± 333.5 MPa, respectively. Also the mechanical properties of some of the subtalar ligaments such as interosseous and cervical ligaments are undocumented and the properties of these ligaments are estimated by scaling the mechanical properties of ATFL ligament's since ATFL have the broad insertion areas as ITCL and CL. The experimental comparison indicated that the model over-estimated motion at the subtalar joint [18], therefore this assumption may be inappropriate. To develop the model further, mechanical testing of the subtalar ligaments is necessary.

Constant Labrum Thickens

The literature shows that the thickness of labrum in hip joint is variable between 2mm-3mm Hip joint of the model uses the constant labral thickness as 2mm [46]. The assumption of a uniform labral thickness will force the contact stiffness to be uniform across the articular surface. This may not be physiological because the contact stiffness may be a function of the thickness of the labrum and therefore may spatially vary.

Elimination of Cartilage in the Hip Model

The cartilage is not used in the dynamic model of hip joint as the interference between cartilage to cartilage is not considered as FAI as defined previously and further load

transmission characteristics are not the point of interest in this study, in which case the cartilage plays a vital role.

Spherical Joint of Hip Joint

The motion of the hip joint is approximated to ball and socket joint by using a Spherical joint between femur and acetabulum in the dynamic model. Using this joint would depict the early interference produced by any aspherical nature of femoral head or acetabular rim. Future development of model should include ligament constraints to produce the motion.

CHAPTER 7 FUTURE WORK

Long term goals of the study include

1. Studying the variations in forces generated in other ligaments by changing the orientation of CFL.
2. Improving the dynamic model by introducing cartilage geometry and loading the joint using tendons.
3. Finding the mechanical properties such as elastic modulus of ligaments such as ITCL and CL and using those values in the model.
4. Developing the hip model by using ligament constraints and variable thickness labrum.
5. In order to solve the surgical failures of Femoroacetabular Impingement at the hip joint. Subjects with failed FAI surgeries will be considered and to find if any of the morphological parameters that are proposed to affect FAI are a cause for the surgical failures.

CHAPTER 8: REFERENCES

1. Gupta, S.C., C.D. Gupta, and A.K. Arora, *Pattern of talar articular facets in Indian calcanei.* J Anat, 1977. **124**(Pt 3): p. 651-5.

2. Tannast, M., K.A. Siebenrock, and S.E. Anderson, *Femoroacetabular impingement: radiographic diagnosis--what the radiologist should know.* AJR Am J Roentgenol, 2007. **188**(6): p. 1540-52.

3. Sarrafian, S., *Anatomy of the Foot and Ankle: Descriptive, Topographic, Functional*. 1993, Philadelphia: Lippincott.

4. Barbaix, E., P. Van Roy, and J.P. Clarys, *Variations of anatomical elements contributing to subtalar joint stability: intrinsic risk factors for post-traumatic lateral instability of the ankle?* Ergonomics, 2000. **43**(10): p. 1718-25.

5. Ruth, C.J., *The surgical treatment of injuries of the fibular collateral ligaments of the ankle.* J Bone Joint Surg Am, 1961. **43-A**: p. 229-39.

6. R. E. Isman, V.T.I., *ANTHROPOMETRIC STUDIES OF THE HUMAN FOOT AND ANKLE.* Bulletin of Prosthetics Research, 1969. **97**.

7. Lundberg, A., *Kinematics of the ankle and foot. In vivo roentgen stereophotogrammetry.* Acta Orthop Scand Suppl, 1989. **233**: p. 1-24.

8. Siegler, S., J. Chen, and C.D. Schneck, *The three-dimensional kinematics and flexibility characteristics of the human ankle and subtalar joints--Part I: Kinematics.* J Biomech Eng, 1988. **110**(4): p. 364-73.

9. Roaas, A. and G.B. Andersson, *Normal range of motion of the hip, knee and ankle joints in male subjects, 30-40 years of age.* Acta Orthop Scand, 1982. **53**(2): p. 205-8.

10. Lundberg, A., et al., *The axis of rotation of the ankle joint.* J Bone Joint Surg Br, 1989. **71**(1): p. 94-9.

11. Chen, J., S. Siegler, and C.D. Schneck, *The three-dimensional kinematics and flexibility characteristics of the human ankle and subtalar joint--Part II: Flexibility characteristics.* J Biomech Eng, 1988. **110**(4): p. 374-85.

12. Bedi, A., et al., *Surgical treatment of femoroacetabular impingement improves hip kinematics: a computer-assisted model.* Am J Sports Med, 2011. **39 Suppl**: p. 43S-9S.

13. Kennedy, M.J., *The Effect of Cam Femoroacetabular Impingement on Hip Maximal Dynamic Range of Motion.* Journal of Orthopedics, 2009. **1**: p. 41-50.

14. Anderson, A.E., et al., *Effects of idealized joint geometry on finite element predictions of cartilage contact stresses in the hip.* J Biomech, 2010. **43**(7): p. 1351-7.

15. Eckhoff, D.G., et al., *Three-dimensional mechanics, kinematics, and morphology of the knee viewed in virtual reality.* J Bone Joint Surg Am, 2005. **87 Suppl 2**: p. 71-80.

16. Rose, M.D., *Kinematics of the trapezium-1st metacarpal joint in extant anthropoids and Miocene hominoids.* Journal of Human Evolution, 1992. **22**(4–5): p. 255-266.

17. Davis, P.R., *Observations on vertebrae in different races.* 6th Congres des Sciences Anthropologiques et Ethnologiques, 1960: p. 443-450.

18. Imhauser, C.W., et al., *Subject-specific models of the hindfoot reveal a relationship between morphology and passive mechanical properties.* J Biomech, 2008. **41**(6): p. 1341-9.

19. Toy, J, *Subject Specific Models of the Hindfoot Reveal a Relationship between Morphology and Passive Mechanical Properties*. 2009, Drexel University.

20. AnatomyAnkle. Available from: http://www.kenhub.com/en/library/anatomy/the-ankle-joint

21. AnkleAnatomy. Available from: http://www.scoi.com/specialties/anatomy-ankle.

22. Inman, V.T., *The Joints of the Ankle*. 1991, Baltimore: Williams&Wilkins.

23. Barnett, H.J. and H.H. Hyland, *Tumours involving the brain-stem; a study of 90 cases arising in the brain-stem, fourth ventricle, and pineal tissue.* Q J Med, 1952. **21**(83): p. 265-84.

24. Hicks, J.H., *The mechanics of the foot I, the joints.* Journal of Anatomy, 1953. **87**: p. 345-357.

25. Sammarco, J., *Biomechanics of the ankle. I. Surface velocity and instant center of rotation in the sagittal plane.* Am J Sports Med, 1977. **5**(6): p. 231-4.

26. Bunning, P.S. and C.H. Barnett, *A Comparison of Adult and Foetal Talocalcaneal Articulations.* J Anat, 1965. **99**: p. 71-6.

27. Laidlaw, P.P., *The Varieties of the Os Calcis.* J Anat Physiol, 1904. **38**(Pt 2): p. 133-43.

28. Drayer-Verhagen, F., *Arthritis of the subtalar joint associated with sustentaculum tali facet configuration.* Journal of Anatomy, 1993. **183**(Pt 3): p. 631-634.

29. Beynnon, B.D., et al., *First-time inversion ankle ligament trauma: the effects of sex, level of competition, and sport on the incidence of injury.* Am J Sports Med, 2005. **33**(10): p. 1485-91.

30. Holmer, P., et al., *Epidemiology of sprains in the lateral ankle and foot.* Foot Ankle Int, 1994. **15**(2): p. 72-4.

31. Freeman, M.A., M.R. Dean, and I.W. Hanham, *The etiology and prevention of functional instability of the foot.* J Bone Joint Surg Br, 1965. **47**(4): p. 678-85.

32. Buckwalter, J.A., C. Saltzman, and T. Brown, *The impact of osteoarthritis: implications for research.* Clin Orthop Relat Res, 2004(427 Suppl): p. S6-15.

33. Lundberg, A., et al., *Kinematics of the ankle/foot complex--Part 2: Pronation and supination.* Foot Ankle, 1989. **9**(5): p. 248-53.

34. Allinger, T.L. and J.R. Engsberg, *A method to determine the range of motion of the ankle joint complex, in vivo.* J Biomech, 1993. **26**(1): p. 69-76.

35. Stauffer, R.N., E.Y. Chao, and R.C. Brewster, *Force and motion analysis of the normal, diseased, and prosthetic ankle joint.* Clin Orthop Relat Res, 1977(127): p. 189-96.

36. Close, J.R., *Some applications of the functional anatomy of the ankle joint.* Journal of Bone and Joint Surgery, 1956. **38-A**(4): p. 761-781.

37. Valderrabano, V., et al., *Kinematic changes after fusion and total replacement of the ankle: part 1: Range of motion.* Foot Ankle Int, 2003. **24**(12): p. 881-7.

38. Close, J.R. and V.T. Inman, *The action of the ankle joint*, in *Prosthetic Devices Research Project*. 1952, Institute of Engineering Research: University of California, Berkeley.

39. Barnett, C.H. and J.R. Napier, *The axis of rotation at the ankle joint in man; its influence upon the form of the talus and the mobility of the fibula.* J Anat, 1952. **86**(1): p. 1-9.

40. Isman, R.E. and V.T. Inman, *Anthropometric Studies of the Human Foot and Ankle*. Bulletin of Prosthetic Research, 1969. **Spring**: p. 97-129.

41. Manter, J.T., *Movements of the subtalar and transverse tarsal joints.* The Anatomical Record, 1941. **80**(4): p. 397-410.

42. Wu, G., et al., *ISB recommendation on definitions of joint coordinate system of various joints for the reporting of human joint motion--part I: ankle, hip, and spine. International Society of Biomechanics.* J Biomech, 2002. **35**(4): p. 543-8.

43. Bremer, S.W., *The unstable ankle mortise--functional ankle varus.* J Foot Surg, 1985. **24**(5): p. 313-7.

44. Berry, D.J., *surgery of the hip book* 2013. p. 2-18.

45. Mechlenburg, I., et al., *Cartilage thickness in the hip joint measured by MRI and stereology – a methodological study.* Osteoarthritis and Cartilage, 2007. **15**(4): p. 366-371.

46. Groh, M.M. and J. Herrera, *A comprehensive review of hip labral tears.* Current Reviews in Musculoskeletal Medicine, 2009. **2**(2): p. 105-117.

47. HipAnatomy. Available from: http://ernestschilders.com/hip-anatomy.php.

48. Ganz, R., et al., *Femoroacetabular impingement: a cause for osteoarthritis of the hip.* Clin Orthop Relat Res, 2003(417): p. 112-20.

49. Beck, M., et al., *Hip morphology influences the pattern of damage to the acetabular cartilage: femoroacetabular impingement as a cause of early osteoarthritis of the hip.* J Bone Joint Surg Br, 2005. **87**(7): p. 1012-8.

50. Lavigne, M., et al., *Anterior femoroacetabular impingement: part I. Techniques of joint preserving surgery.* Clin Orthop Relat Res, 2004(418): p. 61-6.

51. Tannast, M., K.A. Siebenrock, and S.E. Anderson, *Femoroacetabular Impingement: Radiographic Diagnosis—What the Radiologist Should Know.* American Journal of Roentgenology, 2007. **188**(6): p. 1540-1552.

52. Philippon, M.J., et al., *Revision hip arthroscopy.* Am J Sports Med, 2007. **35**(11): p. 1918-21.

53. Heyworth, B.E., et al., *Radiologic and intraoperative findings in revision hip arthroscopy.* Arthroscopy, 2007. **23**(12): p. 1295-302.

54. Ilizaliturri, V.M., Jr., *Complications of arthroscopic femoroacetabular impingement treatment: a review.* Clin Orthop Relat Res, 2009. **467**(3): p. 760-8.

55. Matsuda, D.K. and D. Hanami, *Hip arthroscopy for challenging deformities: posterior cam decompression.* Arthrosc Tech, 2013. **2**(1): p. e45-9.

56. Kubiak-Langer, M., et al., *Range of motion in anterior femoroacetabular impingement.* Clin Orthop Relat Res, 2007. **458**: p. 117-24.

57. Roach, K.E. and T.P. Miles, *Normal hip and knee active range of motion: the relationship to age.* Phys Ther, 1991. **71**(9): p. 656-65.

58. Bergmann, G., et al., *Hip contact forces and gait patterns from routine activities.* J Biomech, 2001. **34**(7): p. 859-71.

59. Cappozzo, A., *Gait analysis methodology.* Human Movement Science, 1984. **3**(1–2): p. 27-50.

60. Leardini, A., et al., *Validation of a functional method for the estimation of hip joint centre location.* J Biomech, 1999. **32**(1): p. 99-103.

61. Bell, A.L., D.R. Pedersen, and R.A. Brand, *A comparison of the accuracy of several hip center location prediction methods.* Journal of Biomechanics, 1990. **23**(6): p. 617-621.

62. Davis Iii, R.B., et al., *A gait analysis data collection and reduction technique.* Human Movement Science, 1991. **10**(5): p. 575-587.

63. Seidel, G.K., et al., *Hip joint center location from palpable bony landmarks—A cadaver study.* Journal of Biomechanics, 1995. **28**(8): p. 995-998.

64. Piazza, S.J., N. Okita, and P.R. Cavanagh, *Accuracy of the functional method of hip joint center location: effects of limited motion and varied implementation.* J Biomech, 2001. **34**(7): p. 967-73.

65. Noble, P.C., et al., *The anatomic basis of femoral component design.* Clin Orthop Relat Res, 1988(235): p. 148-65.

66. Byrd, J.W.T., C.A. Guanche, and R.K.N. Ryu, *AANA Advanced Arthroscopy: The Hip*. 2010: Elsevier Health Sciences.

67. Peelle, M.W., et al., *Acetabular and femoral radiographic abnormalities associated with labral tears.* Clin Orthop Relat Res, 2005. **441**: p. 327-33.

68. Hammer, W.I., *Functional Soft-tissue Examination and Treatment by Manual Methods*. 2007. p. 260.

69. Louahem M'sabah, D., C. Assi, and J. Cottalorda, *Proximal femoral osteotomies in children.* Orthop Traumatol Surg Res, 2013. **99**(1 Suppl): p. S171-86.

70. Cordes, S., D.R. Dickens, and W.G. Cole, *Correction of coxa vara in childhood. The use of Pauwels' Y-shaped osteotomy.* J Bone Joint Surg Br, 1991. **73**(1): p. 3-6.

71. Clippinger, K.S., *Dance Anatomy and Kinesiology*. 2007. p. 182.

72. Cibulka, M.T., *Determination and significance of femoral neck anteversion.* Phys Ther, 2004. **84**(6): p. 550-8.

73. Osteotomy, F.D.; Available from: http://www.hss.edu/conditions_femoral-osteotomy-overview.asp#.VUj15vlVhBc.

74. Stulberg SD, C.L., Harris WH. *Unrecognized childhood hip disease: a major cause of idiopathic osteoarthritis of the hip*. in *The Hip*. 1975.

75. Reid, G.D., et al., *Femoroacetabular impingement syndrome: an underrecognized cause of hip pain and premature osteoarthritis?* J Rheumatol, 2010. **37**(7): p. 1395-404.

76. Gear, C.W., *Simultaneous Numerical Solution of Differential-Algebraic Equations.* IEEE Trans Circ Theory, 1971. **18**: p. 89-95.

77. ADAMS manual, M.S.A.S. 2011. p. 188-191.

78. Gottschalk, S., M.C. Lin, and D. Manocha, *OBBTree: a hierarchical structure for rapid interference detection*, in *Proceedings of the 23rd annual conference on Computer graphics and interactive techniques*. 1996, ACM. p. 171-180.

79. Park, S., C.T. Hung, and G.A. Ateshian, *Mechanical response of bovine articular cartilage under dynamic unconfined compression loading at physiological stress levels.* Osteoarthritis Cartilage, 2004. **12**(1): p. 65-73.

80. Treppo, S., et al., *Comparison of biomechanical and biochemical properties of cartilage from human knee and ankle pairs.* J Orthop Res, 2000. **18**(5): p. 739-48.

81. Izambert, O., et al., *Dynamic stiffness and damping of human intervertebral disc using axial oscillatory displacement under a free mass system.* Eur Spine J, 2003. **12**(6): p. 562-6.

82. Funk, J.R., et al., *Linear and quasi-linear viscoelastic characterization of ankle ligaments.* J Biomech Eng, 2000. **122**(1): p. 15-22.

83. Grood, E.S. and W.J. Suntay, *A joint coordinate system for the clinical description of three-dimensional motions: application to the knee.* J Biomech Eng, 1983. **105**(2): p. 136-44.

84. Eberly, D., *Least Squares Fitting of Data*. 2008: Geometric Tools, LLC.

85. Ilizaliturri, V.M., Jr., et al., *A geographic zone method to describe intra-articular pathology in hip arthroscopy: cadaveric study and preliminary report.* Arthroscopy, 2008. **24**(5): p. 534-9.

86. Field, A., *Discovering Statistics using SPSS*. Third ed. 2009: SAGE.

87. Lequesne, M., J. Malghem, and E. Dion, *The normal hip joint space: variations in width, shape, and architecture on 223 pelvic radiographs.* Ann Rheum Dis, 2004. **63**(9): p. 1145-51.

88. Cibulka, M.T. and J. Threlkeld, *The early clinical diagnosis of osteoarthritis of the hip.* J Orthop Sports Phys Ther, 2004. **34**(8): p. 461-7.

89. Athanasiou, K.A., G.G. Niederauer, and R.C. Schenck, Jr., *Biomechanical topography of human ankle cartilage.* Ann Biomed Eng, 1995. **23**(5): p. 697-704.

90. Calhoun, J.H., et al., *A comprehensive study of pressure distribution in the ankle joint with inversion and eversion.* Foot Ankle Int, 1994. **15**(3): p. 125-33.

91. Siegler, S., J. Block, and C.D. Schneck, *The mechanical characteristics of the collateral ligaments of the human ankle joint.* Foot Ankle, 1988. **8**(5): p. 234-42.

92. Y.C, F., *Biomechanics: Mechanical Properties of Living Tissues*. 1981, New York: Springer-Verlag.

APPENDIX A

RIGID BODY DYNAM IC MODEL DEVELOPMENT

Contact Mechanics

The force developed between contacting articular surfaces is defined as a non-linear function of penetration depth, x and the penetration velocity, $\dot{x}$

$$\boldsymbol{Force} = \boldsymbol{k}\,(\boldsymbol{x})^{\boldsymbol{e}} + \boldsymbol{step}(\boldsymbol{x}, \boldsymbol{0}, \boldsymbol{0}, \boldsymbol{dmax}, \boldsymbol{c})\dot{\boldsymbol{x}} \qquad \textbf{Equation 7}$$

The penetration depth x is scaled by stiffness term k. The stiffness term k is calculated using the following equation,

$$\boldsymbol{k} = \boldsymbol{E} * \frac{\boldsymbol{A}}{\boldsymbol{t}} \qquad \textbf{Equation 8}$$

Where *E* is the experimental compressive modulus of cartilage at the distal tibia and talar dome (*E* = 0.374*MPa)* [80]. The modulus is scaled by the local average area, *A* , of the polygons comprising each bone surface mesh at the articulating surfaces, and thickness, *t,* of the articular cartilage at each joint as shown in equation 8.

The exponent, *e* is chosen based on cartilage's non-linear behavior under axial loading [79]. The cartilage cannot exceed a compressive axial strain of 100% as the cartilage cannot compress greater than its original thickness. Therefore, an exponent was chosen that would generate very high compressive forces so that bone penetration would not be greater than the average cartilage thickness at the hind foot. In this case *e*=9 is chosen,

assuming 3mm cartilage thickness allowing no greater than 86% of compressive strain (2.6mm penetration). The step function increases till the penetration value reaches $dmax$ and the damping coefficient reaches *c*. The damping coefficient *c* is chosen to be 2Nmm/s from the literature [81].

Ligament Mechanics

Each ligament is modeled as a tension only non-linear viso-elastic material with stress (*T*)-strain (ε) relation using quasi-linear viscoelastic theory [92] using the following equation,

$$T(\varepsilon) = \left(A(e^{B\varepsilon} - 1) + 0.1 * VR(M1, M2)\right) * step(\mathrm{DM(M1,M2)}, L_o, 0, L_o + 0.1, 1)$$

Equation 9

The constants A and B are obtained from previous experimental studies [81] by fitting the equation to experimental load-displacement tests for individual lateral-collateral bone-ligament-bone preparations. The term *VR* monitors the magnitude of the first time derivative of the displacement vector between the ligament insertion points *M1* and *M2*. The step function as described in equation 10 monitors independent time variable *A*. The function starts when $A=x_0$ and activates initial value h_0, this function continues cubically till the final value reaches h1 when $A=x_0$ and stops when $A=x_1$.

$$STEP(A, x_0, h_0, x_1, h) \qquad \textbf{Equation 10}$$

The subtalar ligament's structural properties have not been characterized; therefore their load-strain properties were represented as a function of their calcaneal insertion areas. Since

the ITCL and CL appear to have similar physical structures than the ATFL [3] this ligament was scaled by a factor of the ratio: *AreaITCL/AreaATFL*. *AreaATFL* was calculated in the previous experimental studies [91].

APPENDIX B

Changing the Neck-Shaft Angle of Femur

The neck-shaft angle of the femur is changed in the computer model using the software Geomagic™ by following the intertrochanteric osteotomy which is successfully used by surgeons [68, 69].

A wedge is cut near the femoral neck region and the femoral head is aligned on the cut plane of femoral shaft and fused. Figure 111 shows the wedge cut performed on femoral shaft to increase the neck-shaft angle and Figure 112 shows the wedge cut performed on femoral shaft to decrease the neck-shaft angle.

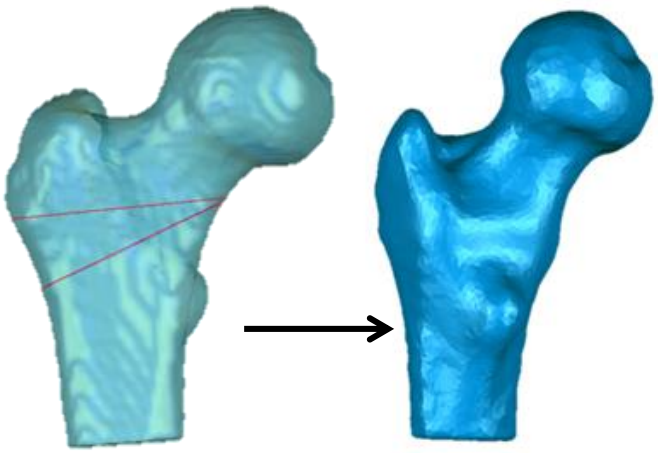

Figure 111. Wedge cut to increase the femoral neck-shaft angle.

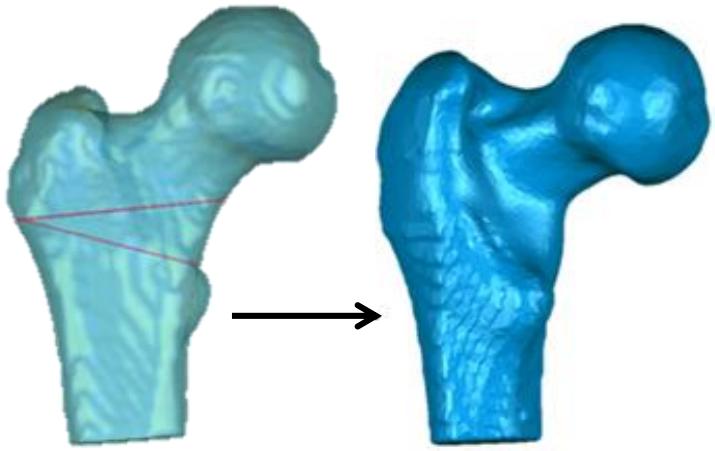

Figure 112. Wedge cut to decrease the femoral neck-shaft angle

Changing the Anteversion Angle

The femoral anteversion angle is changed by following derotational osteotomy, a procedure used by surgeons [72].

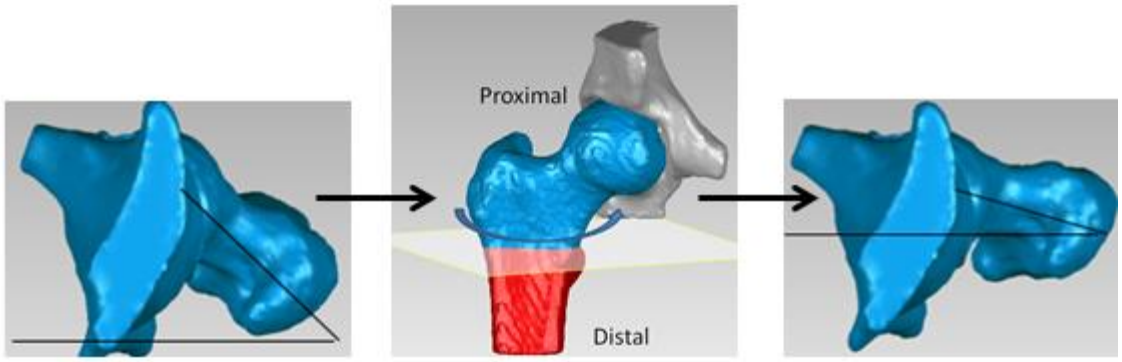

a) Normal anteversion angle b) Process of osteotomy c) Reduced anteversion angle

Figure 113. Process of Derotational Osteotomy (b) to reduce the femoral anteversion angle by 20 degrees to induce retroversion

The shaft of the femur is cut by plane (Figure 113b) and now the femur is divided into two parts-proximal and distal, the proximal part is rotated anticlockwise in right hip to decrease the anteversion angle and the proximal part is rotated clockwise to increase anteversion angle. Then the distal part and proximal part are fused together in the end.

VITA

Ramya Namani

Education

Ph.D. Mechanical Engineering, 2015, Drexel University, Philadelphia, PA, Advisor: Sorin Siegler, Ph.D.
M.S. Mechanical Engineering, 2008, University of Pennsylvania, PA
B.S. Mechanical Engineering, 2007, Andhra University, India

Honors and Awards

Matching dissertation grant award by International Society of Biomechanics, 2013
Engineering Design Education Fellowship, COE, Drexel University 2012-2015
Drexel Coulter foundation Grant 2013-2015
Academic Topper Gold Medal, Andhra University, India

Publications

Steven B. Cohen, Daniel P. Woods, Sorin Siegler, Christopher C. Dodson, **Ramya Namani**, Michael G. Ciccotti "Biomechanical comparison of graft fixation at 30o and 90o of elbow flexion for ulnar collateral ligament reconstruction by the docking technique", Journal of Shoulder and Elbow Surgery, 2015 Feb,265-72

Paolo Caravaggi, Sorin Siegler, James Tangorra, Mary Milone, **Ramya Namani**, Paul A Marchetto "The Envelope of Motion of the Cervical Spine and its Influence on the maximum torque generating capability of the Neck Muscles", Journal of Biomechanics, 2015 Aug.

Research Experience

Research Assistant, Drexel University, September 2012-2015.

- Developed A new total ankle replacement (TAR) device with conic saddle shaped joint.
- Modified a 6 DOF mechanical linkage to do the in-vitro testing of ankle specimens to compare Range of motion, coupling behavior of various TAR devices
- Created CAD models of various ankle implants and used the 3D printed models in in-vitro testing
- Developed a systematic approach to conduct in-vitro experiments on four degrees of freedom loading system to evaluate the Biomechanics of the elbow joint.
- Specialized in using an efficient data acquisition system and sensor technology to record the bone position movement in various motions
- Developed hip and ankle dynamic models to study the effect of morphology on biomechanical function
- Advised/mentored 3 M.S students and 1 undergraduate student

Teaching and Administrative assistant

- Teaching Fellow – Freshman Engineering Design Laboratory Sequence
- Teaching Assistant in various Mechanical Engineering courses such as Dynamics, Computer Aided Design and Evaluation and Presentation of Experimental Data
- Accreditation Board for Engineering and Technology (ABET) administrative assistant 2012-2013

Professional Organizations

- International Society of Biomechanics (ISB)
- Drexel Graduate Women in Science and Engineering (DGWISE)